# D2.1

# Intermediate integrated summary report about advanced technologies for the production of high-purity RBM

*Lead beneficiary:* LENZ

Due date: 30.4.2021 (M12)

Type of deliverable: R

| Dissemination level | | |
|---|---|---|
| PU | Public | X |
| PP | Restricted to other programme participants | |
| RE | Restricted to a group specified by the consortium | |
| CO | Confidential, only for members of the consortium | |

| History of changes | | | |
|---|---|---|---|
| Version | Date | Organisation | Modifications |
| 0.1 | 30.03.2021 | WP2 participants | 1st draft |
| 0.2 | 16.04.2021 | WP2 participants | 2nd draft |
| 0.3 | 30.04.2021 | WP2 participants | Completed version, review and additional contents |
| 1.0 | 18.06.2021 | LENZ, TECN | Final version |

| Main author(s) (in alphabetical order) | | |
|---|---|---|
| Name | Surname | Organisation |
| Jacobo | Alvarez | Lenz Instruments |
| Íñigo | Cacho | Fundación GAIKER |
| Jef | Bergmans | VITO |
| Miguel | Castro-Díaz | Loughborough University |
| Francesco | Di Maio | TUDelft |
| José Francisco | Fernández | ICV - CSIC |
| Abraham | Gebremariam | TUDelft |
| Asghar | Gholizadeh-Vayghan | VITO |
| Eunate | Goiti | TECNALIA |
| Debabrata | Gosh | VITO |
| Petri | Jetsu | VTT |
| Tülay | Ozlu | BESE |
| Kanda | Philippe | Keey Aerogel |
| Maximilian | Rech | RAMPF Eco Solutions |
| Mustafa | Sahmaran | Hacettepe University |

*ICEBERG website:* [www.iceberg-project.eu](www.iceberg-project.eu)

Legal Disclaimer

# Executive Summary

This document overviews a set of activities carried out in first year of the ICEBERG project dealing with the development of novel advanced technologies for the production of high purity recycled building materials (RBM).

In the frame of the ICEBERG project, a novel automatic sorting tool for the industrial scale processing of building demolition waste is being developed. The technology relies on the use of Near Infrared Hyperspectral Imaging to identify the composition of individual fragments in mixed ceramic fractions. The optimization of the measuring parameters has allowed defining the design parameters for the future implementation of a mobile automatic sorting line.

While the separation and purification of mixed ceramic fractions is an important step towards the production of high purity RBM, the ICEBERG project also explores the development of novel processes to achieve this goal. In particular, a novel process for the multi-step recycling of concrete has been set-up based on the use of a thermal step, followed by the separation of the ultrafine cement powder fraction by a cyclone process.

The project also aims to develop a sensor technology to monitor the quality of End-of-life (EOL) concrete in terms of the presence of pollutants, and thus to ensure compliance with target specifications. An in-line Laser Induced Breakdown Spectroscopy (LIBS) sensor-based equipment has been developed and coupled to an RFID traceability control system. At this initial stage, efforts have been focused on the optimization of the sensor set-up and spectral processing algorithms, and on the conceptual design of the industrial scale quality control line.

As a complementary strategy to recycle concrete and to avoid downgrading, a novel concrete processing technology based on accelerated carbonation is being investigated, and optimized for its pre-industrial scale implementation. Results show that this novel process allows reducing water absorption in recycled concrete, and improving its quality.

In terms of the recycling process for the ceramic fractions, the project addresses the development of a microgrinding process to improve the quality and homogeneity of the recycled material, thus allowing its reusability. The process has been developed, optimized and characterized at the lab scale.

The reuse of wood containing demolition waste represents another important recycling challenge. ICEBERG project intends to develop an integrated crushing and sorting process for the production of high quality wood fibers, which is under optimization. Bench scale pyrolysis experiments at three different temperatures have been conducted successfully. Initial lignin separation tests were also done.

A novel gypsum purification process is under development, which relies on a sequential multistep process involving hydrocyclone separation, acid treatment and leaching. Work is in progress to define the optimum configuration in terms of separation yield and cost, and to scale the process up to the pilot scale.

A last project goal deals with the recycling of post-consumer foams. A glycolysis process to recover polyols from foams commonly used in construction industry

has being established. Studies are being performed to investigate the possible reuse of the recovered materials.

Finally, a last relevant activity focuses on setting up a production line of silica closed-loop aerogels using EBM. Silica precursor synthesis has been tested with two concretes and one sample of construction glass waste. The continuous silica aerogel production at lab scale using jet cutting has been validated.

## Acronyms

ADR: Advanced Dry Recovery

AFm: Alumina, ferric oxide, monosulfate

CDW: Construction, refurbishment and Demolition Waste

C-S-H: Calcium silicate hydrate

CTP: Cloud traceability platform

EBM: End-of-life Building Materials

EoL: End-of-life

FT: Fourier transform infrared

HAS: heating air classification system

HSI: Hyperspectral imaging

IP: Intelectual property

IR: Infra-red

ITZ: Interfacial transition zone

LIBS: Laser-induced breakdown spectroscopy

LTSCD: Low Temperature Supercritical Drying

NA: Natural aggregates

PIR: Polyisocyanurate

PU: Polyurethane

PVA: polyvinyl acetate

PVA: polyvinyl alcohol

RAC: Recycled aggregates concrete

RBM: Recovered Building Materials

RCA: Recycled concrete aggregates

RFID: Radio Frequency Identification

RH: Relative humidity

SEM: Scanning electron microscopy

SWIR: short-wave infrared

UV-Vis-NIR: Ultraviolet-Vision- Near infrared

w/c: water/cement

WP: Work package

XRD: X-ray diffraction

# Contents

## List of figures

## List of tables

# 1. Introduction

Construction and demolition waste (CDW) accounts for more than a third of all waste generated in the EU28 (>350 Mt, excluding excavation earths). It contains a wide variety of materials such as concrete, bricks, wood, glass, metals and plastic. It includes all the waste produced by the construction, maintenance and demolition of buildings and infrastructure, as well as road planning and maintenance.

The average recycling rate is of 50% for the stony fraction (concrete, stone and ceramics which are at present down-cycled) and of less than 30% for wood; 25% for plastics; 10% for gypsum and 6% for glass.

During the first year of the ICEBERG project, several cost-effective advanced sorting and processing technologies for the production of high-purity secondary raw materials have been researched.

The following sections of this report include the progress on the research, upscaling and integration of those technologies and their use on the recycling of mixed aggregates (concrete and ceramic fractions); concrete; ceramic; wood; plasterboard; polymeric insulating foams; and glass and silica based for superinsulation materials.

# 2. Composition of Construction and Demolition Waste

The precise knowledge of the composition of CDW-based materials is important in order to develop and optimise novel advanced solutions for the production of high purity RBM. In the frame of the ICEBERG project, a characterisation study has been performed to evaluate the composition and characteristics of different waste materials.

In determining the composition of CDW-based materials, concrete waste (CW), glass waste (GW) and masonry units which include red clay brick (RCB), hollow brick (HB) and roof tile (RT) were used as obtained from an urban transformation area located in Ankara, Turkey. These materials were subjected to a non-complex, two-step, crushing-grinding procedure. The first step of the procedure consisted of loading the CDW-based materials into a laboratory-type jaw crusher which provided initial size reduction, followed by the second step which included the loading of the crushed materials into a ball mill and further grinding for an hour. In Figure 1, the images of a building that is planned to be demolished within the scope of an urban transformation and the materials after demolition are presented.

Figure 1. Demolition site in Ankara/Turkey

In Figure 2, views of CDW-based masonry units taken with the help of a video camera and scanning electron microscope (SEM) are shown. In Figure 3, gradation curves that give information about the particle size distributions of the precursors are displayed. X-ray diffraction (XRD) analysis results of the CDW-based materials are shown in Figure 4. X-ray fluorescence (XRF) analysis was performed to determine the chemical composition of the CDW-based precursors and the results are shown in Table 1.
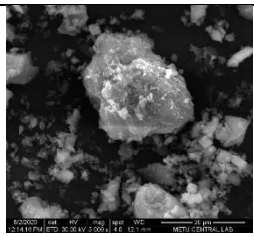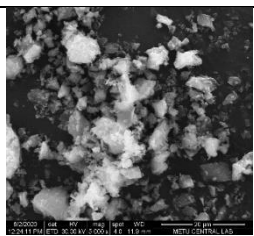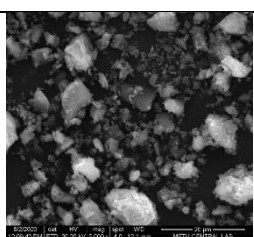
| | Original Form | Crushing Stage | Grinding Stage | SEM Images |
|---|---|---|---|---|
| (a) | | | | |
| (b) | | | | |
| (c) | | | | |

Figure 2. Photographs and SEM Images of CDW-based materials: (a) Red Clay Brick, (b) Hollow Brick, (c) Roof Tile, (d) Concrete Waste, (e) Glass Waste
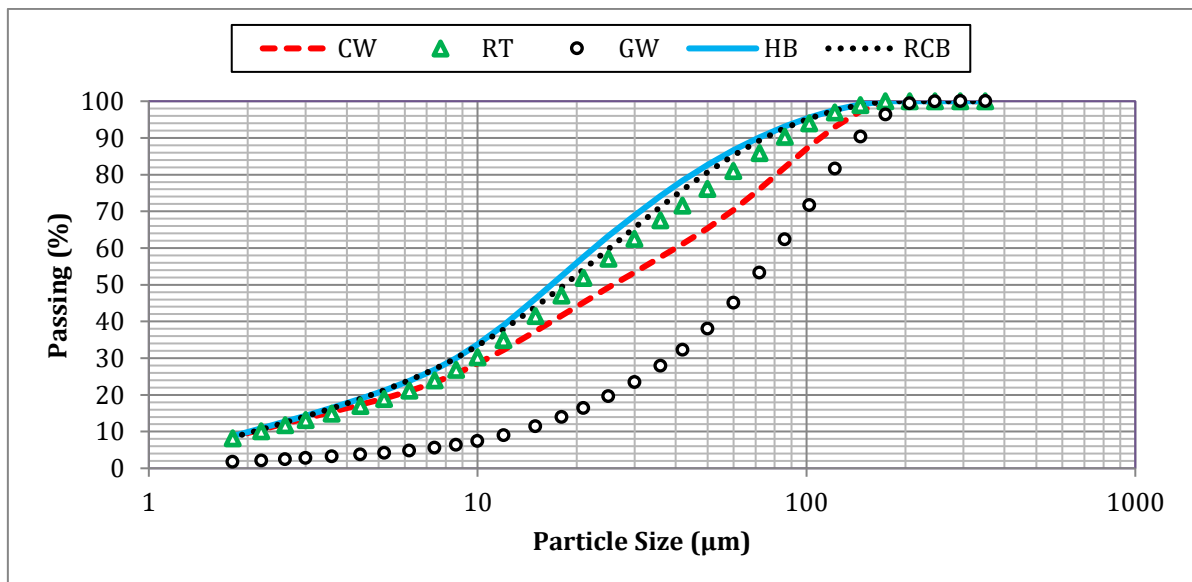


Figure 3. Particle size distributions of different CDW-based materials after ball milling
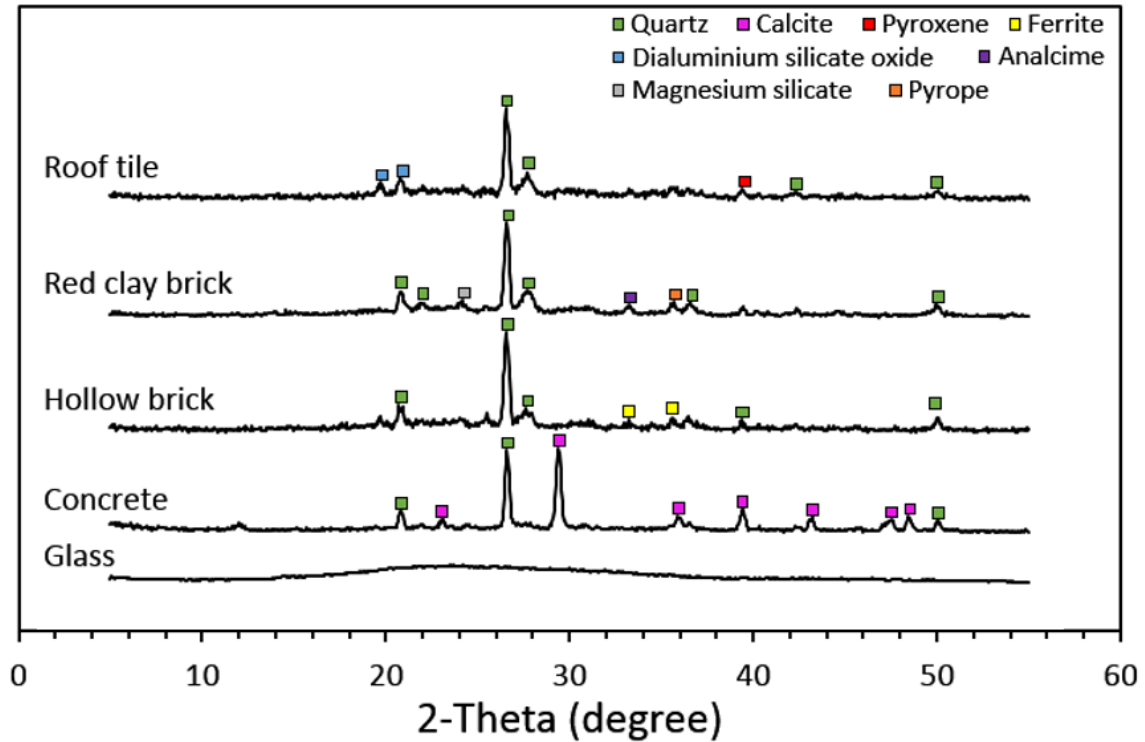
Figure 4. XRD Analysis of CDW-based materials

Table 1. Chemical composition of CDW-based materials

| Chemical Composition (%) | SiO$_2$ | Al$_2$O$_3$ | Fe$_2$O$_3$ | CaO | MgO | SO$_3$ | TiO$_2$ | K$_2$O | Na$_2$O | LOI |
|---|---|---|---|---|---|---|---|---|---|---|
| **Hollow Brick** | 39.7 | 13.8 | 11.8 | 11.6 | 6.45 | 3.4 | 1.65 | 1.55 | 1.45 | 7.8 |
| **Red Clay Brick** | 41.7 | 17.3 | 11.3 | 7.69 | 6.49 | 1.41 | 1.57 | 2.66 | 1.15 | 7.96 |
| **Roof Tile** | 42.6 | 15.0 | 11.6 | 10.7 | 6.26 | 0.71 | 1.82 | 1.6 | 1.6 | 7.49 |
| **Glass Waste** | 66.5 | 0.93 | 0.25 | 10.0 | 3.93 | 0.24 | 0.06 | 0.20 | 13.6 | 4.15 |
| **Concrete Waste** | 31.6 | 4.76 | 3.50 | 31.3 | 5.12 | 0.92 | 0.24 | 0.71 | 0.45 | 20.9 |

LOI: Loss of Ignition

In Figure 2, the original form, crushing stage, grinding stage and SEM images of the CDW-based materials are presented. According to the SEM images of the

CDW-based materials, it is observed that the particles observed in 20 μm cross section are quite similar to each other and do not have any specific characteristics.

As can be seen from Figure 3, HB is the finest CDW-based precursor after ball milling followed by RCB, RT, CW and GW. Further grinding to reach finer particle fractions for precursors is not intended in this study, since further milling is more labourious and energy-intensive. Another reason for the avoidance of further grinding of the precursors is related to a more realistic simulation of the situation in practice. Upon construction/demolition of a certain structure, different waste types are obtained collectively and it is therefore more logical and representative of the actual situation to keep the grinding period constant, if no special separation of wastes is intended.

X-ray diffraction (XRD) technique was also used to analyse the crystalline nature of the CDW-based materials. XRD analysis results of the CDW-based materials are presented in Figure 4. All materials except glass waste have a crystalline microstructure. It is known that the amorphous structure of the material and its low crystalline structure show positive results in terms of reactivity. Clayey materials do not have pozzolanic activity and are crystalline/semi-crystalline in nature. However, when calcined at temperature ranges of 600–900 °C, they lose their combined water and their crystallographic structure collapses, leading to the formation of silica and alumina in an amorphous state or in a state characterized by a disorder in the lattice structure. Under such circumstances, clay can exhibit pozzolanic activity since silica and alumina can react with calcium hydroxide. However, when the calcination temperature exceeds 900 °C, reorganization of alumina and silica can take place, which leads to the formation of thermodynamically stable compounds such as mullite and tridimite. These compounds are also crystalline in nature and non-reactive with calcium hydroxide. Today's so-called clayey building materials are rarely pozzolanic not only because they are calcined at higher temperatures but also they are composed of ingredients that contain no or low amounts of clayey ingredients. In contrast, bricks and tiles produced in other regions (e.g., Flanders) contain around 60% of clay.

The XRD diffractograms of CDW-based precursors can be largely related to the differences in their production processes, calcination temperature and raw materials used in these building materials. Since the initial producer, production stages and the sources of CDW-based raw materials are not known, no further details related to the differences in the mineralogy of these materials can be provided. The big quartz and calcite peaks in the XRD of this concrete show that it's probably produced with siliceous fine aggregates (sand) and limestone coarse aggregates.

X-ray fluorescence (XRF) analysis was performed to determine the chemical composition of the CDW-based materials and the results are shown in Table 1. The analysis shows that while GW was the richest material in siliceous oxides, RCB, RT and HB were also rich in siliceous and aluminous oxides. As expected, concrete waste is rich in calcium compared to other materials. Since the reactivity and pozzolanic activity of the materials are generally dependent on silicon,

aluminum and calcium oxides, designs are planned according to the combination of oxides contained in these materials to give maximum performance.

Future studies include the collection, sorting and individual characterization of CDW-based materials from different demolition sites. In addition, the pozzolanic activity of CDW-based materials will be determined by partial substitution of cementitious systems and the performances of CDW-based materials with different combinations will be analyzed.

## 3. Automated mobile sorting line based on hyperspectral imaging (HSI) to increase sorting efficiency of mixed EBM

### 3.1. Description of the problem

CDW sorting remains one of the main challenges when it comes to recycling these materials. In most of cases, operators classify these materials manually, and only metals and low-density materials are separated automatically through magnetic separation and density separation respectively. This process is time-consuming and expensive besides dangerous for the workers who are exposed to toxic substances present in these wastes.

On the other hand, automated techniques such as robot arms, separation by air flows known as "air jigging"[1] [2], and conveyor belts by imaging techniques [3] are being developed at the laboratory level, without a full implementation on industrial scale. These last techniques seem to be the more promising ones, focusing the efforts of the studies in create information on how to differentiate the materials using spectroscopies such as colour imaging (Vis), near-infrared (NIR), short-wave infrared (SWIR). Nevertheless, these techniques need to be optimized, due to the importance of the quality of the separation for the industrial preparation of new construction materials. Up to date there are only studies on how to sort big groups of materials such as the so-called "greys" including concrete and mortar, "reds", that group bricks, tiles, etc and "impurities" that include plastic, gypsums, wood, etc. Therefore, the ceramic fraction is not being separated in detail, ignoring the wide variety of materials that the term ceramic encompasses. In addition, the current applications of this sorted waste are mainly for the filling of roads and the preparation of aggregate materials such as mortars and concrete [3]. A classification that could differentiate between subgroups such as types of ceramics (bricks, porcelains, wares, etc.) is of vital importance, due to the different chemical and thermal treatments that each of these materials requires for the elaboration of new value-added products.

With the objective of developing an automated mobile sorting line based on hyperspectral imaging (HSI) to increase sorting efficiency of mixed CDW, CSIC and KERABEN are preparing sets of representative patterns of ceramic fractions mixed with other materials such as cement and gypsum-based materials. The resulting patterns of the mixtures of these materials have been analyzed in the NIR range (750-2500 nm). A deep characterization of the chosen materials for the set of pattern preparation can be found in Section 6 of the present report. This information will be used to get to know their hyperspectral images, to help to develop new hierarchical algorithms to recognize and classify the input stream into "grey" (concrete), "red" (ceramics), and impurities (e.g. plastics and gypsum) and possible subgroups inside each steam.

### 3.2. State of the art/technology

Construction, refurbishment and demolition waste (CDW) represents the largest waste stream in industrial countries and is composed of increasingly complex mixtures of different materials, including concrete aggregates, ceramics, wood, gypsum, plastics, metals or insulation foams. A relevant fraction of end-of-life

building materials (EBM) consists of a mixture of stony materials composed by concrete aggregates, ceramics (bricks and tiles) and other impurities (Figure 5). Since the recycling industry of EBM is dominated by relatively simple technologies, said large mineral fraction (85% of all CDW) is normally subjected to crushing and sieving combined with metals separation. The resulting outputs are typically applied as a substitute for natural gravel in unbound applications (e.g. road foundations). However, despite the fact that road foundation is a useful outlet for recycled aggregates, it is not a sustainable application in the long run. In the next years, the demand of materials for road foundations is expected to decline due to a reduction in the net growth of infrastructures, along with a strong increase in Europe of the amount of EBM related to demolition of a large number of constructions built in the middle of the last century[1].



Figure 5. Typical mixtures of stony aggregates from EBM (source: GAIKER)

Therefore, a shift towards more structural applications for recycled aggregates is required in order to foster a recovery based on circular economy approaches. But, for that, higher purity recovered materials (both, concrete aggregates and ceramic fractions) have to be produced from EBM. However, the conventional separation technologies implemented by the recycling industry are not able to obtain high-grade recycled fractions from stony mixtures. Indeed, the current sorting processes are mainly focused on the separation of light components and metallic parts by means of density-based systems and magnetic separators, respectively. Thus, advanced cost-effective sorting technologies are required to obtain high purity recycled concrete aggregates and ceramic fractions to be used as secondary raw materials in new building products. One basic step to achieve this goal is to improve automated separation technologies.

Optical sensors have been successfully implemented in automated sorting lines to classify at industrial scale mixed materials on the basis of differences in colour, transparency or chemical composition. The most common optical sensors integrated in state-of-the-art sorting systems are based on colour imaging (VIS) and/or near infrared spectroscopy (NIR) techniques. In this regard, it is pointed out that NIR spectroscopy has been the most often used identification technique in automated sorting processes when the chemical composition of materials is

---

[1] HISER project. Deliverable D3.12 "Integrated summary report about circular economy cycles for the stony, gypsum, wood, mineral and glass wool from CDW" (2017)

the feature to recognise, as in the case of plastics waste. The separation capacity of these systems depends on bulk density and grain size of the input stream (for plastic waste: 1-2 t/h approximately). The process consists basically of feeding the input material onto a conveyor belt, where it is scanned by an imager. If it detects the target material to be sorted out, it commands the control unit to blow the appropriate valves of the separation module at the end of the conveyor belt. So, these materials are separated from the material flow by jets of compressed air.

In previous research actions, the separation of CDW into big main groups has been developed. Imaging classification has been tested on a pre-industrial scale, using NIR, Vis or hyperspectral imaging (HSI), and computational treatments such as principal component analysis (PCA). Up to date, just a basic number of materials have been explored for the implementation of this technique without any successful transition into the recycling industry. In previous research actions, three main groups such as "greys" including concrete, mortar…, "reds" including bricks, tiles… and "impurities" with plastics, paper…. Nevertheless, results are promising because of the sufficient differences showed in these spectral ranges for these groups. The Vis spectrum range is especially interesting to identify coloured materials such as bricks, however, other materials only show differences in the intensity of the bands (concrete, mortar, and gypsum). IR spectrum was also studied, showing that it is possible to differentiate materials such as concrete and brick, due to their different chemical composition. IR spectrum of gypsum provides very distinguee bands from the rest of the materials [4], [5], [6].

NIR-based sorting solutions have also been researched and applied to EBM with the purpose of improving the quality of mixed recycled aggregates by means of removing non-stony impurities, such as, gypsum, organic materials or autoclaved aerated concrete. This study was carried out in the frame of the EU funded IRCOW project (number: 265212), and it was concluded that the composition of mixed recycled aggregates could be upgraded by using sorting systems based on said spectroscopic technique[2]. Continuing with this line of work, the EU funded HISER project (grant agreement number: 642085) was focused on developing an automated sorting prototype (validated at TRL 5) in order to classify mixtures of stony aggregates in three outputs in one single stage (Figure 6): two recycled fractions *(concrete aggregates and ceramic materials)* and a third one containing *impurities* (plastics, wood, gypsum, and others). So, in this case the focus was placed on fostering the circularity of both, concrete and ceramic materials for sustainability of building material resources.

---

[2] Vegas I., et al, "Upgrading the quality of mixed recycled aggregates from construction and demolition waste by using near-infrared sorting technology", Construction and Building Materials, Volume 75, 2015, Pages 121-128, ISSN 0950-0618
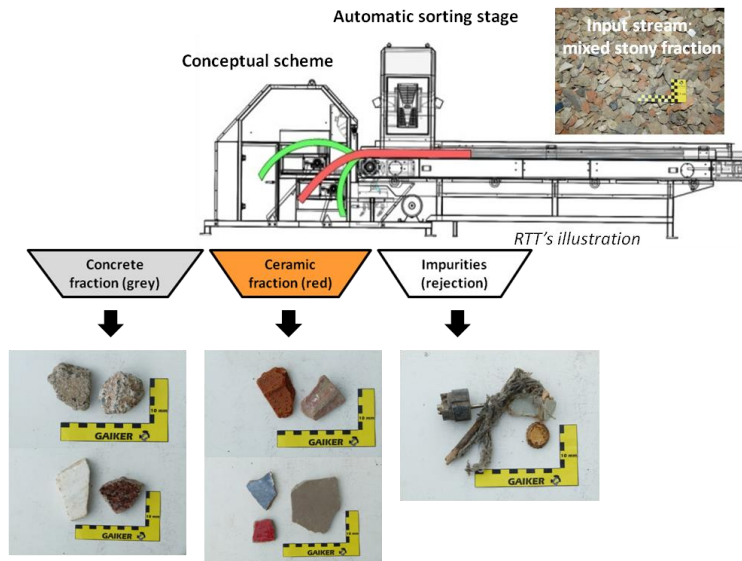
Figure 6. Conceptual scheme of a sensor-based sorting stage of mixed aggregates (source: HISER – H2020 642085)

Hyperspectral imaging (HSI) was the technique investigated in HISER for the automated recognition of concrete aggregates and ceramic materials in pre-processed mixed stony streams. In particular, two hyperspectral imagers with different wavelength range of Inno-spec GmbH were tested: RED-EYE 1.7 (0.9-1.7 µm) and RED-EYE 2.2 (1.2–2.2 µm). The RED-EYE 2.2 camera was finally implemented and evaluated in the experimental sorting prototype mentioned above[3].

The application of sensor-based techniques to sort mixed EBM is relatively recent and addressed by a limited number of research groups. In addition to IRCOW and HISER projects, mentioned above, roughly three groups have been identified with works related to CDW sorting supported by HSI: Bauhaus-University of Weimar and Ilmenau University of Technology (BUW) in Germany, Sapienza University of Rome (SUR) in Italy, and the third group includes some industrial research consortiums supported by various national and international public research funding (EU funded C2CA project and a French initiative named as CDW Recycling)[4].

BUW developed a sorting prototype for CDW including a hyperspectral imager of LLA Instruments GmbH (KUSTA 2.2 MSI, wavelength range: 1.25-2.15 µm). Some results obtained by BUW are summarized as follows: 1) concrete and bricks are well distinguishable in the infrared spectrum, 2) autoclaved aerated concretes and sand lime bricks can also be well recognized, 3) lightweight and normal concretes cannot be distinguished in the near-infrared spectrum,

---

[3] Hollstein F., et al. "Automated sorting of construction and demolition waste by advanced spectral imaging", Proc of IV International Conference Progress of Recycling in the Built Environment, 2018, Pages 37-45 (e-ISBN: 978-2-35158-208-4)

[4] Hollstein F, et al. "Challenges in automatic sorting of construction and demolition waste by hyperspectral imaging", Proc. of SPIE Vol. 9862, pp J01-J10, 2016

4) gypsum as impurity in the waste stream is well detectable and 5) clay brick material is not always recognizable[5]. On the other hand, SUR investigated at laboratory scale the HSI-based detection of impurities (wood, plastic, foam, gypsum and bricks) mixed with stony aggregates. For that, a NIR spectral camera equipped with an ImSpector N17E™ imaging spectrograph (wavelength range: 1.0–1.7 µm) was used, and satisfactory results were claimed[6].

The main advantage of HSI in comparison with NIR spectroscopy is mainly due to the combination of high spatial and spectral resolution. HSI applies reflectance/emittance spectroscopy to every pixel in a spatial image. So, the chemical and spatial analysis of the whole surface of scanned materials is performed. Thus, complex sorting tasks could be possible since the complete spectral footprint of every pixel of a material image is recorded.

A hyperspectral image is formally to be considered as a 3D data cube in which two dimensions represent a surface (x, y) and the third dimension comprises the energy content equivalent of reflected/transmitted electromagnetic radiation beams as a function of radiation frequency, called spectrum (Figure 7).



Figure 7. Conceptual scheme of a hyperspectral image (two spatial and one spectral dimensions)

There are several methods to generate the data cube. The whiskbroom and push-broom methods are the most common in industrial sensor-based classifications. In brief, the whiskbroom method scans a surface pixel by pixel to measure the full spectrum of the surface point in one time step, and the push-broom scanning performs the same but a full (finite) straight line of pixels is scanned in one time step (Figure 8).

---

[5] Linß E., et al. "Sensor-based sorting of mineral construction and demolition wastes by near-infrared". Proc. OCM 2015 - Optical Characterization of Materials, Karlsruhe, March 18 – 19, 2015, ISBN 978-3-7315-0318-7, pp 179 – 189

[6] Palmieri R., et al. "Automatic detection and classification of EOL-concrete and resulting recovered products by hyperspectral imaging". Proc. SPIE 9106, Advanced Environmental, Chemical, and Biological Sensing Technologies XI, 91060D (22 May 2014), doi: 10.1117/12.2049399
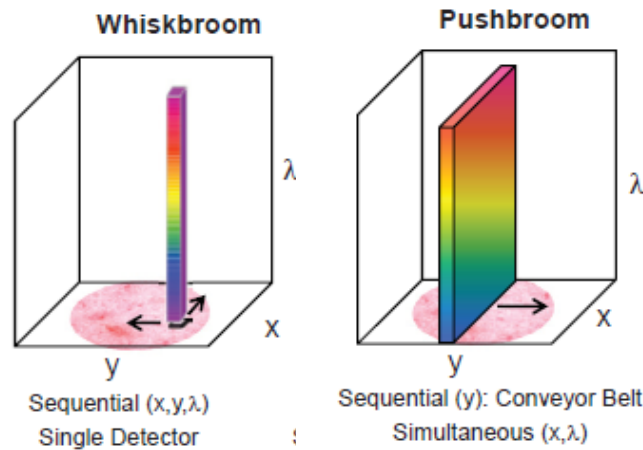
Figure 8. Whiskbroom and pushbroom scanning methods[7]

On the market there are hyperspectral cameras that work in the spectral ranges of Vis-NIR, NIR, SWIR and mid wade infrared (MIR). Their cost is related to the spectral range, the SWIR and MIR cameras being the most expensive ones (Figure 9). The choice depends on the user's application.
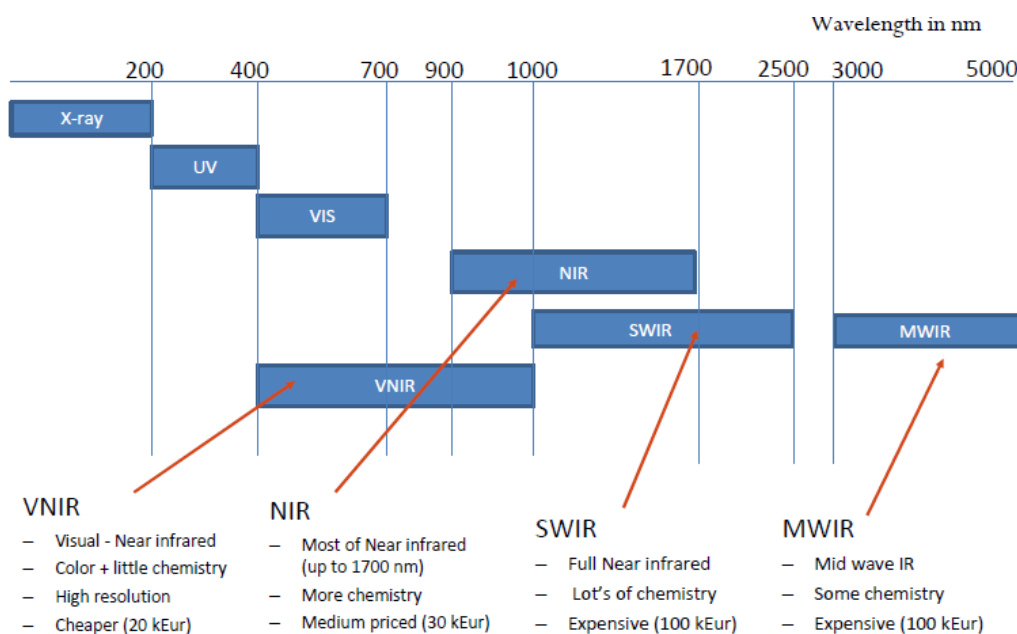


Figure 9. Types of hyperspectral cameras on the market (source: Prediktera)

## 3.3. Extended methodology

As a first approach to the problem presented adobe, different construction materials have been studied by UV-Vis-NIR spectroscopy using a Perkin Elmer

---

[7] Boldrini B, et al., "Hyperspectral imaging: a review of best practice, performance and pitfalls for in-line and on-line applications", Journal of Near Infrared Spectroscopy 20, 483-508 (2012)

Lambda 950 spectrometer in the range of 200 - 3500 nm. Once these spectra were obtained, element of classification for all the materials were stablished. Based on these preliminary results, different sets of representative patterns were prepared as explained in the next subsection. In the same way, these mixtures were studied in the range of 750 - 2500 nm using the same spectrometer in order to obtain a relation between the content of material in the mixture and the intensity of the bands.

The automated classification of stony fractions coming from EBM is still a challenge, and therefore, more efforts in innovation are required in order to develop efficient sorting lines. In this purpose, HSI plays a relevant role. As mentioned above, the HISER project designed and assessed (TRL 5) a pilot sorting prototype based on HSI and pneumatic ejectors to produce both recycled concrete and ceramic aggregates from mixed stony fractions in one single step[8]. The hyperspectral imager implemented in the HISER prototype covered the 1.2-2.2 µm wavelength range, being essential the region of 1.7–2.1µm. Limitations due to mobility, multiphasic nature, shape and size of materials were noticed at TRL 5. Thus, further innovation to gain in efficiency (>90%) at both identification and classification stages is needed.

In comparison with earlier developments, ICEBERG will extend the functionality and upgrade the performance of an innovative mobile automated sorting technology based on HSI by incorporating advanced hyperspectral imagers and data processing software to recover high-grade secondary raw materials (concrete and ceramic fractions with purity ≥92%) contained in pre-processed mixed stony aggregates (particle size: 20–50 mm). So, ICEBERG aims to develop a <u>pre-industrial sorting prototype</u> with representative capacities (≥1 t/h). Likewise, this new technology is pretended to be versatile and easily adaptable in real time to treat other complex mixed fractions from EBM: PUR/PIR foams and gypsum.

Considering this objective, the ICEBERG methodology consists of, on one hand, studying at laboratory scale the automated HSI-based recognition of the target materials (concrete and ceramics aggregates, gypsum and, PUR and PIR foams), and on the other hand, implementing the lab results in the new HSI-based sorting prototype:

- Acquisition by a push-broom laboratory system (line scanning method) of hyperspectral images of the target reference samples.
- Hyperspectral data pre-processing: removal of background and other bad pixels (only information from samples are left) and spectral transformation by filtering algorithms.
- Development of classification (calibration) models based on multivariate data analysis (chemometrics).
- Validation of models at lab by test data (with samples that were not used for the models construction)
- Transfer of the calibration models from the lab to the sorting prototype.

---

[8] HISER project: Deliverable 3.1 "Prototype: novel automatic system" (2016)

- Testing of the prototype processing real EBM mixtures (functional trials of the demonstrator for optimization)

In addition to the calibration of HSI technology to get an efficient inline recognition of mixed materials, the design of the mobile sorting prototype is also a relevant issue addressing in ICEBERG and, it is crucial to ensure the future industrial feasibility. Considering this, the prototype under development consists of a conveyor-based concept in order to (1) guarantee particle stabilization before the scanning stage, (2) improve the accuracy of the ejection stage located at the end of the line, and (3) get a proper isolation of the identification instruments (HSI imager) to protect them from harsh working conditions.

## 3.4.  Materials (source, sampling, preconditioning)

Materials typically found in building construction were chosen. These materials can be classified in 3 different groups: In group 1, seven representative ceramics can be found, such as sanitary ware (ROCA washbasin), extruded stoneware, facade and common bricks and porcelain, red body and white body tiles (common construction materials). In group 2, two type of gypsums can be found, gypsum plasterboard and gypsum plaster. Finally, three "concrete-type" materials can be found in group 3: concrete (sidewalk curb), mortar (sidewalk tile) and sand (common construction sand). The investigations were done on new, not used building materials, for availability and reproducibility reasons. In Figure 10, pictures of each material, sorted by groups, are shown. These materials were cut, milled and sieved until the required particle size was obtained. Further details of this process and a complete characterization of these materials can be found in Section 6.3 and 6.4 of the present report.

Once the necessary particle size was obtained, sets of representative patterns were prepared by mixing the materials in known proportions as follows. Firstly, they were mechanically mixed using an electric blade mill without solvent and sieved under 200 ⬚m to ensure homogeneity. Chosen proportions are shown in Figure 11: in blue for binary mixtures (ceramic-cement and ceramic-gypsum) and marked in green, ternary material mixtures (plaster-ceramic-cement).
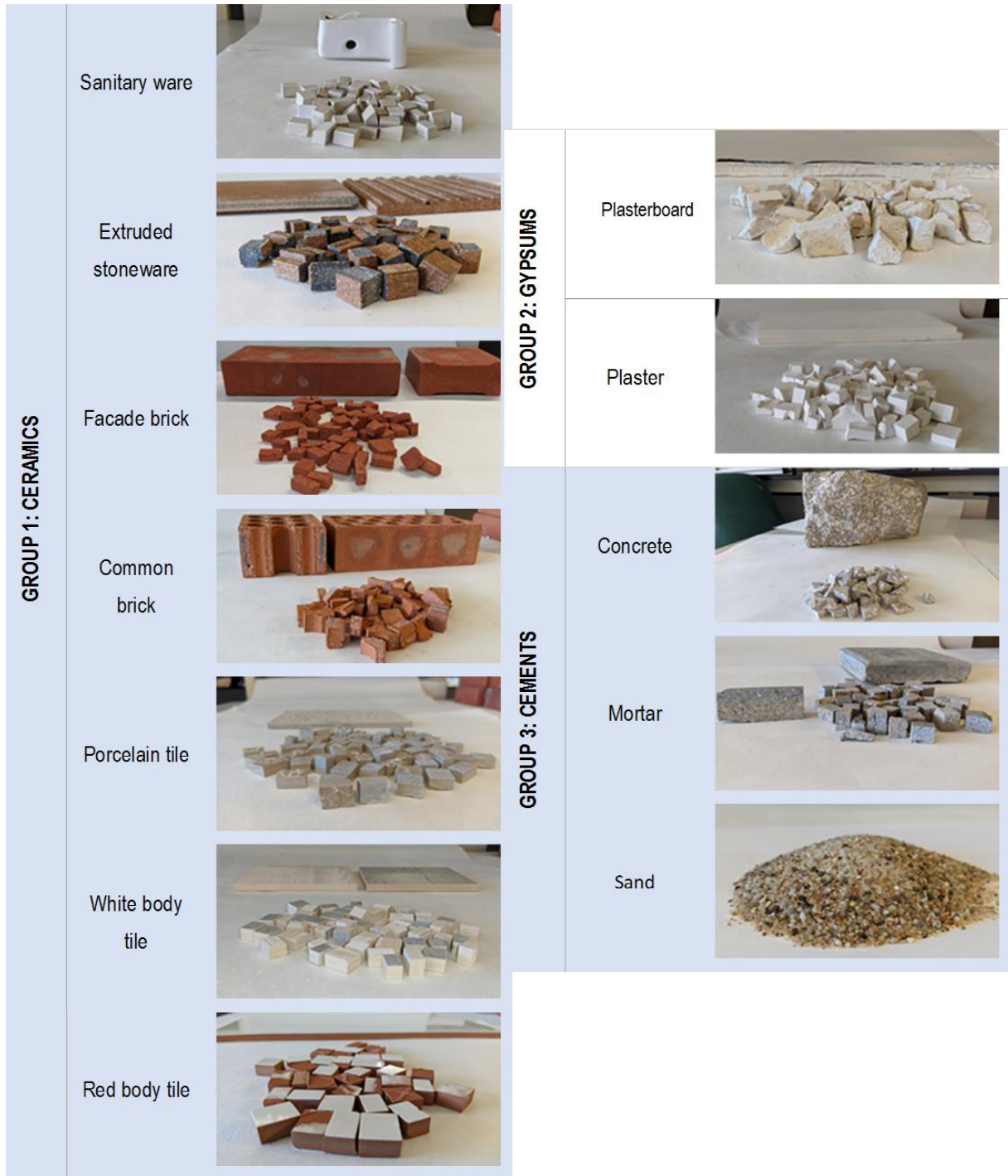
Figure 10. Pictures of the chosen construction materials: Ceramics, gypsums and cements groups.
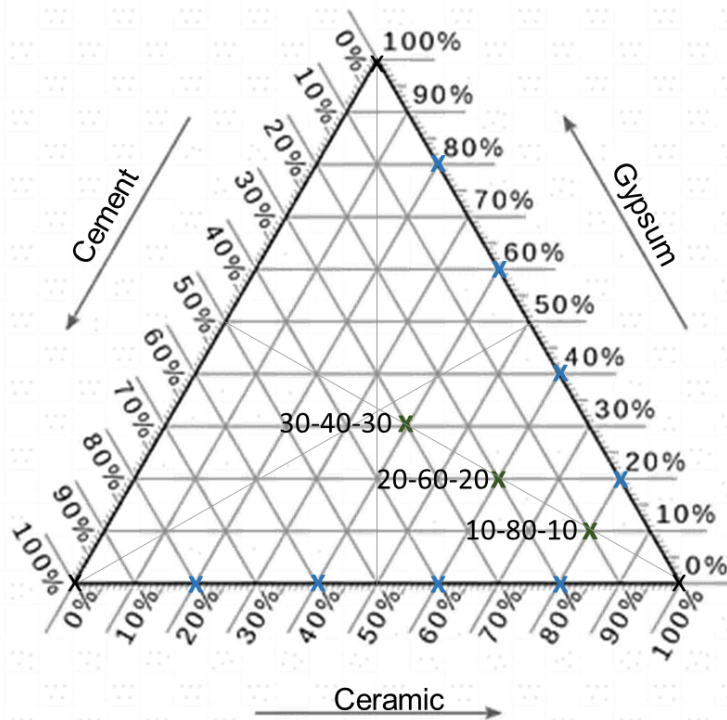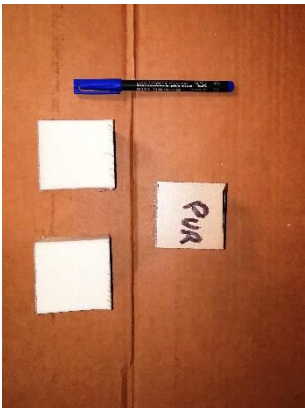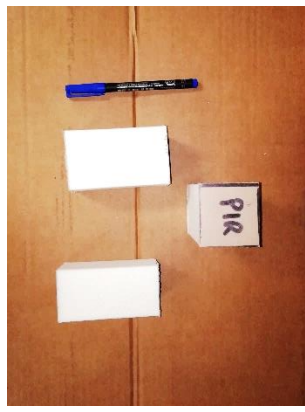
Figure 11. Ternary diagram with the composition of the binary patterns (indicated in blue) and ternary patterns (in green).

Reference samples of the target materials contained in mixtures of EBM have been collected. These known materials are used to develop the laboratory calibration models based on chemometrics tools that later on will be implemented in the novel sorting prototype. So, the reference samples have been clustered in concrete aggregates, red ceramic bricks, ceramic tiles, PUR foams, PIR foams and plasterboards from construction, refurbishment and demolition works, as shown in Table 2.

Table 2. Reference samples from EBM



| Siliceous concrete | Limestone concrete | Ceramic bricks |

| | | |
|---|---|---|
| N/A |  |  |
| Ceramic glazed tiles | Plasterboard from demolition | Plasterboard from refurbishment |
|  |  |  |
| Plasterboard from construction | PUR foam | PIR foam |

## 3.5.  Activities in progress

As a first approximation to obtain a standard for classifying the materials discussed above, a wavelength scan of 200-2500 nm of the unmixed materials was performed. The resulting UV-VIS-NIR spectra of the materials, grouped by type, are shown in Figure 12. The abrupt peak at c.a. 860 nm present in all the spectra is due to the lamp shift of the equipment. The response obtained according to the functional groups visible for this technique is described below. Firstly, water and -OH (hydroxyl) produce particularly diagnostic absorptions in minerals. The overtones of water are seen in adsorption spectra of $H_2O$-bearing minerals (plaster, plasterboard, mortar and concrete). The first overtones of the OH stretches occur at ~1400-1500 nm and the combinations of the H-O-H bend with the -OH stretches are found ~1900 nm [7]. These and other characteristic bands for each material will be discussed in detail below.

**Group 1: ceramics.** As showed in Figure 12 *a* and *b*, all these spectra only differ from each other in the case of both types of bricks and red body tiles, which present broad bands at ~400 nm, 500 nm and 670 nm. These bands are related to Fe-bearing characteristic minerals, such as phyllosilicates. Octahedrally coordinated $Fe^{2+}$ and $Fe^{3+}$ generate broad bands of absorption at 900 nm and 650 nm, as well as absorptions centred about 500 nm. In addition, $Fe^{3+}$ in tetrahedral coordination can generate an absorption near 430 nm. Finally, two

broad bands at c.a. 1900 and 2200 nm are shown for all the presented ceramics materials, corresponding to the hydroxyl group presence [8].

**Group 2: gypsums**. In Figure 12 *c*, UV-Vis-NIR absorption spectra of plaster and plasterboard are presented. Both materials contain a high amount of gypsum ($CaSO_4.2H_2O$) and bassanite ($CaSO_4.1/2H_2O$) in their composition, as studied by XRD and XRF in Section 6 of the present report. These two minerals exhibit characteristic bands near 1400-1550 nm (triplet), 1930-1950 nm (doublet), 2200-2300 nm (triplet) and a broad band at 2500 nm due to $H_2O$ vibrations, as well as bands near 1760-1790 nm probably due to combinations of $SO_4^{2-}$ and $OH^-$ or $H_2O$ vibrations [9]. The remaining bands around 1170 and 2100 nm present in plaster are probably associated with impurities and additives in the gypsum.

**Group 3: concrete-type**. In Figure 12 *d*, UV-Vis-NIR absorption spectra of mortar, sand and concrete can be seen. The difference in the absorption bans between these three materials in the NIR range is due the presence of $H_2O$, which is decreasing from the concrete to the mortar and it is absent in sand, due the lack of water in its structure.

Based on these results, the ceramic types could be differentiated into ceramic containing iron or the so-called "red ceramic", that includes different types of bricks and red body tiles and ceramic that does not contain iron, or "white ceramic", including extruded stoneware, porcelain, sanitary and white body tiles in this range (200-2500 nm). On the other hand, gypsum-base materials are very easy to differentiate using this technique due to the presence of calcium sulfate minerals in their structure. Finally, concrete-type materials present a similar behavior as white ceramic, showing few possibilities of sorting based on their spectroscopy response. However, the absorption of this materials is lower than the absorption of white ceramic materials in the UV range of the spectra, making this a possibility to consider.
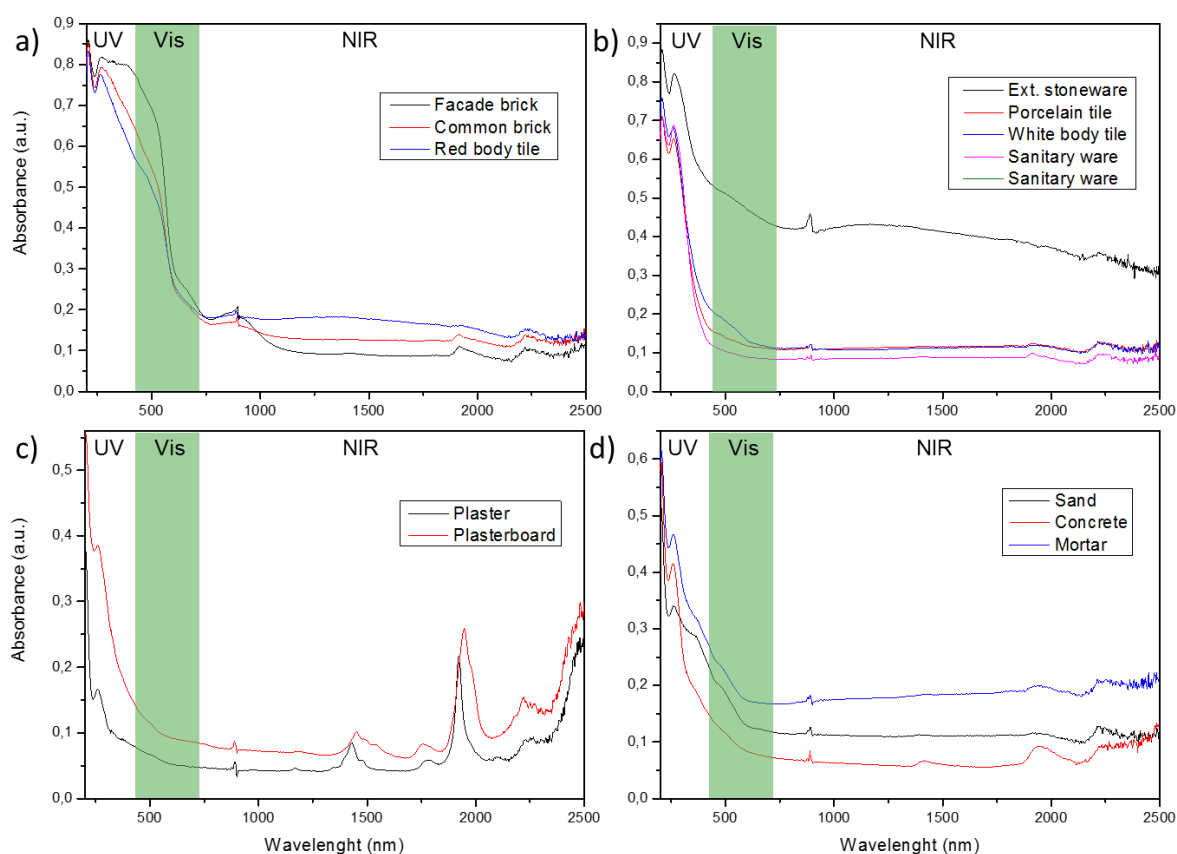
Figure 12. UV-Vis-NIR spectra of the materials, grouped by type: a) red ceramic materials, b) white ceramic materials, c) gypsums and d) cements.

Table 3. Summary of the UV-Vis-NIR response for the tested materials, sorted by group. Legend: (t): triplet, (d): doublet.

|  | Group 1: | Group 2: | Group 3: |
|---|---|---|---|
| *Main peaks (nm)* | Red ceramics: 400, 500 and 670 | 1400-1550 (t), 1930-1950 (d) and 2200-2300 (t) | ~1400-1500 and ~1900 |
| *Preference range for their classification* | Visible - NIR | NIR | NIR |

Based on these results, Fe-bearing ceramics can be easily distinguished from non-containing Fe ceramics. One "red" ceramic (Façade brick) and one "white" ceramic (porcelain tile) were chosen for the preparation of the sets of representative patterns. These two ceramics were mixed with plasterboard as a representative material from the gypsum group and with concrete in the case of the concrete-type group. Firstly, ceramic materials were mixed with gypsum-based and cementitious materials separately, in binary compositions (20-80, 40-60, 60-40 and 80-20), resulting in 16 different compositions. These mixtures were measured in the NIR spectrum range from 750 to 1500 nm

(Figure 13). As in previous measurements, the materials show bands at 1416 nm for the concrete-bearing compositions, 1450 nm for the plasterboard compositions, and 870 nm for the façade brick compositions. As expected, band intensities increase as the presence of the responsible material does. However, overlapping problems arise when two materials with similar bands are mixed. This is the case of the plasterboard and façade brick mixtures (Figure 13), which present the band c.a. 1430 nm, as a result of the gypsum (1450 nm) and façade brick (1416 nm) bands overlapping.

In further steps, these data can be used to create calibration curves for these mixtures, permitting the identification of mixtures of these materials. Moreover, tertiary mixtures of these materials (cement-ceramic-gypsum) are being prepared to provide more detailed information on representative CDW standard sets.
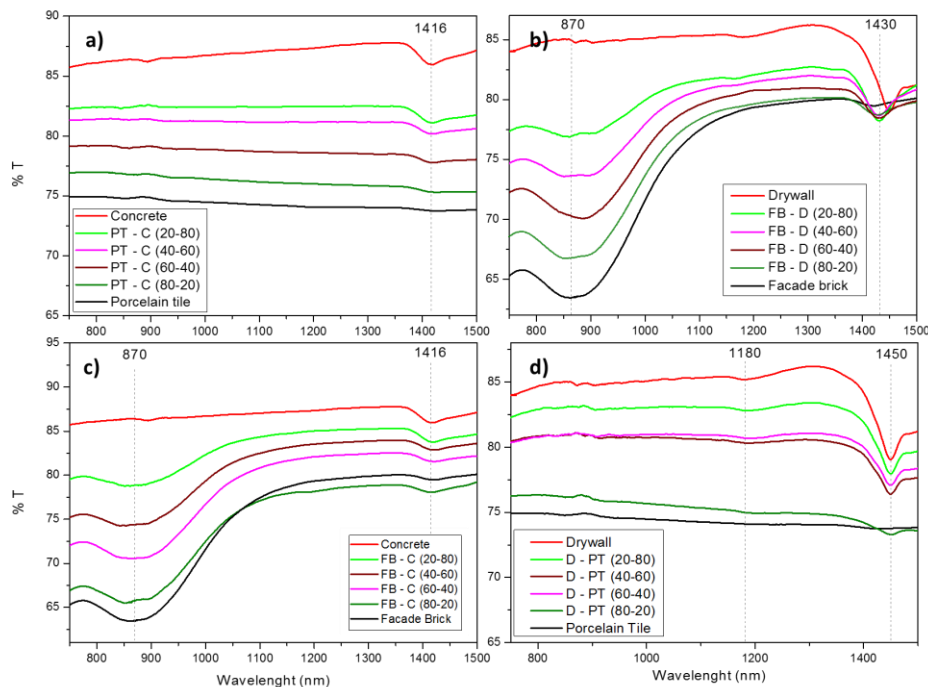


Figure 13. Transmittance NIR spectra of the set of representative patterns of materials.

The ICEBERG activities related to the development of advanced sensor-based sorting technology to increase the recovery efficiency of mixed EBM are focused first, on the laboratory study of the automated identification of the target materials by HSI (lead by GAIKER), and second, on the design and construction of an innovative mobile sorting prototype (lead by LENZ). Considering this, the laboratory work aims to develop chemometrics-based calibration models capable of successfully classifying EBM materials. The modelling result will be later on transferred and implemented in the prototype.

The research is executed using a dedicated table-top laboratory setup available at GAIKER. This setup includes an advanced HSI imager (or camera), two halogen lamps and a sliding scanning table (Figure 14Figure 14). The system is

controlled by a specific software pack that allows to adjust operational parameters (for instance, scanning length or integration time), acquire and analyse hyperspectral images of materials, and develop and validate classification models based on multivariate data analysis algorithms. The selection and installation of said laboratory HSI setup has been carried out within the scope of ICEBERG. So, it has been part of the work executed in the project.
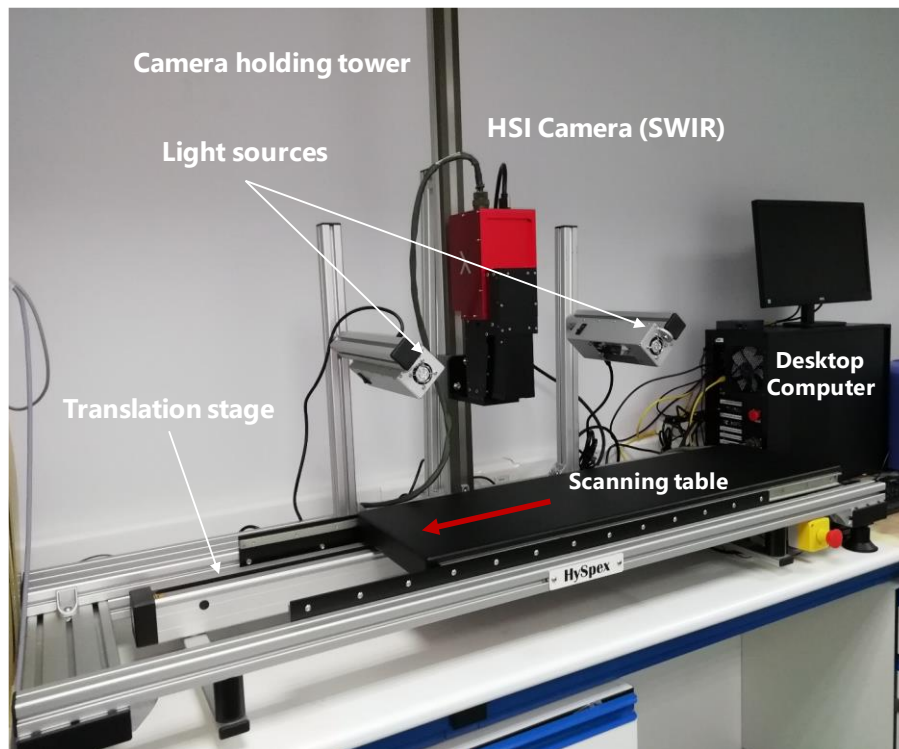


Figure 14. Laboratory setup of hyperspectral imaging (GAIKER)

The key component of the system is the hyperspectral camera or imager. After evaluating different alternatives available on the market and considering conclusions derived from the HISER project related to the necessary spectral range to address the analysis of stony materials (1.2–2.2µm wavelength range), a SWIR HSI camera (model: HySpex SWIR – 384) from NEO (www.hyspex.com) was finally selected for ICEBERG. This camera covers a wide wavelength range (930–2500 nm) within the region of shortwave infrared (SWIR), and it uses the push-broom scanning method (when acquiring data, the camera captures all spectral information simultaneously from a narrow line of the spatial scene). The technical specifications are shown in Table 4.

Table 4. Specifications of the HySpex SWIR – 384 camera (source: NEO)

| MAIN SPECIFICATIONS | |
|---|---|
| Spectral range | 930-2500 nm |
| Spatial pixels | 384 |
| Spectral channels | 288 |
| Spectral sampling | 5.45 nm |
| FOV* | 16° |
| Pixel FOV across/along* | 0.73/0.73 mrad |
| Bit resolution | 16 bit |
| Noise floor | 150 e- |
| Dynamic range | 7500 |
| Peak SNR (at full resolution) | > 1100 |
| Max speed (at full resolution) | 400 fps |
| Power consumption | 30 W |
| Dimensions (l–w–h) | 38 – 12– 17.5 cm |
| Weight | 5.7 kg |
| Camera Interface | CameraLink |

Concerning the laboratory study, the activity currently in progress is focused on adjusting the camera parameters for an optimal scanning and acquiring hyperspectral images of the reference materials. After pre-processing, this experimental data will be later on used to develop the calibration models that will be transferred to the sorting prototype. Some examples of hyperspectral images in JPG format are some below (Table 5).

Table 5. Hyperspectral images in JPG format



| Concrete aggregates | Ceramic bricks | Plasterboard |
|---|---|---|
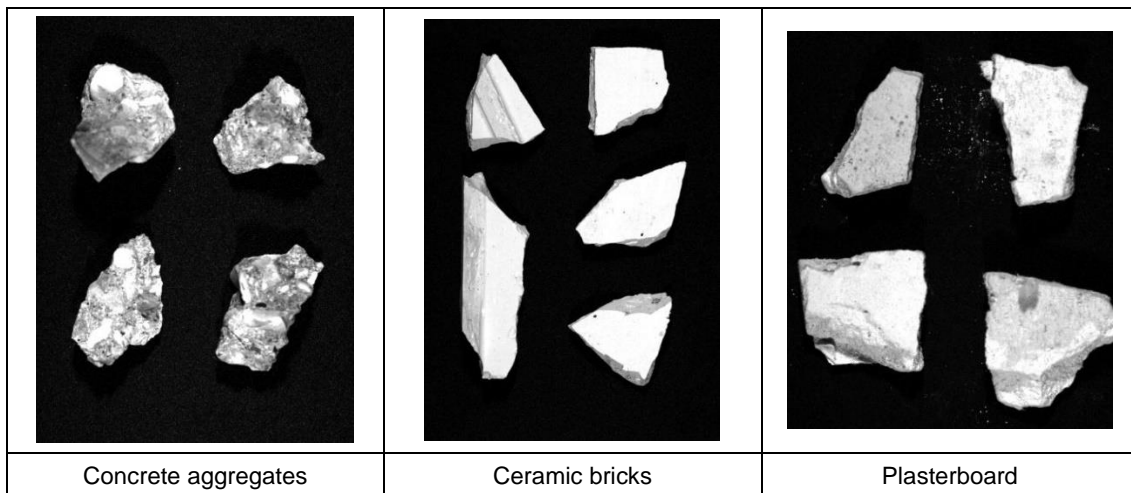
## 3.6.  Planning for the rest of the activities

The obtained results to date from both the separate materials and the mixtures show that a more detailed sorting of these materials could be possible. For the next few months, it is expected to complete these results with the ternary mixtures in order to obtain more complete information. Once all these calibration curves are obtained from the treatment of these data, the computational analysis such as PCA could be a good direction to continue. These data, in addition to the

samples produced to obtain them, will be shared with the other consortium member to favour the transfer of knowledge.

Regarding the laboratory study, the next action points are as follows:

- To complete the dataset with hyperspectral images of the reference samples (chemical and spatial information of the whole surface of patterns)
- To pre-process the hyperspectral data
- To develop classification models based on multivariate data analysis algorithms specific for every stream of mixed EBM (stony aggregates, plasterboards and PUR/PIR foams)
- To validate the models with test data (different than those used for the modelling stage)

## 3.7. Preliminary conclusions

Preparation and identification of sets of representative patterns of CDW have been done using UV-Vis-NIR spectroscopy. Preliminary results obtained with the unmixed materials show the possibility of sorting mixture of this materials using the cited technique. Moreover, results provided by binary compositions of ceramic and cementitious or gypsum-based materials shows the possibility of sorting these mixed materials, based in calibration curves that can be calculated from these results. However, these data need to be completed with the measurement of ternary compositions. Moreover, computational techniques such as PCA are being considered for the data treatment in further steps.

The development of advanced cost-effective sorting technologies based on sensors to be integrated in CDW recycling processes is a key aspect in order to obtain pure material fractions. In this context, hyperspectral imaging (HSI) covering the range of shortwave infrared (SWIR) and supported by chemometrics-based algorithms is a feasible technique for an effective inline identification and classification of EBM. So, the implementation of HSI in an innovative mobile separation line (prototype under construction) will foster the circularity of the valuable resources contained in CDW, and new market opportunities will be generated.

## 3.8. References

[1]   W.M. Ambrós, C.H. Sampaio, B.G. Cazacliu, G.L. Miltzarek, L.R. Miranda, Usage of air jigging for multi-component separation of construction and demolition waste, Waste Manag. 60 (2017) 75–83. doi:10.1016/j.wasman.2016.11.029.

[2]   C.H. Sampaio, B.G. Cazacliu, G.L. Miltzarek, F. Huchet, L. Le Guen, C.O. Petter, R. Paranhos, W.M. Ambrós, M.L. Silva Oliveira, Stratification in air jigs of concrete/brick/gypsum particles, Constr. Build. Mater. 109 (2016) 63–72. doi:10.1016/j.conbuildmat.2016.01.058.

[3]   J.D. Lau Hiu Hoong, J. Lux, P.Y. Mahieux, P. Turcry, A. Aït-Mokhtar, Determination of the composition of recycled aggregates using a deep learning-based image analysis, Autom. Constr. 116 (2020).

doi:10.1016/j.autcon.2020.103204.

[4]    S. Hansen, P. Sadeghian, Recycled gypsum powder from waste drywalls combined with fly ash for partial cement replacement in concrete, J. Clean. Prod. 274 (2020) 122785. doi:10.1016/j.jclepro.2020.122785.

[5]    R. L. S. Ferreira, M. A. S. Anjos, C. Maia, L. Pinto, A. R. G. de Azevedo, J. de Brito, Long-term analysis of the physical properties of the mixed recycled aggregate and their effect on the properties of mortars, Constr. Build. Mater. 274 (2021). doi:10.1016/j.conbuildmat.2020.121796.

[6]    A. Karrasch, M. Landmann, Sorting of Mineral Construction and Demolition Wastes by Near-Infrared Technology, n.d. https://www.researchgate.net/publication/338402849.

[7]    R.N. Clark, Remote Sensing for the Earth Sciences, John Wiley and Sons, 1999. https://archive.usgs.gov/archive/sites/speclab.cr.usgs.gov/PAPERS.refl-mrs/refl4.htmlhttp://speclab.cr.usgs.gov.

[8]    G.R. Rossman, B.L. Ehlmann, Electronic spectra of minerals in the visible and near-infrared regions, in: Remote Compos. Anal. Tech. Underst. Spectrosc. Mineral. Geochemistry Planet. Surfaces, Cambridge University Press, 2019: pp. 3–20. doi:10.1017/9781316888872.003.

[9]    J.L. Bishop, Visible and Near-Infrared Reflectance Spectroscopy, in: Remote Compos. Anal., Cambridge University Press, 2019: pp. 68–101. doi:10.1017/9781316888872.006.

## 4. Thermal attrition mobile unit for concrete recycling

The thermal attrition unit is intended to recycle the fine fraction (0-4mm) of crushed concrete which are usually wet (6-13% moisture). The unit is aimed to dry and separate the wet feed into clean sand (0.25-4mm) and hydrated cement rich powder (<0.25mm). This is possible by exposing the crushed fine concrete fraction to heat and later separating the ultrafine powder in cyclone. The thermal attrition unit is composed of different units; such as, the burner, which supplies hot air; the cyclone, which separates ultrafine powder dragged by the hot air; the Blower, which circulates air into the system; the feeder and the cascades. Under this task, the existing prototype heating air classification system (HAS) which has a capacity of 3 t/h will be redesigned and up scaled into 20 t/h thermal attrition unit. The basic principles of operation remain similar to the existing HAS while some design parameters will be optimized or changed.

### 4.1. Description of the problem

The construction and infrastructure sector consumes large amount of raw materials and produces the most waste. The sector is also responsible for the emission of a large amount of greenhouse gases not only due to the use of cement but also due to the heavy traffic created due to construction activities, which is directly linked to increased levels of CO2 and NOx emissions. During the last century, the global volume of natural resources used in buildings and transport infrastructure has increased 23-fold [1]. Sand and gravel are the most extracted group of materials worldwide, exceeding fossil fuels [2]. This problem seems to get worse with the present global increase in population and demand for infrastructures. The shortage of sand has been already envisaged and is a subject of current debate [3][1]. One option to address these problems is to make use of the large amount of material stock accumulating in buildings and infrastructure by improving the recycling rate of material resources. In fact, the continuous growth of material stock in buildings/infrastructure remains a challenge to close the materials loop and this may hinder the ambition of the construction sector towards circularity. Nevertheless, the need for large scale recycling facilities to improve the recycling rate proportionally to the extent of waste generation is necessary. With this regard, designing and upscaling a thermal attrition unit that can process the fine fraction of crushed concrete into clean recycled sand and cement rich powder is crucial.

### 4.2. State of the art/technology

Usually the fine fraction of recycled aggregates (<4mm) is composed of sand, hydrated cement paste and other pollutants. This fraction accounts for about 30% of the crushed EoL concrete, thus, it presents an environmental and economic burden because it has no practical use. Further treatments are necessary to entirely separate the hydrated cement paste from the sandy fraction, among which thermal treatment methods took the upper hand in recycling the fine fraction [4][5]. Consequently, efforts are undergoing to turn the fine fraction of recycled aggregates into clean fine fraction by separating the adhered cement either by further crushing or by thermally activating the hydrated cement paste.

According to Shui et al [4], when recycled fine aggregates (RFA) and hydrated cement paste (HCP) recovered from EoL concrete is subject to heating up to 800 ˚C, it has the ability to dehydrate and improve its binding capability. The addition of cementitious materials such as fly ash further increases the density of hydration products and thereby the mechanical property of mortar made of recycled fine fraction.

Recycled fine aggregates (RFA), are usually least favoured for concrete applications. The detrimental factors that influence the use of recycled fine aggregates are the amount of adhered cement paste, their angular shape and their high water of absorption. These properties greatly influence the strength and durability of the recycled concrete adversely. In order to offset such weaknesses, different methods have been used to enhance the performance of recycled aggregates. Xuan et.al [6] has examined of recycled aggregates by treating with $CO_2$ during curing and found greater beneficial impact on the durability of recycled aggregates. Cartuxo et al [7] also suggested the use of superplasticizers to improve the workability, porosity and also found an increase in compressive strength of concrete made of recycled fine aggregates. It was also indicated that the use of mineral admixtures such as fly ash along with recycled fine aggregates would improve the workability and strength of recycled concrete [4]. Recycled fine aggregates which are produced by thermal attrition unit are believed to have less cement paste attached to the surface and are expected to display better property in a concrete mix. Since the ultrafine fraction is rich in hydrated cement paste, it can be used for several purposes. For instance, as a raw meal for the production of low carbon clinker [5], as supplementary cementitious materials or as additives in concrete.

## 4.3.  Extended methodology

The HAS setup is complementary to the ADR technology. The input material for the HAS technology is a mix of the airknife product (1-4mm) and the rotor product (0-1mm) that comes from ADR. The HAS technology, which is the preceding design of thermal attrition unit, is designed to further expose the fine fraction aggregates into a hot gas so as to dry the fine aggregates and to get rid of undesirable tiny CDW contaminants, mainly wood and plastic shards. The entire process involves the interaction of particle-gas system in a fluidized-type reactor, where air is used to carry the heat and at the same time classify fine aggregates based on their particle size. The use of heating is to dry the material and somehow activate the ultrafine particles which are mainly composed of hydrated cement. The contact between the hot air and the aggregates is maximized at the cascade of tubes which are embedded in the vertical structure of the HAS setup. Cascades are positioned at the upper and lower section of the HAS. The use of cascades is twofold: first to facilitate an efficient heat and mass transfer between aggregates and the hot gas, and second, to enable the spalling of aggregates while jumping from cascade to cascade after being exposed to higher temperatures.  While the ultrafine particles are swept up by the air flow and get collected in the cyclone, the heavier particles settle down into the bin of the HAS where the clean fine fraction is collected. A sketch of the thermal attrition unit is shown in Figure 15.
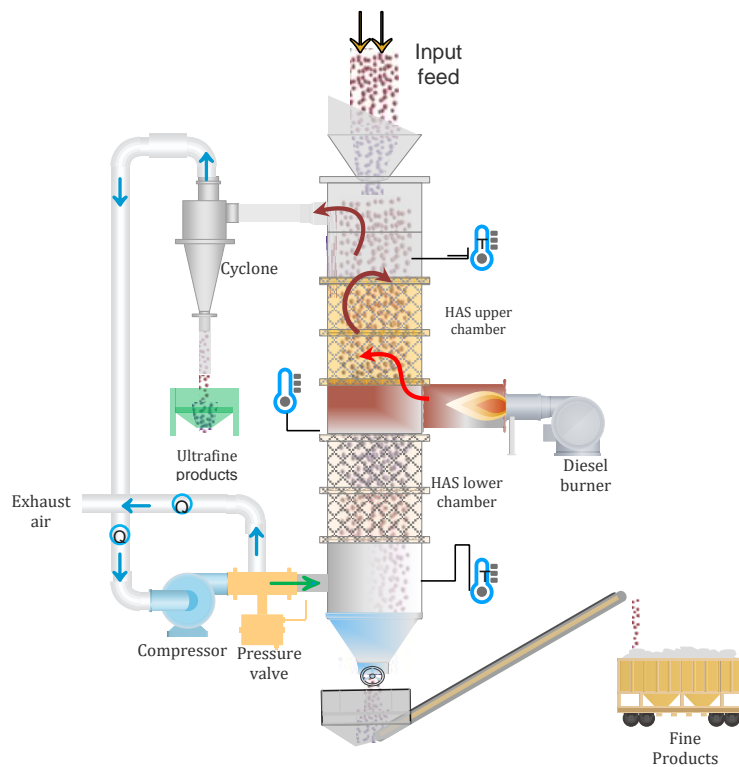
Figure 15: A sketch of thermal attrition unit

The system is made of several components such as the burner, vibrator motors, compressor, cyclone and rotary sluice. The burner uses diesel to generate hot gas at temperatures up to 600 ˚C. This heat is dragged into the system to dry the fine aggregates. The compressor is used to draw air, circulate the warm air from the cyclone and blow part of the vapor saturated air into the atmosphere. Vibrators are used to ensure the down flow of fine aggregates through the staggered arrangement of tubes inside the HAS chamber. The Cyclone is a vortex separation system used to separate the ultrafine particles (extracted from the feed) from the air stream. While the solid particles hit the wall of cyclone and decelerate to fall into the base, the warm air will pass upwards to the recirculation. A patent has been filed for the technology and for the method of recycling cement paste from EoL concrete waste by TU Delft.

The classification of the particles occurs in the separation zone, where the particles interact with the air flow [8]. There are four basic separation zones in most of the air classification systems. These are: gravitational-counter flow, gravitational-crossflow, centrifugal-counter flow and centrifugal-crossflow zones. The HAS technology comprises the principles of gravitational-counter flow zone and centrifugal counter flow zone, where the classifier is designed around a rising airflow inside a vertical chamber. The aggregate particles fall from top of the chamber and the drag force acts in the opposite direction to gravity. Consequently, classification occurs where the drag force is larger than gravity. Coarse particles will continue downwards while fines will be carried out by airflow,

where they are dominated by centrifugal counter flow zone inside the cyclone. The major drawback of this system may be the low separation efficiency because coarse particles may block fines from rising with the air stream.

Unlike conventional air classifiers, the unique feature in the technology is the presence of horizontally staggered tubes inside the vertical chamber. The function of these tubes is to increase the residence time of aggregates for efficient heat/mass transfer between wet fine aggregates and the hot gas. It is believed that the complex interaction between particle-particle, particle-heat, and particle-horizontal bars give rise to some important phenomena like spalling. The thermal stresses generated by rapid heating and the increase in pore pressures due to thermal shock contributes to spalling.

## 4.4.  Materials (source, sampling, preconditioning)

The input material used as an input for the thermal attrition unit is the fine fraction of crushed concrete. It is prepared by crushing End of life (EoL) concrete according to the following diagram shown in Figure 16. The fine products generated from ADR are the airknife (1-4mm) and the rotor fraction (0-1mm). Both products are mixed together and are used as a feed to the thermal attrition unit.
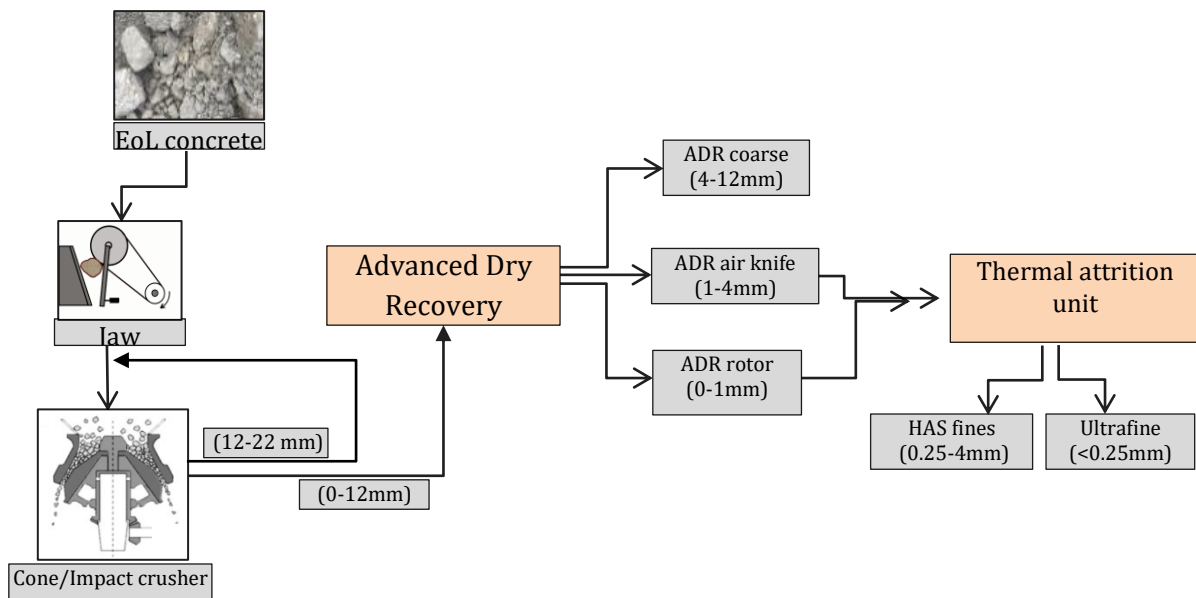


Figure 16: Input material preparation for the thermal attrition unit

## 4.5.  Activities in progress

As the main objective of this task is to design and optimize a biofuel based 20 t/h thermal attrition mobile unit for the production of higher quality recycled concrete fine fractions (0.25-4 mm) and ultrafine cementitious fractions (<0.25 mm), different guidelines were established to achieve the objectives. In one hand, the R&D is continually carried out to deliver basic design parameters; and on the

other hand, designing the unit has been launched side by side to the research based on the milestones shown in Table 6.

Several research activities have been carried out to optimize the property of recycled fines and recycled ultrafine powder. Based on optimum properties of the products, the process parameters are defined which are used an input to the design conditions. Some of the research activities carried out to lie a foundation on the basic understanding of the dominant phenomena when particles are thermally treated at about 600 °C. For such reason, the conditions inside the thermal attrition has been imitated to perform some experiments using the prototype HAS and using an oven. The objective of such experiments is to quantify spalling, to determine the residence time inside the thermal attrition unit and assess the effect of radiation on spalling. The input sample used throughout the experiment is EoL concrete processed by ADR. The fine fraction (0-4mm) is sieved into three distinct particle sizes (0.5-1mm, 1-2mm and 2-4mm) and are used for all experiments separately. The major activities are summarized as follows:

- Spalling plays a crucial role in recovering clean sand during recycling process. When particles are exposed to sudden heat, the temperature gradient at the surface and the centre of the particle gives a corresponding difference in thermal expansion and gives rise to internal stress, causing the material to disintegrate. This has been evidenced by the PSD analysis. At the same time, coarser particles (2-4mm) were observed to crack (split) when spalling suggesting an optimum residence time inside the thermal attrition unit.
- As the residence time inside the oven increases, spalling also increases. At the same time coarser gravel aggregates split. Thus, there should be a compromise in residence time. Accordingly, it should not surpass 35 seconds.
- Based on the experiments conducted, the amount of particles generated by spalling is higher for the experiments conducted in Hoorn (prototype thermal attrition unit) compared to oven experiments (where particles are exposed to only radiation). This could be due to the influence of multiple factors such as convection, radiation, bouncing, and soon.  Although the contribution of radiation in spalling is significant.
- Milling HAS processed fines clearly showed an impact on the recovery of CaO from the particle surface. Milling the heat treated particles displayed almost similar PSD as in acid dissolution test (which is assumed as perfect spalling condition).
- The study covers particles with size 0.5-4mm. It does not include particles <0.5 mm in size. Since most of the cement paste is part of these products, this fraction will be studied in the future to quantify the recovery of hydrated cement powder.

## 4.6. Planning for the rest of the activities

The major activities and milestones are given in Table 6. There are several setbacks discovered in due process. Some to mention, the cost of thermal

attrition unit has been quoted beyond the budget set in ICEBERG and some IP related issues with the manufacturer of thermal attrition unit may delay the planned milestones.

Table 6: Milestones and activities planned

| Activity | september | october | november | december | january | february | march | april | may | June |
|---|---|---|---|---|---|---|---|---|---|---|
| Project initiation/kick-off | | | | | | | | | | |
| Progress meeting 1: October 6th | | | | | | | | | | |
| Additional testwork TUD with HAS Mockup | | | | | | | | | | |
| Program of Requirements HAS | | | | | | | | | | |
| *Milestone 1: approve Program Requirements* | | | | | | | | | | |
| General Arrangement Drawings FH Crone | | | | | | | | | | |
| Progress Meeting 2: November 3rd | | | | | | | | | | |
| *Milestone 2: approve General Arrangement Drawings* | | | | | | | | | | |
| Detailed Design FH Crone | | | | | | | | | | |
| Progress Meeting 3: december 1st | | | | | | | | | | |
| *Milestone 3: approve detailed design* | | | | | | | | | | |
| Technical and structural drawings en list of external parts | | | | | | | | | | |
| Progress Meeting 4: December 29th | | | | | | | | | | |
| Progress Meeting 6: February | | | | | | | | | | |
| *Milestone 4: approve technical and structural drawings* | | | | | | | | | | |
| Order long lead items | | | | | | | | | | |
| Manufacturing of frames and HAS body | | | | | | | | | | |
| Assembly | | | | | | | | | | |
| Progress meeting 5: March | | | | | | | | | | |
| **Milestone 5: Factory Acceptance Test** | | | | | | | | | | |
| Clear Punch item list | | | | | | | | | | |
| Commissioning of HAS onsite (Hoorn) | | | | | | | | | | |
| **Milestone 6: Site Acceptance Test** | | | | | | | | | | |
| Clear Punch item list | | | | | | | | | | |
| Project ICEBERG / VW | | | | | | | | | | |

## 4.7. Preliminary conclusions

The input parameters that are crucial for designing the modular 20 t/h thermal attrition unit has been identified and known. The parameters such as residence time, temperature and airflow, will be implemented in the design of thermal unit. When the right process conditions are implemented, the thermal attrition unit not only does dry and separate the feed into clean recycled sand and hydrated cement rich powder but also glued particles spall to increase the recovery of clean sand. Besides, thermally treated particles also seem to be crackled, thus soft milling may help to loosen such particles.

## 4.8. References

[1]    F. Krausmann, D. Wiedenhofer, C. Lauk, W. Haas, H. Tanikawa, T. Fishman, A. Miatto, H. Schandl, H. Haberl, Global socioeconomic material stocks rise 23-fold over the 20th century and require half of annual resource use, Proc. Natl. Acad. Sci. U. S. A. 114 (2017) 1880–1885. https://doi.org/10.1073/pnas.1613773114.

[2]    A. Torres, J. Brandt, K. Lear, J. Liu, A looming tragedy of the sand commons, Science (80-. ). 357 (2017) 970–971. https://doi.org/10.1126/science.aao0503.

[3]    United Nations Environment Programme, Sand, rarer than one thinks, Environ. Dev. 11 (2014) 208–218. https://doi.org/10.1016/j.envdev.2014.04.001.

[4]    Z. Shui, D. Xuan, H. Wan, B. Cao, Rehydration reactivity of recycled mortar from concrete waste experienced to thermal treatment, Constr. Build. Mater. 22 (2008) 1723–1729. https://doi.org/10.1016/j.conbuildmat.2007.05.012.

[5]    D. Gastaldi, F. Canonico, L. Capelli, L. Buzzi, E. Boccaleri, S. Irico, An

investigation on the recycling of hydrated cement from concrete demolition waste, Cem. Concr. Compos. 61 (2015) 29–35. https://doi.org/10.1016/j.cemconcomp.2015.04.010.

[6]  D. Xuan, B. Zhan, C.S. Poon, Durability of recycled aggregate concrete prepared with carbonated recycled concrete aggregates, Cem. Concr. Compos. 84 (2017) 214–221. https://doi.org/10.1016/j.cemconcomp.2017.09.015.

[7]  F. Cartuxo, J. De Brito, L. Evangelista, J.R. Jiménez, E.F. Ledesma, Increased durability of concrete made with fine recycled concrete aggregates using superplasticizers, Materials (Basel). 9 (2016). https://doi.org/10.3390/ma9020098.

[8]  M. Shapiro, V. Galperin, Air classification of solid particles: A review, Chem. Eng. Process. Process Intensif. 44 (2005) 279–285. https://doi.org/10.1016/j.cep.2004.02.022.

## 5. Upgraded industry-scale LIBS-based quality assessment system

### 5.1. Description of the problem

To close the loop of concrete waste and to implement a circular economy, the value in materials/products must be retained as long as possible. To achieve this, innovative recycling technologies that can separate concrete waste into its various components (e.g., aggregates and minerals) play a crucial role, but they are not enough to bring the recycled materials (secondary raw materials) on the market. The replacement of virgin aggregates is hampered because the industry is hesitant to replace primary with secondary raw materials. Therefore, to effectively achieve circularity, it is also necessary to make sure that the product satisfies the industry's needs by measuring the quality and by explicitly displaying the quality of the products (recycled aggregates).

Recycled concrete differs from primary concrete in that:

• It is made from source materials (End-of-Life concrete) with a high variability: each concrete element of a building (wall, façade, foundation, etc.) is made from a different concrete recipe;

• The supply chain from source to final concrete product involves more different parties.

This means that special technological and organizational instruments are needed to guarantee that recycled concrete, despite these problems, has the same quality as primary concrete.

### 5.2. State of the art/technology

To remove this bottleneck, TUDelft designed and is developing a system/process (patented) through which the quality of the aggregate can be assessed and then traced throughout the value chain using RFID tags.

The system is made of an in-line Laser-Induced Breakdown Spectroscopy (LIBS) based online sensor system that can continuously measure and control the quality and homogeneity of the aggregates produced by the ADR (5000-10000 chemometric analyses per ton) (see Figure 17).
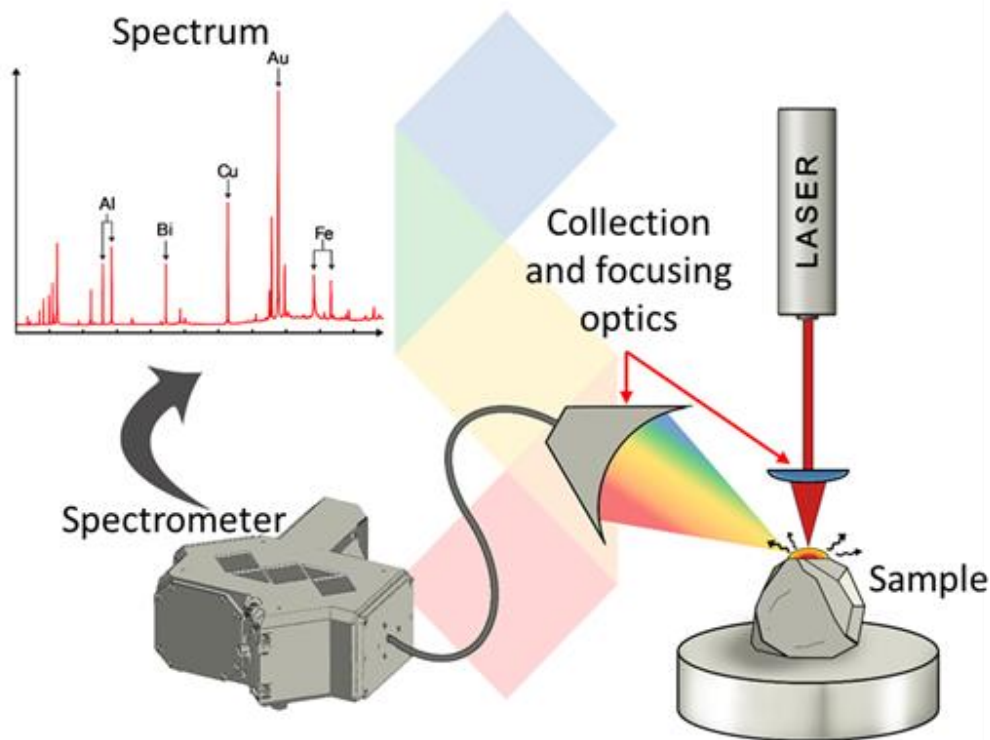
Figure 17: Schematic of a LIBS system and an example of the spectrum.

The LIBS-based equipment is coupled with contactless identification and tracking system based on RFID sensors as well as with the CTP. The tags store the information about quality received from the LIBS system and link it with the larger cloud databases. Each separate fraction of the product holds a dedicated information carrier, which contains the information of the fraction being assessed by the LIBS-based system. The dedicated RFID information carriers are easily noticeable by cost-effective RFID readers, and their presence can thus be established even if the tags are not visible and embedded in the recycled or final product (see Figure 18).



Figure 18. The RFID reader and writer system (left). RFID embedded in concrete (right).

## 5.3. Extended methodology

In order to implement the process schematically presented in the below figure (Figure 19), a lab facility is being arranged at the TUD recycling laboratory.
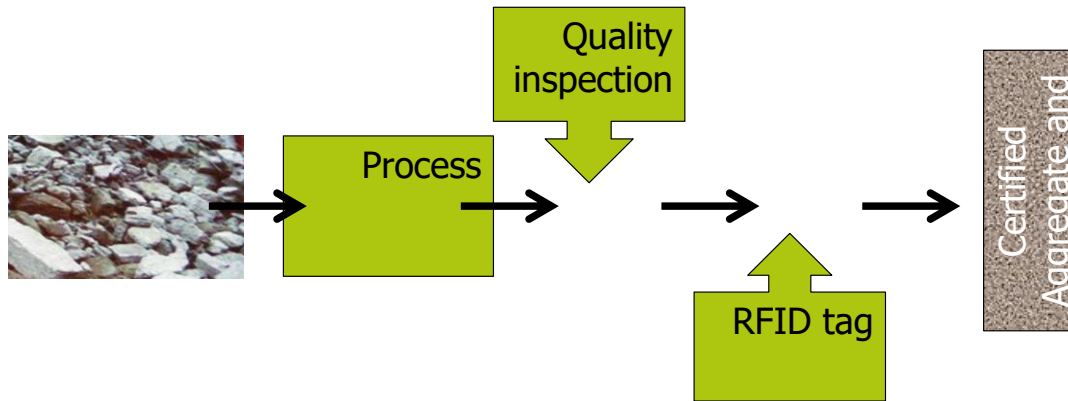


Figure 19. Quality assessment and monitoring system.

Figure 20 shows the LIBS quality assessment facility. The facility has been used to acquire the spectra of the most common pollutants which are usually present in end-of-life (EoL) concrete.
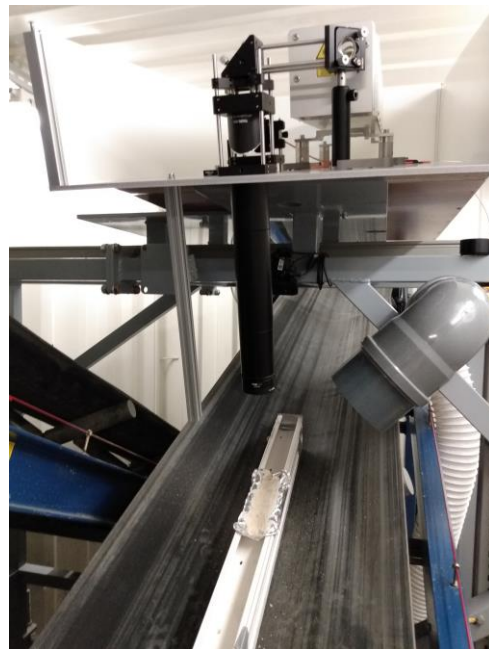


Figure 20. LIBS based quality assessment facility

The acquired spectra will be used in combination with the spectra of the EoL concrete, to facilitate the identification of pollutants in the produced aggregates.

## 5.4.   Materials (source, sampling, preconditioning)

Figure 21 shows an example of the samples for spectra acquisition (top) and an
example of spectra acquired (bottom). The target of the ongoing analysis of the
spectra is to obtain an estimation of the presence of contaminants like wood,
gypsum, glass, etc.
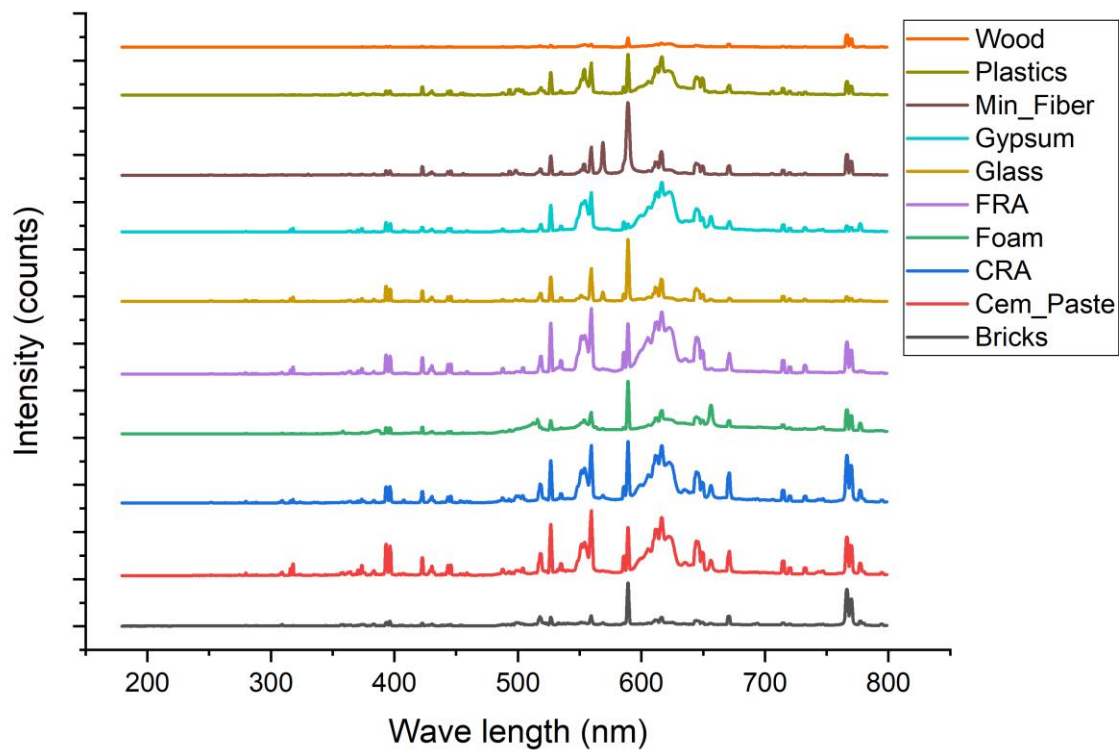


Figure 21. Sample for LIBS analysis (top). Spectra acquired (bottom).

## 5.5. Activities in progress

To obtain a reliable outcome from the LIBS quality assessment measures, it is important to properly direct the laser beam on the materials' heap transported by the conveyor belts (Figure 22).
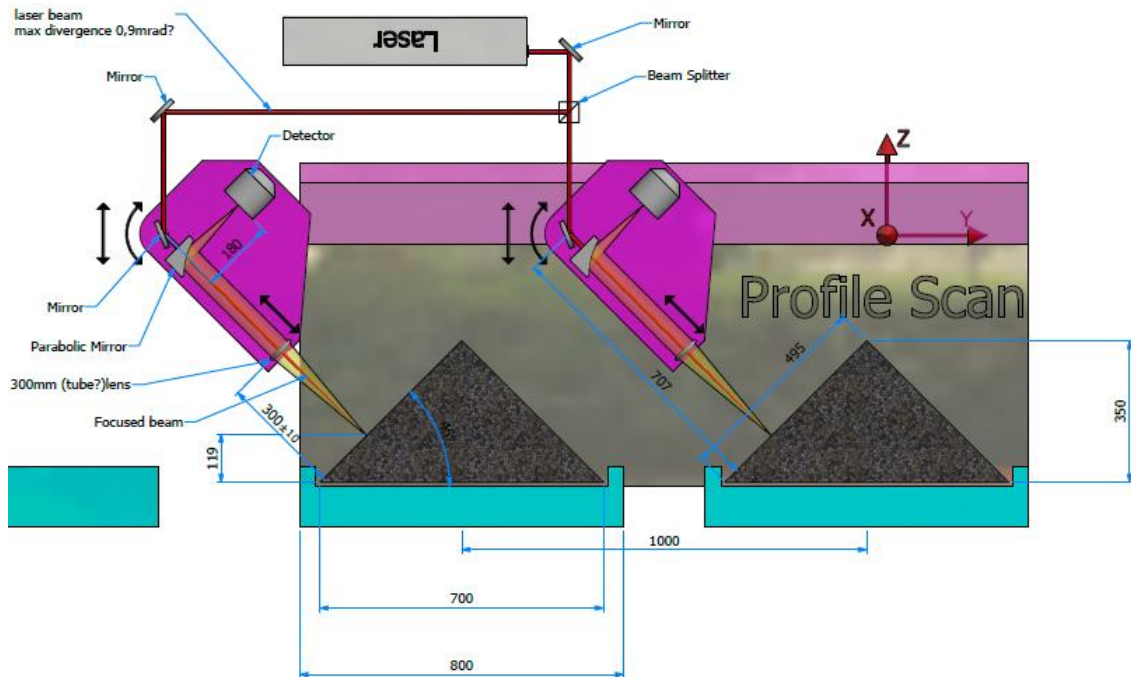


Figure 22. LIBS positioning.

Therefore, experiments are being carried out to find out what is the shape and representative particle size (at a specific position) of the heap transported by a conveyor belt. Below a description of the experiments follows:

Experiments design:

Experimental tests are designed based on the following criteria:

- Feeding rate: 0.8 - 1.2 kg/s
- Conveyor speed: 2.5 - 5 cm/s
- Bulk density of recycled coarse aggregates (4-12mm): 1.23 kg/l
- Bulk density of recycled fine aggregates (0.25-4mm): 1.28 kg/l

All tests are carried out by simulating a conveyor belt (by moving a plastic flat surface placed on a table) where a transparent glass dissects across the direction of flow. The shape of the heap is observed by looking through the transparent glass placed at the conveyor surface. The feeder is placed at a right angle to the conveyor's direction. Figure 23 shows the experimental setup for the experiment.
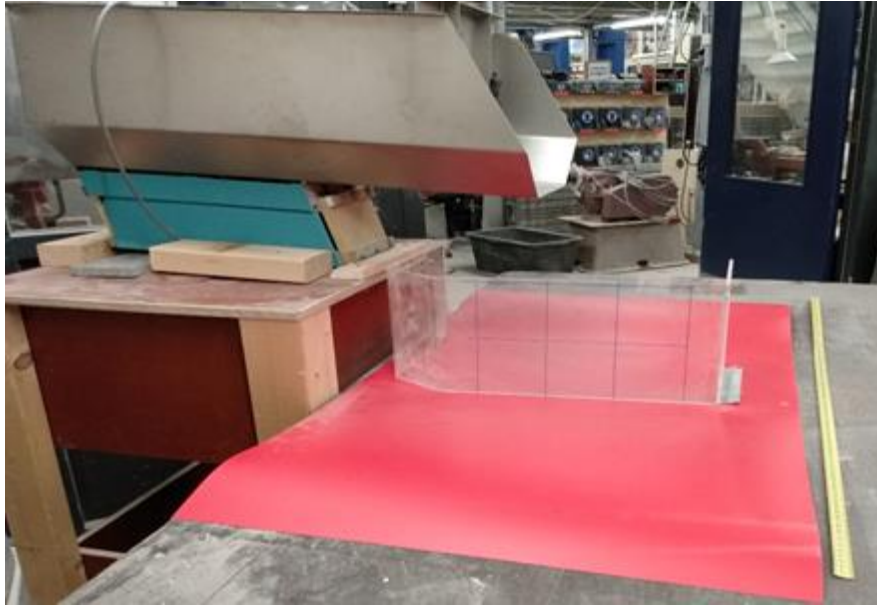
Figure 23. Heap experimental setup.

Measurements:

Figure 24 below shows the shape of the heap for both fine and coarse aggregates. As shown on the glass surface, the square dimensions shown on the glass surface are 10 cm by 10 cm. Thus, for fine aggregates, the height of the peak varies from 8 cm – 12 cm; and the bottom width varies 25 cm – 40 cm.  For the coarse aggregates, the height varies from 14 cm – 20 cm and the bottom width varies 40 cm – 50 cm. The heap shape and profile are shown in Figure 24 and Figure 25.

Figure 24. The heap shape for aggregates of different size (Left: Fine fraction and Right: coarse fraction).



Figure 25. Side view of the heap profile for coarse fraction aggregates.

The design of the LIBS-RFID quality assessment system is ongoing. To make a transportable system, a few options are being considered. Figure 26 below shows one of the options being studied where two conveyor belts (one for the coarse and one for the sand) are installed on the movable container.
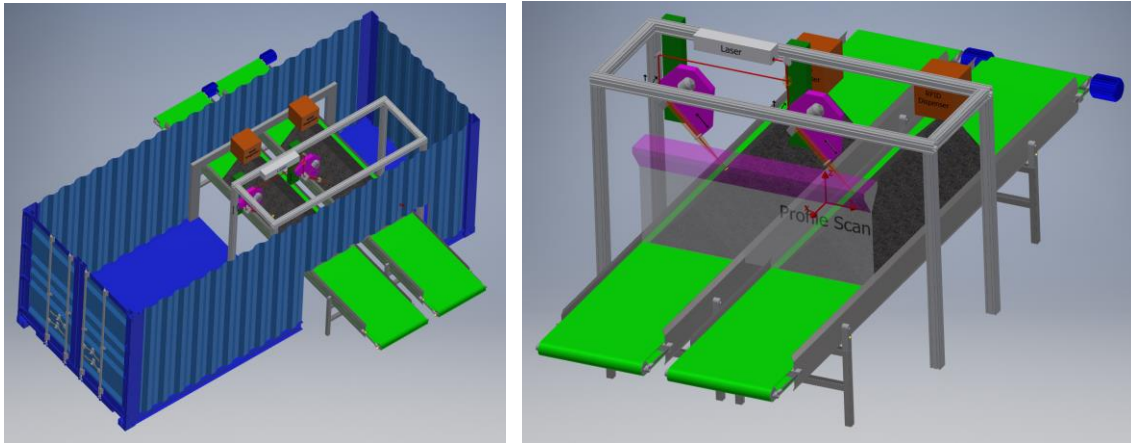


Figure 26. Conceptual LIBS-RFID system design.

The benefits and disadvantages of this layout are being investigated. For example, the easy placement on location over existing conveyor belts and accessibility of equipment on the conveyor belt against the weakening of the structural integrity of the container due to the large openings in the container (1.2 x 2.2 m).

RFID Dispenser Concept

To store the composition of the sampled materials, an RFID tag will be used. Data obtained from LIBS will be matched with the number (tag) stored on the RFID chip, creating an accessible database. The design and operation of the writing and reading and tagging procedure must be very robust and have a low failure rate. The RFID dispenser will consist of a few parts. The tags need to be stored and probably sorted. The tags need to be dispensed every 1 ton of material. Since there are two conveyers, it would be advisable to have two separate readers. One reader will scan the 0-4 mm aggregate conveyer tags and the other reader will scan the 4-12 mm aggregate conveyer tags. Using this configuration all the data coming from the readers will correspond with the matching conveyer. Reader A will only be transmitting tags from the 0-4 mm conveyer and reader B will only be transmitting tags from the 4-12 mm conveyer. Missing a scan or read will only result in an empty read, but there will not be a mix-up.

RFID cartridge

Using a linear
actuator, each tag is
pushed out of a
cartridge

RFID Development
board

RFID
Antenna

PVC hollow tube

Rotated clockwise &
anticlockwise with
the help of a servo
motor to drop the tag
in the concrete heaps

PVC hollow tube

Heap 0-4mm

Heap 4-16
mm
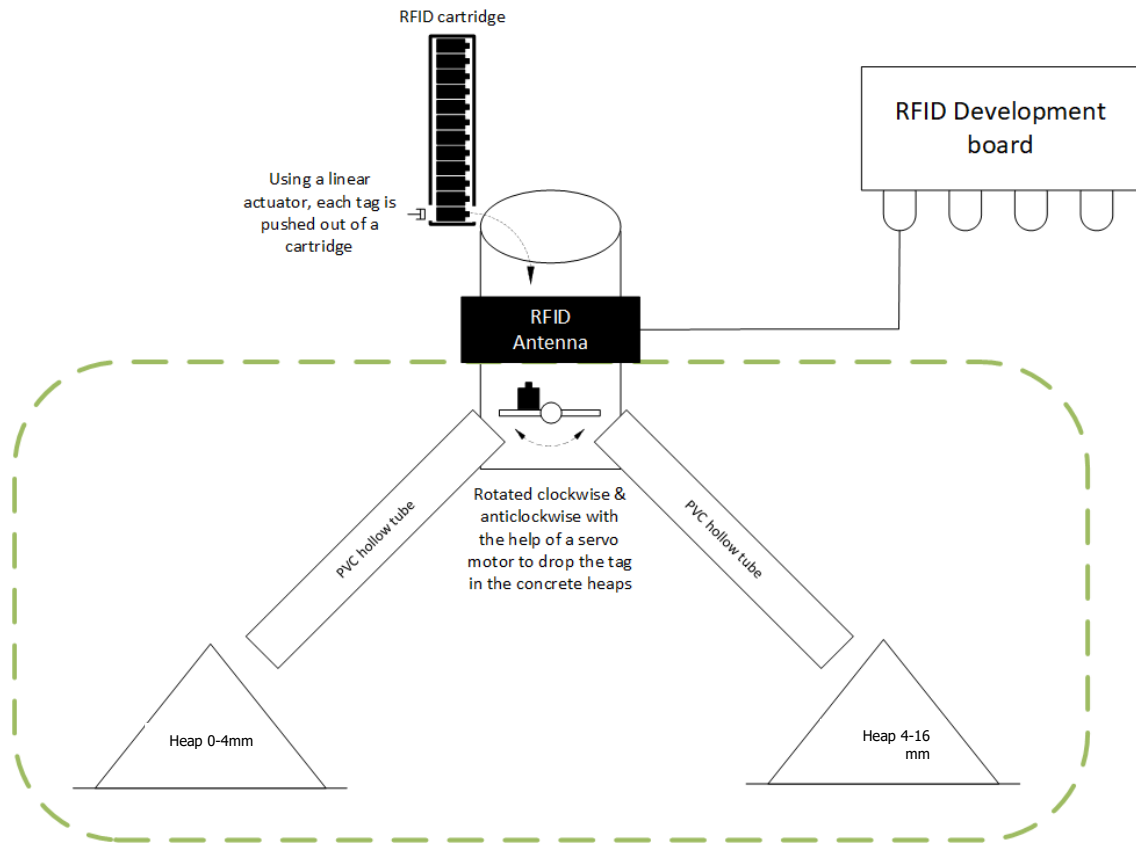
Figure 27. RFID dispenser concept.

Figure 27 describes the RFID dispenser concept, while Figure 28 shows the RFID
first prototype.
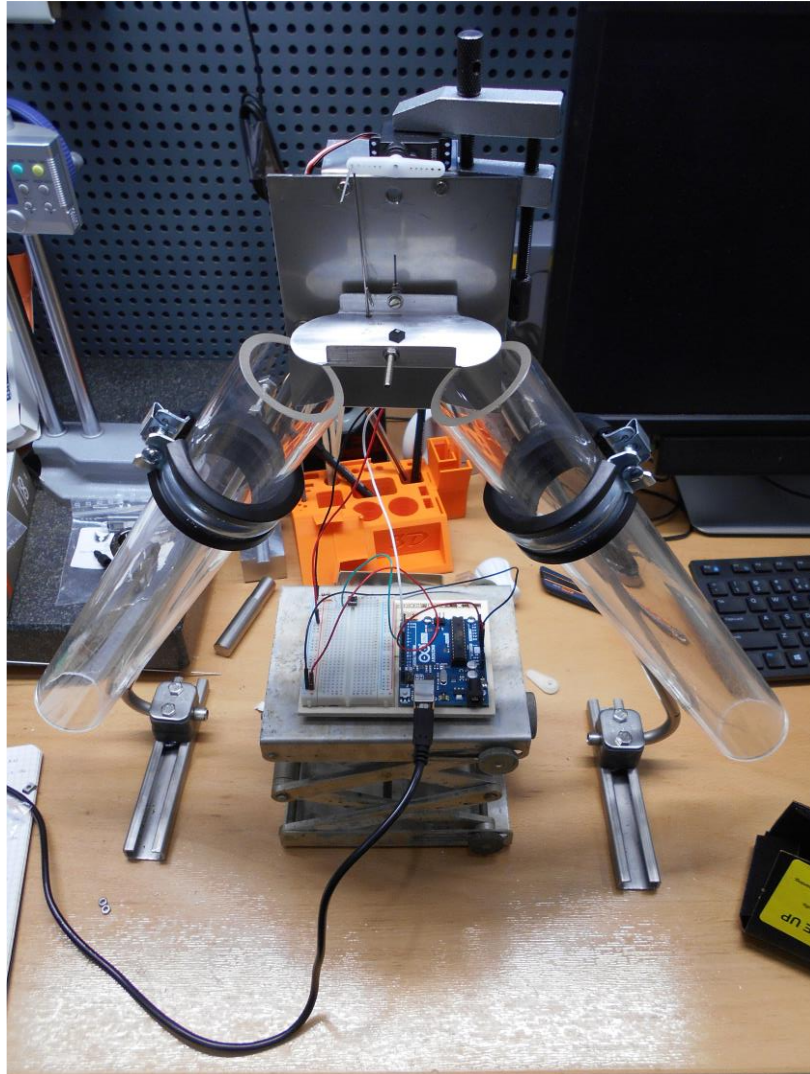
Figure 28. RFID first prototype.

## 5.6. Planning for the rest of the activities

TUD will complete the design of the transportable LIBS-RFID quality assessment facility. Then the first prototype will be built. These works include the design of the optics of the laser system which will work in combination with a Gocator to gain more information on the materials being analysed.

Concerning the RFID tags dispenser, the following activities will be considered:

1) As soon as the hardware design will be finalized, the communication protocol will be programmed for each of the devices;

2) Further control loop will be programmed integrating the entire process with all the hardware;

3) Graphical user interface will be built on top of it;

4) The database storage will be developed.

## 5.7. Preliminary conclusions

The results achieved so far show that the LIBS quality assessment system identifies the contaminants which affect the quality of EoL concrete. The spectra acquired reveal that the system is selective towards different materials.

The spectra measured with the spectrometers show some difference in the peaks. The optimum frequency of the laser is 100Hz. This means the measurements of the Avantes spectrometer were at the optimum laser operation conditions that ensure the highest output power of the laser. This may explain the more peaks present in the Avantes measurements. It should be noted that more peaks do not automatically imply better results. To conclude the results further analysis is required.

The study carried out with the transportable container show that it will be possible to enclose all equipment needed for the quality assessment and monitoring system within one standard container. This will facilitate transportation while reducing costs. The preliminary results on the RFID dispenser show that the RFID tags can be used as information carriers and that a suitable dispenser can be developed without major impacts on the EoL concrete recycling process.

# 6. Upcycling of concrete demolition waste using Accelerated Carbonation

## 6.1. Description of the problem

Currently, the main application for recycled CDW aggregates is as a base material for road construction or as (sub)foundation material. On the contrary, the building sector seldom uses recycled aggregates in high-grade products (e.g. concrete). Secondary materials constitute to about 3-4% of all the building materials used in Netherlands [1]. According to Mulders (2013) 92% of concrete was recovered in the Netherlands in 2012 [2]. However, only 20% of the recovered concrete was recycled in the concrete industry. The capacity of the road construction sector to absorb recycled aggregates as base materials is limited in mature infrastructure system. To ensure enough recovery options for the concrete fraction of CDW in the future, the development of increased high-value applications of C&D waste through innovation is necessary.

High-grade applications of CDW are defined by the incorporation in structural elements of buildings. Concrete accounts for about 42% of used construction materials, thereby reiterating the importance of high-grade concrete recycling [3]. In the standard EN 206, the replacement of natural aggregates (NA) by recycled coarse concrete aggregates is limited up to 30% for most concrete applications.

The main barriers for using recycled concrete aggregates (RCAs) are variability of composition of the RCA and a higher water absorption by RCA when compared to NA [4]. The variability in the composition of the RCA can be tackled by an improved value chain from demolition to new product. By keeping a high-quality concrete fraction separate during the demolition phase, and processing this high-quality concrete into high-grade concrete aggregates for new concrete products, the quality of the RCA is assured.

The increased water absorption of RCA can negatively impact the performance of the concrete mixture [5]. The higher water absorption of RCA will reduce the concrete workability and hence increase the water demand. However, increasing the water amount in the concrete mixture can have detrimental effects. The water/cement ratio (w/c ratio) of concrete is an important indicator of its strength and workability. Joseph et.al. (2015) reported a decrease of 5 GPa in elasticity modus of a concrete mixture for every 1% additional water content [6]. Experimental results show that the compressive strength decreases in a linear manner as a function of additional water added, with reductions around 10-25% of compressive strength [7] [8].

High water absorption is linked with the presence of old mortar attached to the recycled natural aggregates (De Juan et.al., 2009). A further factor are the air voids and capillary pores at the interfacial transition zone (ITZ) [9] [10]. Values of water absorption may be less than 1% for natural aggregates whereas for recycled aggregates, the values can be up to 10% [11].

The amount of water absorption is also influenced by the crushing and grinding process, generating recycled aggregates with varying amount of mortar paste attached to it [5]. De-attaching mortar paste from the NA will strongly decrease the water absorption of the RCA. In Chapter 3, we follow this approach.

## 6.2. State of the art/technology

In order to enable a more substantial high-grade application of RCA in concrete, researchers have proposed different methods to improve the water absorption and surface properties of RCA. Surface coating of RCA with a pozzolanic slurry (e.g. silica fume, fly ash) [12] [13], a polyvinyl alcohol (PVA) emulsion [14] and water glass [15] [16] have been explored in the past with satisfactory results. However, the pozzolanic materials are frequently used and/or wanted SCMs in the construction sector and water glass increases the risk of alkali-aggregate reactions [17]. Furthermore, polymer coating like PVA can even further reduce the compressive strength of the produced concrete. Shi et al. (2016) indicates that the polymer groups can make the cement paste hydrophobic, hindering the hydration of unhydrated cement [18].

Shi et al. (2016) reviewed different RCA treatment techniques reported in literature [18]. The authors stated that the carbonation method is an efficient, feasible and environmentally friendly method for enhancing the properties of RCA.

Carbonation of RCA is gaining more attention among researchers because of its positive influence on the physical and mechanical properties of the aggregate, ease of application, and environmental implications [19] [20]. Furthermore, mineral carbonation routes are a way to utilize captured $CO_2$ and store it for a long period of time.

In the research by Li et al. (2017) where replacement of aggregates with non-carbonated RCA was found to cause ~13% drop in strength, similar concrete mixtures with carbonated RCA showed no drop in strength compared to the reference mixture [21]. The authors applied carbonation on air-dried RCA under 100% $CO_2$ concentration at ambient pressure for 7 days. Zhang et al. (2015) also reported comparable compressive strength results for the reference concrete mixtures and the mixtures incorporating carbonated RCA ($CO_2$ concentration of 20% for 7 days), while that of the non-carbonated RCA was 8–15% less than the reference [17].

The calcium- and magnesium-bearing hydration products (portlandite, C–S–H, ettringite and AFm phases) in the hardened cement paste are prone to carbonation and can form stable phases like calcite or dolomite. In the case of portlandite, carbonation leads to an 11–12% increase in solid volume [22]. This can be correlated to a decrease in the porosity of the old cement matrix, an enhancement in the ITZ and an increase in the mechanical strength of the RCA [20] [23]. On the other hand, carbonation of C–S–H is a complex process with implications to the porosity which are still subject to debate [24]. Some researchers are convinced that carbonation of C–S–H leads to 23% increase in volume and contributes to reduction in water absorption [20] [18] while others refrain from reiterating such value or the perceived increase in volume as a whole [25]. Nonetheless, the carbonation of ettringite entails as much as 50% volumetric shrinkage as a result of full carbonation. As such, care should be taken when choosing the carbonation conditions to maximize the reduction in RCA porosity.

A number of factors during the carbonation process seem to affect the porosity of carbonated RCA. The $CO_2$ concentration, gas pressure, ambient temperature and relative humidity, carbonation time, and aggregate moisture condition appear to be the governing carbonation factors. However, most of the existing literature lends itself to the investigation of carbonation under ambient or close to ambient atmospheric pressures. Zhan et al. (2014) reported a 16.7% drop in water absorption of coarse RCA after exposure to accelerated carbonation settings in very low relative humidity conditions obtained by the presence of silica gel (10 kPa $CO_2$ pressure, and an ambient temperature of 23 °C) [23]. Zhang et al. (2015) reported a 23–28% water absorption drop after carbonating aggregates at 20 °C, 60% RH and 20% $CO_2$ concentration (results varied depending on aggregate type) [17]. The duration of the carbonation reaction in these experiments was not reported.

Considerable improvements in the mechanical properties of RCA (e.g., aggregate crushing value, impact value and Los Angeles abrasion value) as a result of carbonation have also been reported [22] [26]. The research by Shi et al. (2016) suggests that if the $CO_2$ pressure exceeds 0.5 MPa (~5 bars), the further strength development of carbonation products will be insignificant [18]. The authors suggested that this is probably because the performance enhancement obtained through carbonation of portlandite is counteracted by the deterioration of other cement hydrates such as C–S–H. A similar conclusion is drawn by Fernandez Bertos et al. (2004) and pressures exceeding 5 bars were deemed impractical [24].

Research on the effect of carbonation temperature is particularly scarce as Kaliyavaradhan and Ling (2017) concluded in their review paper [27]. Fernandez Bertos et al. (2004) argue that while the $CO_2$ uptake increases with increase in temperature up to 60 °C, due to the exothermic nature of the carbonation reaction, increase in temperature promotes formation of meta-stable forms of calcite. The more stable forms of calcite will form at much lower temperatures (0-10 °C) [24]. However, since the carbonation reactions are exothermal, keeping these low temperatures in industrial set-ups might be challenging.

Moreover, carbonation is commonly reported to be the fastest when the relative humidity is 40–70% and most research on carbonation of RCA has been conducted at RH in this range [24] [25] [28]. It appears that the suitable chamber RH is dependent upon aggregate moisture conditions as well, which has been mostly overlooked in the past. As such, finding the optimal carbonation conditions requires further research.

The main objective of this research is to optimize the accelerated carbonation process of coarse RCA in ambient pressure conditions, since a carbonation process at ambient pressure conditions is considered to be more easily to upscale according to the industrial partners. Carbonation conditions (e.g. relative humidity, $CO_2$ concentration, temperature and carbonation time) will be investigated for different types of RCA (e.g. differences in cement type, cement amount, w/c ratio) to obtain robust carbonation conditions and allow upscaling to demonstration scale. In WP3, the carbonated RCA will be used for the production of RAC.

## 6.3. Extended methodology

Different carbonation conditions (e.g. $CO_2$ concentration, temperature, and carbonation time) are performed on samples of coarse RCA. The carbonated and uncarbonated RCA specimens are then tested for apparent particle density and saturated surface-dry density, water absorption and total carbon content.

A nylon tray containing 500 ml of a saturated NaBr solution is place inside the carbonation chamber to obtain a constant relative humidity of ±60%. Next, 0.5 kg of the coarse RCA sample is placed inside the reactor and the carbonation chamber is brought to the test temperature (this takes ±15 minutes). Carbonation is initiated by flushing a $CO_2/N_2$-gas mixture into the chamber for one hour. During this flushing step, the RH inside the carbonation chamber drops to 40% or less because of the constant inflow of a dry gas mixture. After one hour, the reactor is sealed. After the flushing step, the RH inside the reaction chamber increase back to around 60%, this takes approximately 30 minutes. The carbonation chamber is kept at atmospheric pressure. Consumed $CO_2$ in the reactor is refilled by a gas bottle containing 100% $CO_2$ to keep the $CO_2$ concentration constant.

Upon completion of the carbonation experiment, the gas inside the carbonation chamber is replaced by air, the samples are taken out and dried at 80 °C in a ventilated oven for 24 hours to remove all the water trapped or generated during carbonation. After drying, the specimens are stored airtight and dry (in the presence of silica gel). Temperature, $CO_2$ concentration and carbonation time are varied in the different experiments.

The RCA specimens are soaked in water for 24 h and tested for density and water absorption per EN 1097-6. In the same test, also the porosity of the specimens is assessed. It is prudent to bear in mind that there is no unified definition for cement porosity, and no existing test method can explore and characterize the entire pore size range of cement. For practical purposes, however, it can be argued that all the pores that can be filled with water in a 24 h period can be effectively considered as porosity. As such, the ratio of such pores volume to the total volume of grains (i.e., the sum of solid matter volume and pore volume) can be considered as the effective porosity. If this definition is valid, the apparent particle density and the oven-dried density values can be used to estimate the effective porosity. A closer look at the definitions of apparent particle density and oven-dry density in EN 1097-6 shows that the effective porosity of RCA can be easily obtained by dividing the two. After the water absorption test, the samples were again dried at 80 °C and stored airtight and dry.

The total carbon content of the specimen is measured on a milled subsample (particle size <100 μm) through IR spectrometry after incineration of the specimens according to EN 15936.

X-ray powder diffraction was carried out with a PANalytical Empyrean system, operated at 40 kV and 45 mA, with Co tube (fine focus, $\lambda$ = 1.7903 Å). Continuous scans with a step size rate of 0.013°/ 49.725 s were performed within a $2\theta$ range of 5°-120° (2D-detector) with a Bragg-BrentanoHD module. The obtained diffractograms were qualitatively analysed with the aid of HighScore Plus software (version 4.6a).

## 6.4. Materials (source, sampling, preconditioning)

The RCA that were used for the experiments were obtained by crushing laboratory-produced concrete samples. Two concrete samples were produced with the same basic composition but differing in the used cement type (Table 7). A water/cement (w/c) ratio of 0.5 was used after compensating for the water absorption of the used coarse and fine aggregates by prewetting them. Siliceous natural aggregates were used in the concrete mixture to allow for a clear differentiation between NA and the attached cement paste in the RCA with the different used analysis techniques (e.g. XRD, SEM). The samples were sealed and cured for 90 days.

After 90 days, the concrete samples were crushed with a laboratory-size jaw crusher to aggregates <20 mm. The produced aggregates were sieved at 8 mm to become a coarse RCA fraction of 8-20 mm. The coarse RCA are afterwards dried to constant mass at 80 °C and stored airtight and dry (in the presence of silica gel) to avoid carbonation.

The basic characteristics of the coarse RCA and NA are given in Table 8. The RCA show a significantly higher water absorption and lower particle density than the used NA.

Table 7. Composition of the used concrete samples (in kg/m³).

| Composition of the used concrete samples (kg/m³) | | | | |
|---|---|---|---|---|
| Sample | Siliceous gravel 4/16 | Siliceous sand 0/4 | CEM I 52.5 N | CEM III/A 42.5 N |
| Mixture 1 | 1020 | 720 | 340 | |
| Mixture 2 | 1020 | 720 | | 340 |

Table 8. Characteristics of the coarse RCA and NA.

| Characteristics of the coarse RCA and NA | | | |
|---|---|---|---|
| Sample | Oven-dried particle density (kg/m³) | Water absorption (%) | Total carbon (%) |
| Mixture 1 | 2.2 | 6.4 | 1.5 |
| Mixture 2 | 2.2 | 7.3 | 1.2 |
| NA, sample 1 | 2.5 | 3.5 | |
| NA, sample 2 | 2.6 | 2.7 | |

Before using the RCA in the carbonation experiments, the RCA are preconditioned in a climate chamber at 80% RH. The preconditioning step is to improve reproducibility of the experiments by starting with RCA samples with the same water content.

## 6.5.   Activities in progress
### 6.5.1. Experiments at 40 °C, 70% $CO_2$

Carbonation experiments were performed at 40 °C and a $CO_2$ concentration of 70%. The experiments varied in carbonation time (1, 2, 4, 6, 16, 24 and 30 hours). Figure 29 and Figure 30 show the main results for these carbonation experiments. Despite a high variability on the results, some trends are visible. This high variability has a few reasons: 1) there is already a variability on the natural siliceous aggregates, as can clearly be seen from the minimal and maximal water absorption that were measured on these aggregates; 2) not every RCA contains the same amount of attached mortar. More attached mortar means a higher water absorption value and a higher carbonation potential; 3) water absorption and total carbon values can differ for different particle size for the RCA. The particle size distribution of the used RCA samples (8-20 mm) can vary. Despite our effort to take representative subsamples using a sample splitter, some variation cannot be excluded.

The water absorption of the coarse RCA samples decreases with increased carbonation times (Figure 29) to reach a minimal value at around 24 hours of carbonation. At 24 hours, the RCA from mixture 1 (CEM I) show a decrease of 27% in water absorption to a water absorption value of 4.7%. At this time, the RCA from mixture 2 (CEM III/A) show a decrease of 28% in water absorption to a water absorption value of 5.3%.

For the RCA samples from mixture 1 (CEM I), the water absorption decrease clearly coincides with an increase in the total carbon content of the samples (Figure 30). For the RCA samples from mixture 2 (CEM III/A), this is trend is less clear because of a variation in the results. The current results are insufficient to draw a conclusion for the mixture 2 samples.
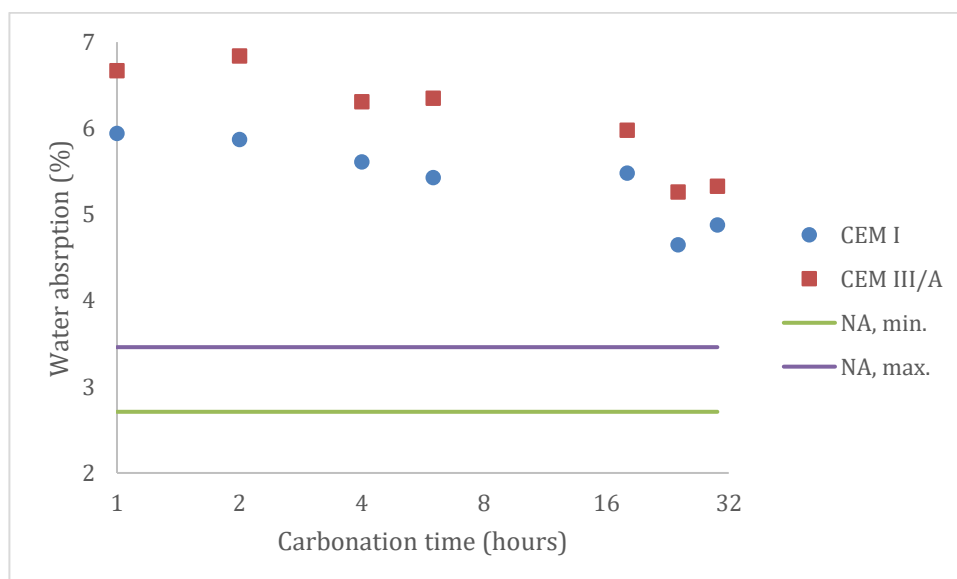


Figure 29. Water absorption values (%) of the RCA samples at different carbonation times.
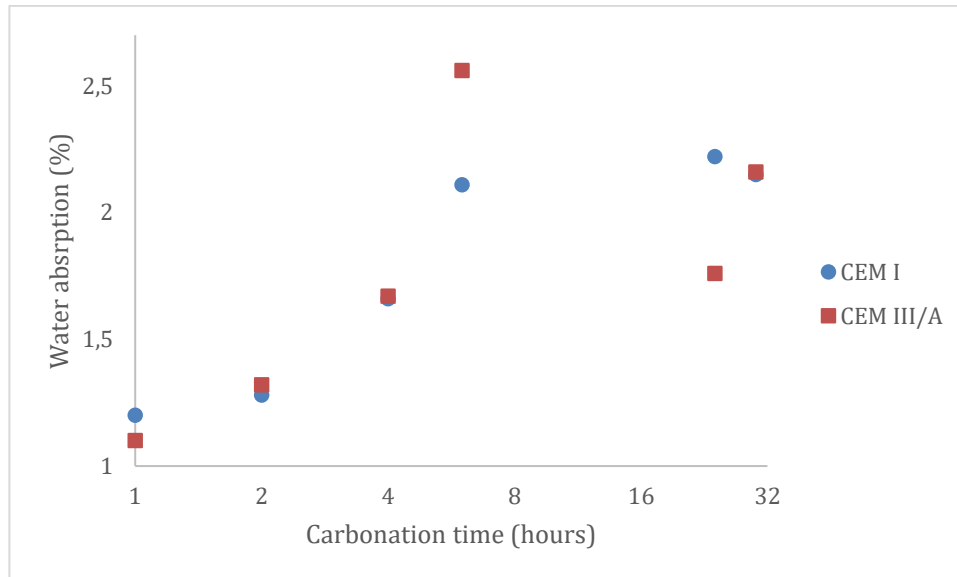
Figure 30. Total carbon content (%) of the RCA samples at different carbonation times.

The XRD diffractogram of the uncarbonated RCA samples is given in Figure 31. The diffractogram is predominated by a big quartz peak from the siliceous fine and coarse aggregates. The XRD results show very variable concentrations of cement phases, because of the high variability in the attached cement content for RCA. This makes it difficult to interpret the results. However, when the ratio of the concentration of portlandite ($Ca(OH)_2$, the major phase that can be carbonated) over the total concentration of carbonates (the sum of the concentration of calcite [$CaCO_3$], vaterite [$CaCO_3$], aragonite [$CaCO_3$] and dolomite[$CaMg(CO_3)_2$]) is plotted on a graph (Figure 32) after Rietveld analysis, a decreasing trend is visible. The initial portlandite content is higher in the RCA from mixture 1 (CEM I), which causes higher ratios.
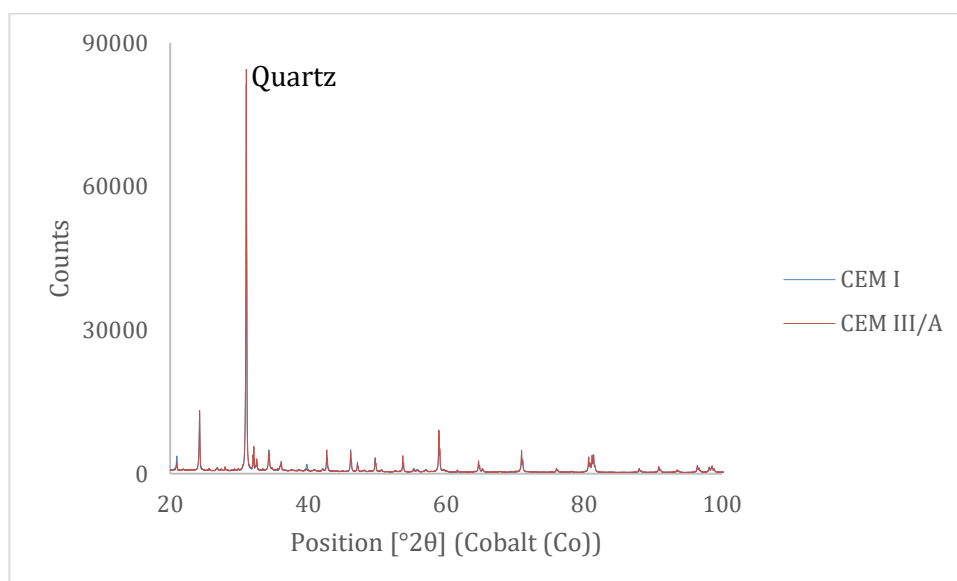


Figure 31. XRD of the uncarbonated RCA samples.
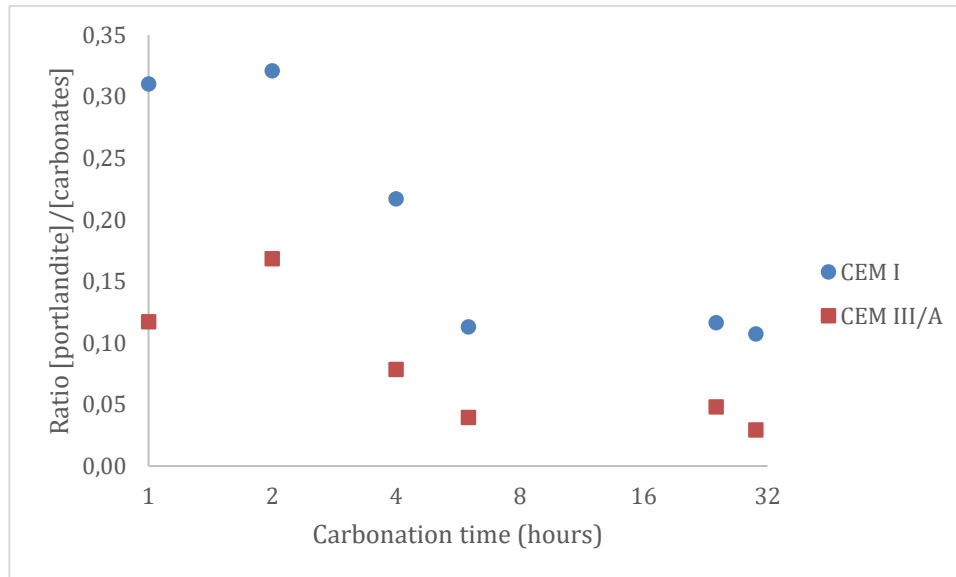
Figure 32. Ratio portlandite/carbonates of the RCA samples at different carbonation times. [Carbonates] =
[calcite] + [aragonite] + [vaterite] + [dolomite].

### 6.5.2. Experiments at higher temperatures or $CO_2$ concentrations

The water absorption values for the carbonated RCA samples from mixture 1
(CEM I) are given in Figure 31. An increase in the $CO_2$ concentration from 70%
to 100% does not show a significant effect on the water absorption of the treated
RCA. But an increase of the temperature in the carbonation chamber from 40 °C
to 60 °C does cause a bigger decrease in water absorption at shorter carbonation
times, with the maximum decrease already reached after 4 hours of carbonation.
An increase in temperature will facilitate the removal of excess water in the RCA.
This excess water is formed by the carbonation reaction (e.g. $Ca(OH)_2$ + $CO_2$ =>
$CaCO_3$ +$H_2O$). The excess water will slow down the diffusion of CO2 inside
the particle and can even leach out $Ca(OH)_2$ from the RCA [28], increasing
porosity.

This means that a faster effect in water absorption could also be obtained by
starting with dried RCA, as reported in literature. However, we chose not to start
from dried RCA because this would mean an extra drying step would have to be
added to the industrial process, increasing treatment costs of the RCA.

The total carbon content of the treated samples (Figure 32) shows a similar trend
as discussed before, with a higher carbon content for the RCA treated at 60 °C
for the shorter carbonation times. Although the RCA treated with 100% $CO_2$
do not show a lower water absorption then the RCA treated with 70% $CO_2$,
they do show a higher carbon content than the RCA treated with 70% $CO_2$ at
shorter carbonation times.
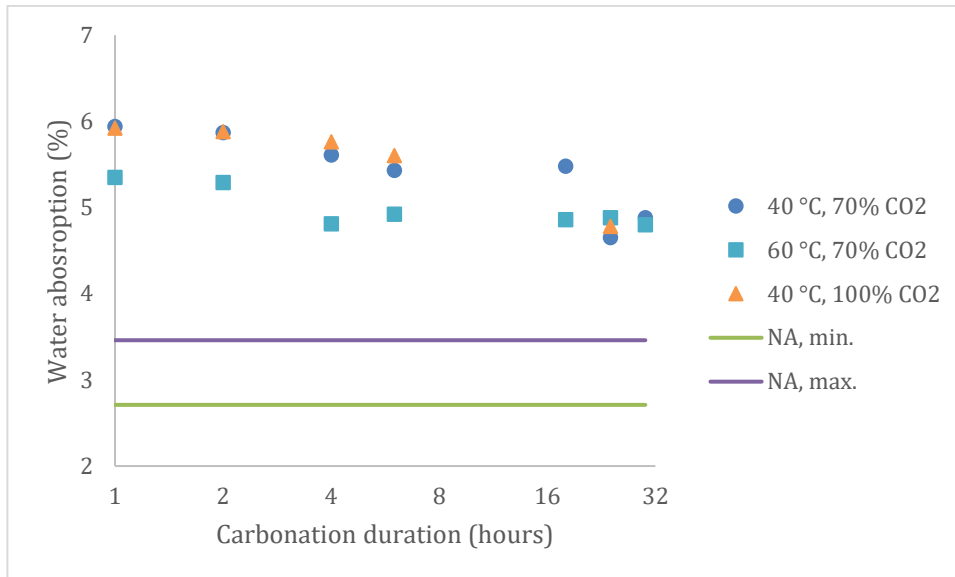
Figure 33. Water absorption values (%) of the RCA samples from mixture 1 (CEM I) at different carbonation conditions.
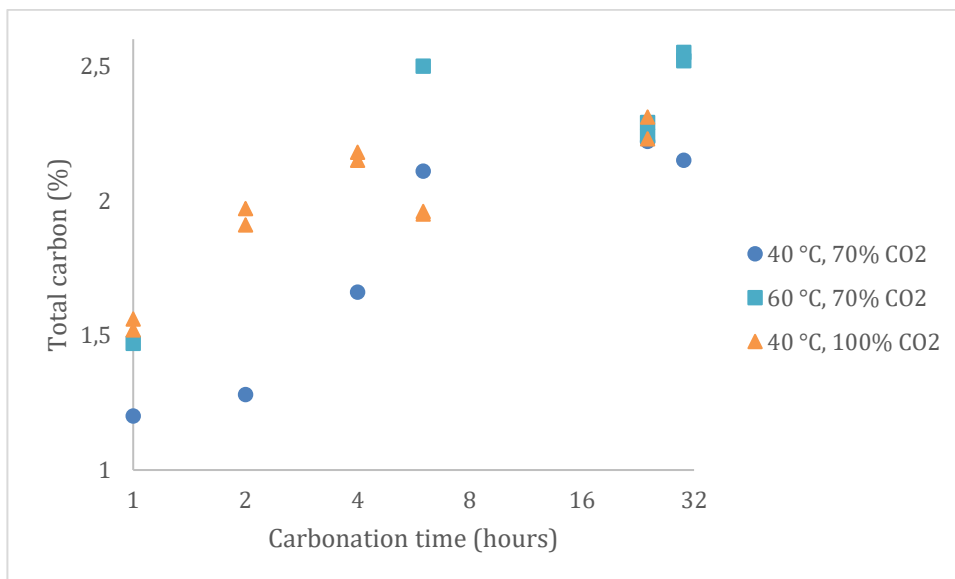


Figure 34. Total carbon content (%) of the RCA samples from mixture 1 (CEM I) at different carbonation conditions.

For the RCA from mixture 1, the ratio of the concentration of portlandite over the total concentration of carbonates in different carbonation conditions is plotted in Figure 35. A decreasing trend is visible as well for the other carbonation conditions. The ratio drops faster for the experiments at 60 °C.
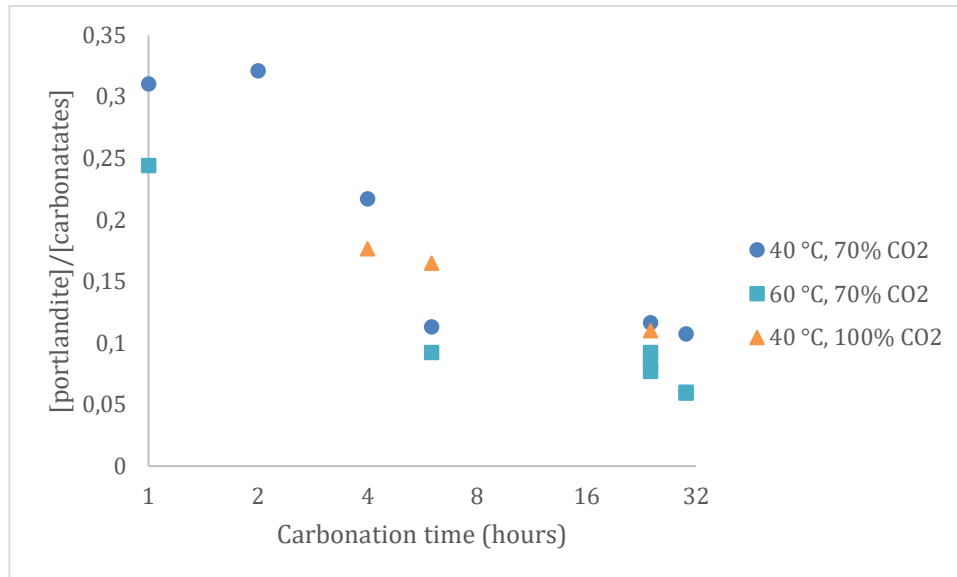
Figure 35. Ratio portlandite/carbonates of the RCA samples from mixture 1 (CEM I) at different carbonation times. [Carbonates] = [calcite] + [aragonite] + [vaterite] + [dolomite].

The water absorption values for the carbonated RCA samples from mixture 2 (CEM III/A) are given in Figure 36. The same conclusions can be drawn as for the RCA from mixture 1: 1) no significant effect from an increase of the $CO_2$ concentration from 70% to 100%; 2) increasing the temperature from 40 °C to 60 °C speeds up the carbonation process, with lower water absorption values at short times.

No conclusions can be drawn yet from the total carbon content of the treated samples from mixture 2 (CEM III/A) because of the big variability of the results. (Figure 37). Repeated experiments are needed to get a better view.
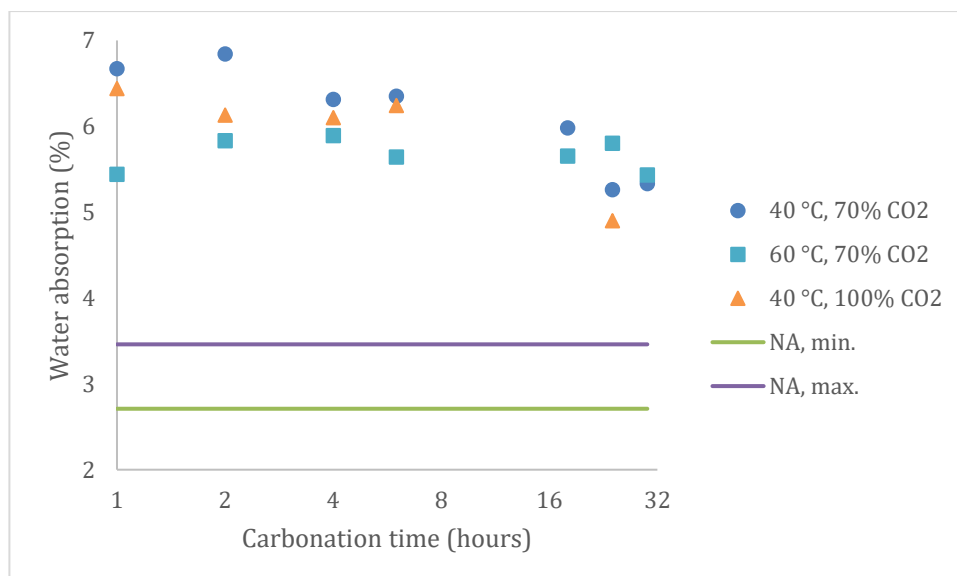


Figure 36. Water absorption values (%) of the RCA samples from mixture 2 (CEM III/A) at different carbonation conditions.
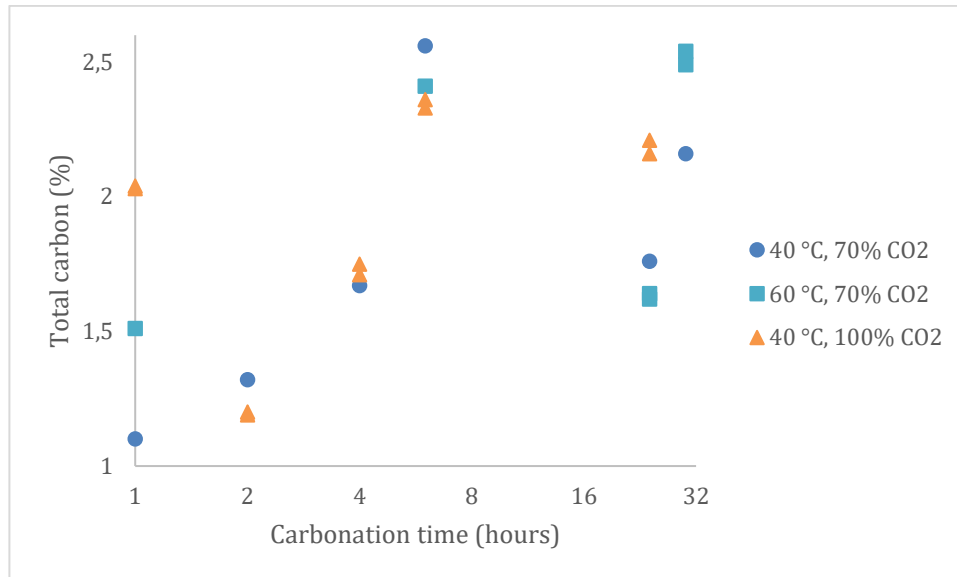
Figure 37. Total carbon content (%) of the RCA samples from mixture 2 (CEM III/A) at different carbonation conditions.

For the RCA from mixture 2, the ratio of the concentration of portlandite over the total concentration of carbonates in different carbonation conditions is plotted in Figure 38. A decreasing trend is visible as well for the other carbonation conditions. The ratio drops faster for the experiments at 60 °C.
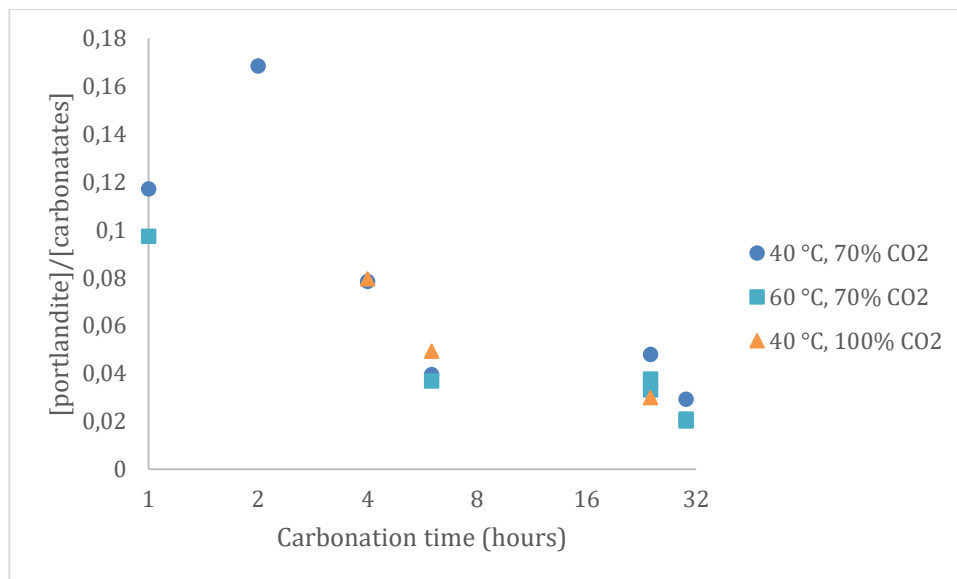


Figure 38. Ratio portlandite/carbonates of the RCA samples from mixture 2 (CEM III/A) at different carbonation times. [Carbonates] = [calcite] + [aragonite] + [vaterite] + [dolomite].

## 6.6.  Planning for the rest of the activities

We're currently focusing on repeating experiments for the experiments performed at 70% $CO_2$. These repeat experiments will focus at the time frame 6-24 hours for the experiments at 40 °C and on the time frame 4-24 hours for the experiments at 60 °C. This will allow to get a better view at trends and the optimal carbonation times for the targeted conditions.

Furthermore, ongoing analyses with x-ray diffraction (XRD) and scanning electron microscopy (SEM) will give a better insight in the type of mineral that are carbonated and on the carbonation depth of RCA. The carbonation depth will also be further investigated through phenolphthalein coloring.

After finding the optimal carbonation times for the experiments at 40 °C and 60 °C, experiments will be performed at 80 °C investigate if the process can be accelerated further by an increase in temperature. Experiments will also be performed at lower $CO_2$ concentrations to investigate the minimal amount of $CO_2$ concentration needed for an efficient carbonation. Lowering the required $CO_2$ concentration will significantly reduce the costs of the process. RCA from the optimized process will be tested on micro-deval and freeze-thaw resistance.

The optimized carbonation conditions will also be used for the carbonation of RCA from other concrete samples. These concrete samples have a higher cement content and a lower w/c ratio. This will give more information on the robustness of the carbonation process.

Afterwards, high-grade RCA obtained from commercial concrete recycling plants will be carbonated at the pilot facilities of Orbix. Concrete will be made containing different amounts of carbonated and non-carbonated RCA in WP3. These concrete samples will be tested with the purpose of obtaining a process for the production of concrete that can be used in the case study at Colruyt (WP4).

## 6.7.  Preliminary conclusions

A carbonation process at elevated temperature (60 °C) and a $CO_2$ concentration of 70% causes a decrease in the water absorption in the RCA of more than 20% after 4-6 hours carbonation. This way, water absorption values of less than 5% are obtained for the RCA samples of mixture 1. This shows that with a selective demolition process combined with an accelerated carbonation can lead to high-quality RCA. Further work in WP2 (optimization carbonation process) and WP3 (concrete formulations and testing) are needed to evaluate the maximal replacement rates with these RCA.

## 6.8. References

[1] E. Schut, M. Crielaard and M. Mesman, "Circular economy in the Dutch construction sector: A perspective for the market and government", Rijksinstituut voor Volksgezondheid en Milieu RIVM, 2016.

[2] L. Mulders, "High quality recycling of construction and demolition waste in The Netherlands", Utrecht University, 2013.

[3] P.-A. Enkvist and P. Klevnäs, "The circular economy - a powerful force for climate mitigation", Material Economics Sverige AB, 2018.

[4] R. Cardoso, R. Vasco Silva, J. de Brito and R. Dhir, "Use of recycled aggregates from construction and demolition waste in geotechnical applications: A literature review", *Waste Management,* vol. 49, pp. 131-145, 2016.

[5] M. Quattrone, B. Cazacliu, S. Angulo, E. Hamard and A. Cothenet, "Measuring the water absorption of recycled aggregates, what is the best practice for concrete production?", *Construction and Building Materials,* vol. 123, pp. 690-703, 2016.

[6] M. Joseph, L. Boehme, Z. Sierens and L. Vandewalle, "Water absorption variability of recycled concrete aggregates", *Magazine of Concrete Research,* vol. 67, no. 11, pp. 592-597, 2015.

[7] S. C. Kou, C. S. Poon and D. Chan, "Influence of Fly Ash as Cement Replacement on the Properties of Recycled Aggregate Concrete", *Journal of Materials in Civil Engineering,* vol. 19, no. 9, 2007.

[8] J. Li, J. Xiao and J. Huang, "Influence of recycled coarse aggregate replacement percentages on compressive strength of concrete", *Journal of Building Materials,* vol. 9, no. 3, pp. 297-301, 2006.

[9] P. M. Basheer, "Permeation Analysis", in *Handbook of Analytical Techniques in Concrete Science and Technology*, William Andrew Inc., 2001, pp. 658-737.

[10] L. Basheer, J. Kropp and D. J. Cleland, "Assessment of the durability of concrete from its permeation properties: a review", *Construction and Building Materials,* vol. 15, pp. 93-103, 2001.

[11] Z. Sierens, L. Vandewalle, M. Joseph and L. Boehme, "Water absorption variability of recycled concrete aggregates", *Magazine of Concrete Research,* vol. 67, no. 11, pp. 592-597, 2015.

[12] A. Katz, "Treatments for the Improvement of Recycled Aggregate", *Journal of Materials in Civil Engineering,* vol. 16, no. 6, 2004.

[13] D. Kong, T. Lei, J. Zheng, C. Ma, J. Jiang and J. Jiang, "Effect and mechanism of surface-coating pozzalanics materials around aggregate on

properties and ITZ microstructure of recycled aggregate concrete", *Construction and Building Materials,* vol. 24, no. 5, pp. 701-708, 2010.

[14] S. C. Kou and C. S. Poon, "Properties of concrete prepared with PVA-impregnated recycled concrete aggregates", *Cement and Concrete Composites,* vol. 32, no. 8, pp. 649-654, 2010.

[15] J. Li, H. Xiao and Y. Zhou, "Influence of coating recycled aggregate surface with pozzolanic powder on properties of recycled aggregate concrete", *Construction and Building Materials,* vol. 23, no. 3, pp. 1287-1291, 2009.

[16] L. X. Yang, Y. L. Qian, Q. Q. Fang and Y. T. Han, "Effects of Recycled Coarse Aggregate Reinforcing Treated by Water-Glass on the Performance of Recycled Concrete", in *Proceedings of the 3rd International Conference on Material Engineering and Application*, Hong Kong, 2016.

[17] J. Zhang, C. Shi, Y. Li and X. Pan, "Performance Enhancement of Recycled Concrete Aggregates through Carbonation", *Journal of Materials in Civil Engineering,* vol. 27, no. 11, 2015.

[18] C. Shi, Y. Li, J. Zhang, W. Li, L. Chong and Z. Xie, "Performance enhancement of recycled concrete aggregate – A review", *Journal of Cleaner Production,* vol. 112, no. 1, pp. 466-472, 2016.

[19] C. Liang, B. Pan, Z. Ma, Z. He and Z. Duan, "Utilization of $CO_2$ curing to enhance the properties of recycled aggregate and prepared concrete: A review", *Cement and Concrete Composites,* vol. 105, 2020.

[20] D. Xuan, B. Zhan and C. S. Poon, "Assessment of mechanical properties of concrete incorporating carbonated recycled concrete aggregates", *Cement and Concrete Composites,* vol. 65, pp. 67-74, 2016.

[21] L. Li, C. S. Poon, J. Xiao and D. Xuan, "Effect of carbonated recycled coarse aggregate on the dynamic compressive behavior of recycled aggregate concrete", *Construction and Building Materials,* vol. 151, pp. 52-62, 2017.

[22] J. Zhang, C. Shi, Y. Li, X. Pan, C. S. Poon and Z. Xie, "Influence of carbonated recycled concrete aggregate on properties of cement mortar", *Construction and Building Materials,* vol. 98, pp. 1-7, 2015.

[23] B. Zhan, C. S. Poon, Q. Liu, S. Kou and C. Shi, "Experimental study on $CO_2$ curing for enhancement of recycled aggregate properties", *Construction and Building Materials,* vol. 67, pp. 3-7, 2014.

[24] M. Fernandez Bertos, S. Simons, C. Hills and P. Carey, "A review of accelerated carbonation technology in the treatment of cement-based materials and sequestration of $CO_2$", *Journal of Hazardous Materials,* vol. 112, no. 3, pp. 193-205, 2004.

[25] A. Morandeau, M. Thiéry and P. Dangla, "Investigation of the carbonation mechanism of CH and C-S-H in terms of kinetics, microstructure changes and moisture properties", *Cement and Concrete Research,* vol. 56, pp. 153-170, 2014.

[26] S. C. Kou, B. J. Zhan and C. S. Poon, "Use of a CO2 curing step to improve the properties of concrete prepared with recycled aggregates", *Cement and Concrete Composites,* vol. 45, pp. 22-28, 2014.

[27] S. K. Kaliyavaradhan and T. C. Ling, "Potential of CO2 sequestration through construction and demolition (C&D) waste—An overview", *Journal of CO2 Utilization,* vol. 20, pp. 234-242, 2017.

[28] A. Gholizadeh-Vayghan, A. Bellinkx, R. Snellings, B. Vandoren and M. Quaghebeur, "The effects of carbonation conditions on the physical and microstructural properties of recycled concrete coarse aggregates", *Construction and Building Materials,* vol. 257, 2020.

# 7. Microgrinding process for processing ceramic fractions

## 7.1. Description of the problem

The production of ceramic products is highly dependent on the physical properties of the powdered ceramic and how it disperses during green body formation. One of the most important quality control parameters is the ceramic particle size and size distribution. The particle size can help define the time and temperature required to attain full density during sintering, with finer particles requiring shorter sintering times due to their high surface area. A direct relationship is also known to exist between the particle size and the pore size observed in the green body prior to sintering. Large particles tend to pack inefficiently, leading to the formation of large pores which persist during sintering, increasing the probability of component failure. Pore formation can be controlled, however, by either using powders with smaller particle sizes or by using polydisperse size distributions where the fine particles within the powder fill the voids between the larger particles. Finally, the presence of large agglomerates must be avoided as these can lead to defect formation during sintering, as agglomerated grains tend to grow more quickly than well-dispersed particles. Again, this reduces the strength of the ceramic component. Reliable particle size analysis is therefore an important requirement as part of ceramic component development and production control.

With the aim of develop new ceramic product made from secondary raw material coming from high-grade sorted ceramic EBM, the design of a grinding process of the ceramic fraction is of vital importance. Therefore, the objective of this tasks is to adapt a micro-grinding process to produce nanometer-sized ceramic materials. Therefore, once the grinding process was designed and tested, particle size was measured to control the particle size distribution achieved in each step.

## 7.2. State of the art/technology

Currently, the discharged waste in the ceramic industry is reduced to packaging waste (paper, plastic, etc.) and organic material. In past years, ceramic pieces that broke during the manufacturing process were discharged, being a considerable waste in the industry. However, currently these wastes have become one more raw material, through their addition in the milling step of a wet milling process in floor tile and bricks manufacturing. With this purpose, the broken pieces of ceramic go through a grinding process to reduce them to powder. Therefore, the approximation that is considered in this study to reduce the ceramic fraction among the CDW is based on the practice of this industrial described process. Briefly, in the industry the materials are put through a crusher mill, and dry milled with a hammer mill unit, both these facilities belonging to a conventional recycling plant [10]. At laboratory scale, in this study a tungsten carbide ring mill rapid mill are used in order to simulate these industrial processes. Specifically, the utilization conditions for the rapid mill are widely described in the literature for its optimization. The parameters to take into account are load of alumina balls and size of them, load of material to be grind, load of solvent, type of solvent and time/speed of grinding.

## 7.3. Extended methodology

Particle size reduction of ceramic fractions were studied using three types of milling processes: WC ring mill, rapid mill and attrition mill (Figure 39, Figure 40). Particle size of each material after the stages was measured.  Briefly, material size was firstly reduced into 2 cm$^3$ pieces in order to place them into de WC ring mill. The working principle of this mill is the friction. The vibration of the bowl produces an impact of the tungsten carbide concentric rings on the materials inside the bowl when it vibrates, causing the size reduction of it within seconds. With this process, the pieces are reduced in microns. Subsequently, this powder was placed into the rapid mill. This mill consists in a ceramic jar with alumina balls that is undergo to circular movements, producing centrifugal force inside it. The grinding of the process relies on the energy release on the point of collision between the alumina balls placed inside the jar and the friction of them with the walls. This stage provides a particle size from 3.5 up to 30 microns for the selected construction materials in 20 min. Finally, part of this powder is placed into the attrition mill as final stage of the process. Milling in an attrition mill is based on the stirring action of an agitator that has horizontal arms, placed vertically in a stain-stell tank filled with metallic balls, the material to grind and a solvent (Figure 40). This motion causes a differential movement between the balls and the material, thus providing a significantly higher degree of surface contact than is achieved in tumbler or vibratory mills. For this study, 3 hours of stirring, 1 mm Zr balls and water as solvent were chosen.



| 1. Cut into pieces | 2. Ring WC mill | 3. Rapid mill |

Figure 39. Outline of the steps followed in conditioning of the materials.



Figure 40. Pictures of the attrition mills used.

Once the milling process is completed, all the materials were characterized as follows:

The determination of the particle size distributions was carried out by the diffraction method with a He-Ne laser, with a λ = 632.8 nm using a Malvern Mastersizer S, on a wet sample. Distilled water was used as dissolvent. Moreover, images of the particles were obtained using a field emission scanning electron microscope (FE-SEM) Hitachi S-4700.

The materials composition was studied by X-ray fluorescence spectroscopy (XRF) using the IQ$^+$ semi-quantitative analysis curve. Samples were prepared with $Li_2B_4O_7$ as additive for the sample. Loss of ignition of the materials was evaluated by their treatment at 1000 ºC during 1 hour in a muffle.

Structural characterization was carried out by X-ray powder diffraction (XRD) patterns which were obtained using a D8 Advanced (Bruker) diffractometer equipped with Cu Kα monochrome radiation (λ = 1.5406 Å) in the range of 10° ≤ 2θ ≤70° at a 1°/min speed. Moreover, UV-Vis-NIR spectroscopy (Perkin Elmer Lambda 950) was used in the range of from 200 nm 2500 nm complemented with Fourier-transform infrared spectroscopy (FT-IR) in the range of 4000-400 cm$^{-1}$ using a Spectrum 100 Optica FT-IR spectrometer (Perkin Elmer) to analyze the chemical bindings. Furthermore, confocal Raman with AFM (WITec / alpha 300AR) measurements have been carried out using a 532 nm excitation laser (Green laser) with a 100x objective lens (N.A. 0.95) with a focus area over the sample at 20mW power.

The thermal characterization was carried out using Differential Thermal Analysis and Thermogravimetry (DTA-TG) using a Netzsch STA 409/C thermal analysis station by heating in air up to 1400 °C at a rate of 10 °C/min, and hot stage microscopy that was carried out using both optical and heating instruments. For optical purposes, a Hesse instrument with Leica-Microsystems optics and Image Analysis (EMI) was used. The furnace used was also from Hesse instruments using rhodium heating elements. These measurements were carried out up to 1400 ºC.

## 7.4. Materials (source, sampling, preconditioning)

The source, sample and preconditioning of the chosen materials have been detailed in previous Sections (2.4 and 6.3) of the present report.

## 7.5. Activities in progress

**Particle size**

Particle size distributions of the materials after both conventional and attrition milling and sieving under 100 ▢m are presented in Table 9. After the first milling, the majority of the materials achieve bimodal distributions with a maximum $d_{50}$ of 10.17µm for the extruded stoneware material and a minimum $d_{50}$ of 3.56µm for the plaster. Particle size increases as the toughness of the material does, going from the hardest materials in the ceramic group to the least hard, the gypsum group. After the attrition milling, the particle sizes are reduced to approximately

half that those obtained in conventional processing, except in the case of gypsum materials. This fact can be explained by the trend of the gypsum to form aggregates in aqueous medium. Therefore, the milling process must be done with an alternative solvent.

Table 9. Particle size distributions (d50 and d90) of the pattern materials after both conventional and attrition milling and sieving under 100 μm.

| | Material | $Al_2O_3$ (μm) | | | Attrition mill (μm) | | |
|---|---|---|---|---|---|---|---|
| | | $D_{50}$ | $D_{90}$ | mode | $D_{50}$ | $D_{90}$ | mode |
| Group 1: | Sanitary ware | 9.39 | 28.42 | bimodal | 4.56 | 11.6 | bimodal |
| | Ext. stoneware | 10.17 | 31.97 | bimodal | 5.52 | 14.6 | bimodal |
| | Common brick | 5.96 | 25.74 | bimodal | 3.03 | 7.83 | bimodal |
| | Facade brick | 5.53 | 21.49 | bimodal | 4.03 | 11.1 | bimodal |
| | Porcelain tile | 4.97 | 21.01 | bimodal | 4.26 | 10.5 | bimodal |
| | Red body tile | 4.88 | 19.34 | bimodal | 4.21 | 11.1 | bimodal |
| | White body tile | 4.89 | 19.33 | bimodal | 4.04 | 11.9 | trimodal |
| G. 2: | Drywall | 5.64 | 22.33 | monomodal | 3.96 | 56.0 | bimodal |
| | Plaster | 3.56 | 14.85 | trimodal | 2.83 | 55.1 | trimodal |
| G. 3: | Concrete | 5.43 | 26.30 | monomodal | 3.42 | 10.0 | monomodal |
| | Mortar | 5.78 | 22.20 | bimodal | 4.86 | 15.3 | bimodal |
| | Sand | 5.90 | 25.64 | bimodal | 4.15 | 10.8 | trimodal |

**Field emission scanning electron microscopy (FE-SEM)**

By means of FE-SEM, the particle size, morphology and distribution of milled and sieved materials (<100 μm) are analyzed in more detail. In order to simplify the SEM measurements, 1 representative material from each group was chosen for this analysis, selecting mortar, porcelain and plasterboard. Figure 41 shows the micrographs of these materials indicating mainly irregularly shaped particles. Porcelain tile images show small irregular particles with the presence of bigger ones up to 8.2 μm. On the other hand, mortar material presents a more regular distribution in the particle size, being c.a. 0.5 - 1.5 μm in diameter. Plasterboard is also composed by small particles of c.a. 1 μm in diameter; however, it presents aggregates, bigger in size than the big particles in the other materials. Therefore, it is clearly seen that the particle size distribution technique is only able to measure the aggregates of this material and cannot distinguish the particles that constitute them.

GROUP 1: Porcelain tile
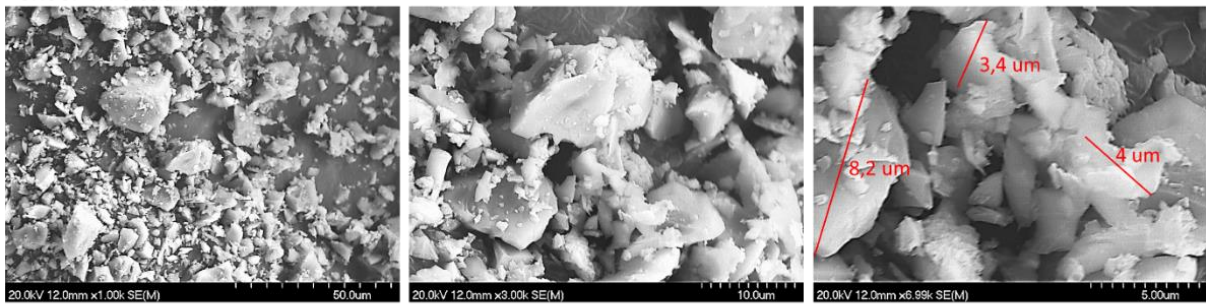
GROUP 2: Plasterboard
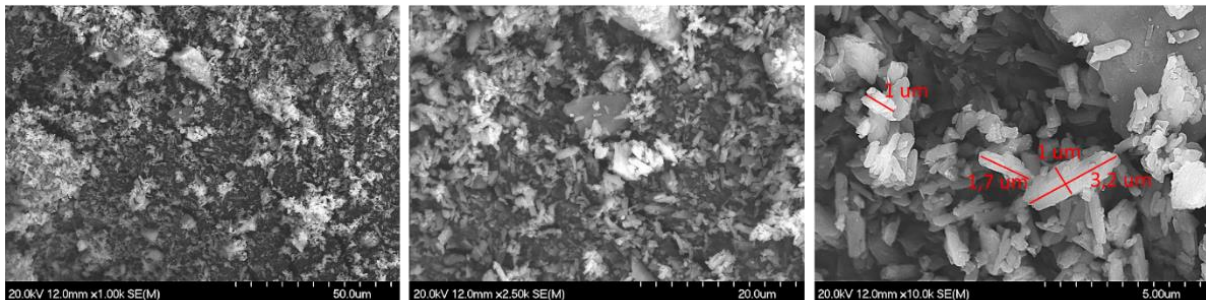
GROUP 3: Mortar
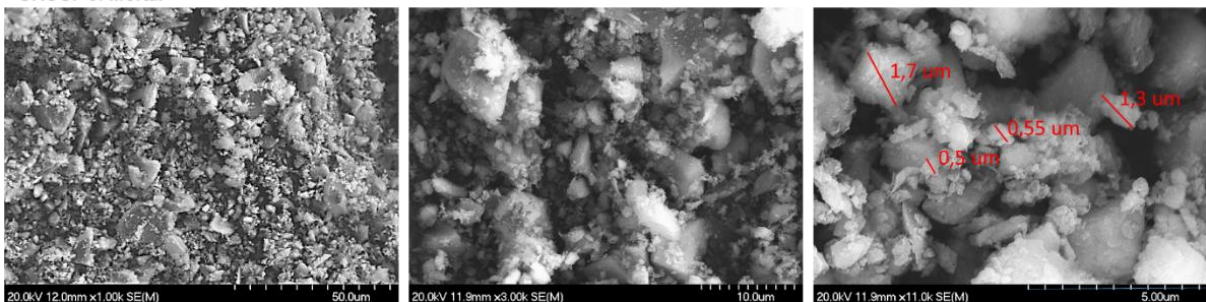


Figure 41. FE-SEM micrographs of a representative material of each group: Porcelain tile from ceramic's group, plasterboard from gypsum's group and mortar from cement's group.

### X-ray fluorescence spectroscopy (XRF)

The composition of each material is expressed in term of equivalent oxides percentages in Table 10 and Table 11. Elements present in <0.10% (such as $ZrO_2$, $P_2O_5$, $Cr_2O_3$, $NiO$ and $MnO$) have been overlooked in these tables. The **ceramic group** stands out for its high $SiO_2$ (<61%) and $Al_2O_3$ (<14%) content. Among the ceramics, three subgroups can be appreciated. First, both bricks present more $Fe_2O_3$ than any other material, while white and red body tiles stand out for their content in $CaO$. Finally, the third subgroup is formed by sanitary wares and porcelain tiles which have similar compositions, with slight variations in $K_2O$ and $Na_2O$ content. **Gypsum group** is easily distinguished by its high content of $SO_3$ and $CaO$, clearly due to the presence of gypsum ($CaSO_4 \cdot 2H_2O$), and its low content of $SiO_2$ (<7%) in its composition. In addition, it is possible to determine the difference between plaster and plasterboard, since plasterboard present higher content in $SiO_2$, which can be related with the impurities that it contains. **Cement group** is characterized by its content in $CaO$, $SiO_2$ and $Al_2O_3$, except in case of sand, which is mainly composed by $SiO_2$ (94.1%). In

comparison with the ceramic group, concrete and mortar have less percentage of $SiO_2$, but they have higher amount of CaO.

Table 10. Composition in equivalent oxides of the group 1 materials obtained by XRF. (In bold those present in >2%). N.d.: Non detected. LoI.: Loss-of-ignition.

| (%) | Group 1: ceramics | | | | | | | |
|---|---|---|---|---|---|---|---|---|
| | Sanitary ware | Porcelain tile | Extruded stoneware | Facade brick | Common brick | Roof tile | White body tile | Red body tile |
| CaO | 1.04 | 0.78 | 0.31 | **3.00** | 1.05 | **3.22** | **8.93** | **8.52** |
| Fe₂O₃ | 0.80 | 0.90 | **4.20** | **7.20** | **6.06** | **6.47** | 1.48 | **4.65** |
| K₂O | **2.40** | 1.43 | 1.62 | **5.36** | **5.00** | **4.15** | 2.04 | **3.61** |
| MgO | 0.16 | 0.46 | nd | 2.00 | **4.54** | **2.62** | 0.31 | 1.80 |
| Na₂O | 1.82 | **4.38** | 0.31 | 0.27 | 1.03 | 0.28 | 1.20 | 0.59 |
| SiO₂ | **71.3** | **71.6** | **61.1** | **61.1** | **62.4** | **64.3** | **67.0** | **64.5** |
| TiO₂ | 0.42 | 0.53 | 1.34 | 0.92 | 0.74 | 0.86 | 0.84 | 0.82 |
| Al₂O₃ | **21.2** | **19.3** | **30.0** | **17.4** | **17.5** | **17.0** | **17.7** | **14.7** |
| MnO | nd | nd | nd | 0.13 | 0.10 | - | nd | 0.050 |
| ZrO₂ | 0.60 | 0.14 | 0.070 | 0.056 | 0.045 | - | 0.12 | 0.21 |
| SO₃ | nd | nd | nd | nd | 0.082 | - | 0.10 | 0.082 |
| ZnO | nd | 0.10 | nd | nd | nd | - | 0.12 | 0.24 |
| BaO | nd | nd | 0.58 | nd | nd | - | nd | nd |
| SrO | 0.025 | 0.033 | 0.21 | 0.043 | nd | - | 0.031 | 0.031 |
| LoI | -- | -- | -- | 2.30 | 1.11 | 0.81 | -- | -- |

Table 11. Composition in equivalent oxides of the group 2 and 3 materials obtained by XRF. (In bold those present in >2%). Nd: Non detected. LoI.: Loss-of-ignition.

| (%) | Group 2: gypsums | | Group 3: cements | | |
|---|---|---|---|---|---|
| | Plasterboard | Plaster | Sand | Concrete | Mortar |
| CaO | **31.7** | **39.3** | 0.21 | **36.1** | **25.4** |
| Fe₂O₃ | 0.72 | 0.11 | 0.90 | 0.67 | 1.31 |
| K₂O | 0.49 | nd | 0.76 | 1.62 | 1.26 |
| MgO | 0.44 | 0.81 | 0.11 | 0.45 | **2.50** |
| Na₂O | nd | nd | 0.17 | 0.31 | 0.26 |
| SiO₂ | **7.70** | 1.13 | **94.1** | **30.5** | **42.4** |
| TiO₂ | nd | nd | nd | nd | nd |
| Al₂O₃ | **2.75** | 0.69 | **3.54** | **4.22** | **3.70** |
| ZrO₂ | 0.072 | 0.060 | nd | nd | 0.021 |
| SO₃ | **35.3** | **49.2** | nd | 0.41 | 0.26 |
| ZnO | nd | nd | nd | nd | nd |
| BaO | nd | nd | nd | nd | nd |
| SrO | 0.50 | 0.28 | nd | nd | 0.060 |
| LoI | 20.3 | 8.40 | nd | 25.6 | 22.8 |

## X-Ray Diffraction (XRD)

### Group 1: Ceramics

As explained before, in ceramics group, three different subgroups can be observed according to their composition and the industrial process that they undergo: brick subgroup, red and white subgroup and porcelain, sanitary and extruded stoneware subgroup. According to this, XRD patterns of the materials of group 1 are shown in Figure 42. Firstly, both bricks present a very similar XRD pattern, containing quartz, hematite, iron silicon oxide, clinoenstatite and calcium silicate hydroxide. Therefore, these two types are indistinguishable by this technique. In the case of red and white tiles, both type of tiles present quartz, feldspars (albite and anorthite), rutile and potassium iron oxide, hence, they are also indistinguishable between them by this technique. Finally, sanitary ware and porcelain tile present a very analogous XRD pattern (containing quartz and mullite). However, sanitary ware presents clear bands corresponding to albite and zircon phases that are not present in the compared material. Based on that, it is possible to recognize these two. Moreover, a small halo around $2\theta = 20\text{-}29^{\circ}$ can be observed, corresponding with the amorphous phase. Finally, extruded stoneware presents a different XRD pattern from all the other studied material, containing tridymite and anorthite besides quartz and mullite. The presence of the mentioned crystalline phases is in well concordance with the composition results obtained by XRF spectroscopy results.
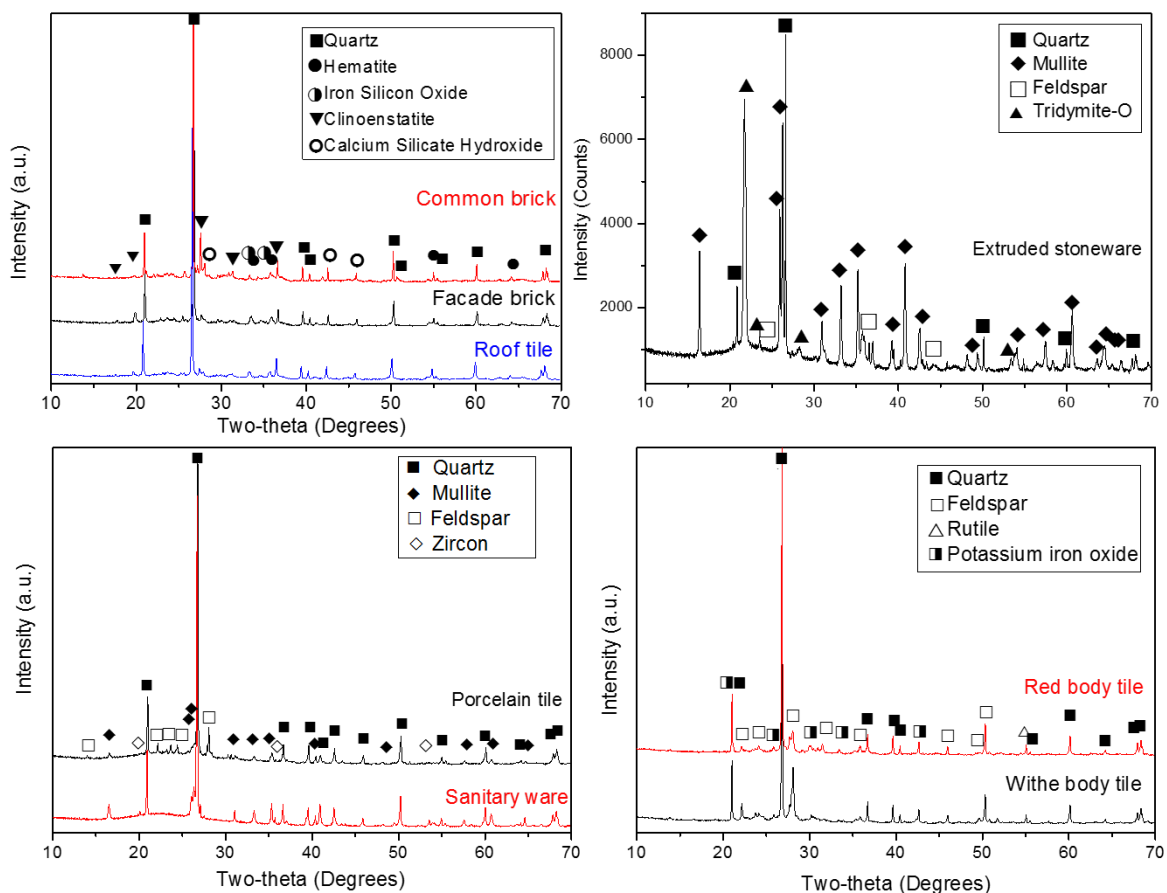


Figure 42. XRD patterns of the ceramic group materials.

## Group 2: Gypsum

XRD patterns of group 2 materials are shown in Figure 43. As mentioned before, plaster and plasterboard have sodium sulfate-bearing minerals in their composition. However, the form in which the sulfate is present differs between them. While plaster presents bassanite and anhydrite ($CaSO_4 \cdot 1/2\ H_2O$ and $CaSO_4$ respectively), plasterboard has gypsum ($CaSO_4 \cdot 2\ H_2O$)), other calcium sulfates forms and other impurities as quartz. Therefore, XRD technique is capable to distinguish the materials since it makes possible to distinguish the form in which the calcium sulfate is present.
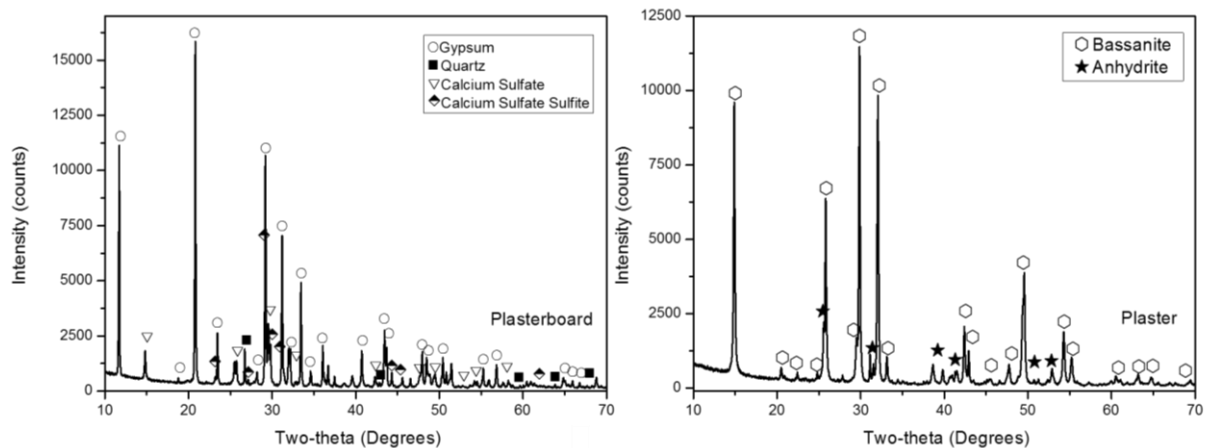


Figure 43. XRD pattern of the gypsum group materials.

## Group 3: Cements

XRD patterns of group 3 materials, concrete, mortar and sand, are presented in Figure 44. As expected, sand pattern only presents quartz phase peaks, whilst mortar and concrete present calcite and clinoenstatite, besides quartz. The main difference between mortar and cement is that mortar possesses sand in addition of cement, therefore it has a higher amount of silica and, consequently, it will present a higher intensity of the quartz phase in the X-ray pattern. Finally, in Table 12 a summary of the found phases in the studied materials and the percentage of vitreous phase is shown.
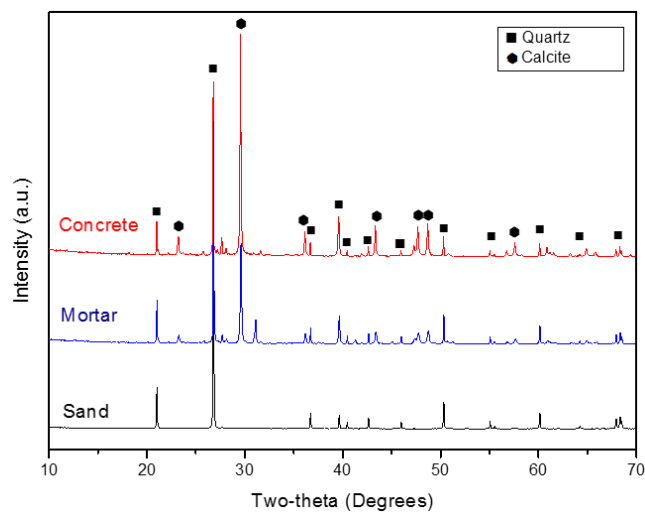


Figure 44. XRD patterns of the cement group materials.

Table 12. Summary of the found phases in the studied materials and the percentage of vitreous phase. n. d. "not detected"

| | Material | Main phase | Secondary phases | Vitreous phase (%) |
|---|---|---|---|---|
| Group 1: ceramics | Sanitary ware | Quartz | Mullite and feldspar (albite, anorthite) | 47 |
| | Porcelain tile | | Mullite and zircon | 32 |
| | Extruded stoneware | | Tridymite-o, mullite and feldspar (albite, anorthite) | 35 |
| | Common brick | | Hematite, iron silicon oxide, calcium silicate hydroxide and clinoenstatite | n.d. |
| | Facade brick | | Hematite, iron silicon oxide, calcium silicate hydroxide and clinoenstatite | n.d. |
| | Roof tile | | Hematite, iron silicon oxide, calcium silicate hydroxide and clinoenstatite | n.d. |
| | Red body tile | | Potassium iron oxide, feldspar (albite, anorthite) and rutile | n.d. |
| | White body tile | | Potassium iron oxide, feldspar (albite, anorthite) and rutile | n.d. |
| Group 2: cements | Plasterboard | Gypsum | Quartz, calcium sulfate and calcium sulfate sulphite | n.d. |
| | Plaster | Bassanite | Anhydrite | n.d. |
| Group 3: gypsums | Concrete | Calcite | Quartz | n.d. |
| | Mortar | Quartz | Calcite | n.d. |
| | Sand | | | n.d. |

## FT-IR

FT-IR spectra of the materials in the range of 4000-400 cm$^{-1}$ are presented in Figure 45 and Figure 46. Spectra of the ceramic materials (Figure 45) are mainly characterized by the presence of an absorption peak centered at 1010 cm$^{-1}$. This absorption is attributed to the asymmetric stretching vibrations of Si-O-Si and/or Si-O-Al bonds. The vibrations at the range 780-685 cm$^{-1}$ are relate to the symmetric stretching vibrations of Si-O-Si and/or Si-O-Al bonds. The band at 570 cm$^{-1}$ is assigned to the Fe-O bond vibrations of hematite, which is present only in Fe-bearing materials. Finally, the absorption peak at ~455 cm$^{-1}$ corresponds to the O-Si-O asymmetric bending vibrations [11], present again in all the ceramic materials.
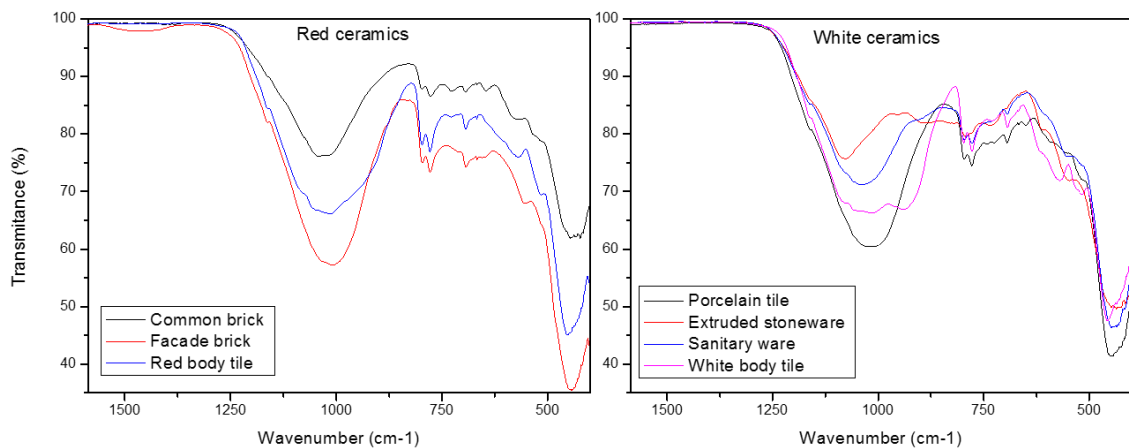
Figure 45. FT-IT spectra of the ceramic group materials.

Figure 46 shows the gypsum-based materials, plaster and plasterboard FTIR spectra. These materials present the characteristic bands for gypsum mineral: The bands in region 3530-3405 cm$^{-1}$ and 1685-1624 cm$^{-1}$ correspond to the stretching vibrational modes and bending vibrational modes of water, respectively. For the sulfate groups, the band at 1116 cm$^{-1}$ is assigned to the asymmetric stretching vibrational mode □3, while the band at 1005 cm$^{-1}$ is attributed to the symmetric stretching vibrational mode □1. The two bands observed at 668 and 600 cm$^{-1}$ correspond to the bending vibrational mode □4 [12].

FTIR spectrum of cementitious materials; mortar, sand and concrete, are shown in Figure 46. The cement and mortar spectra are very similar to those present by ceramic materials. The main difference when compared with brick spectrum are the bands related with the carbonate presence pointed out by the presence of the band at around 1450 cm$^{-1}$ and 877 cm$^{-1}$, related to antisymmetric and out-of-plane bend vibrations of carbonate ions, respectively. [13] This observation is in accordance with the XRD results which showed the presence of calcite in this material. On the other hand, sand presents different response, based on the presence of mainly quartz in its structure.
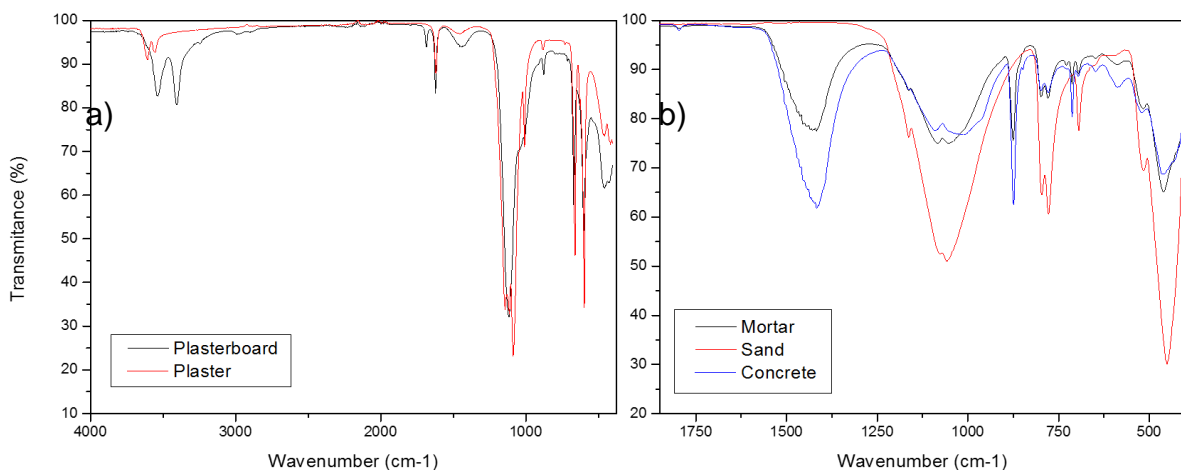


Figure 46. FT-IR spectra of: a) gypsum-based materials and b) cementitious materials.

## Raman

Raman spectra of all the pattern materials were measured using a B&W Tek Portable Raman spectrometer using both, green and red laser. However, the obtained peaks cannot be differentiated, probably due to their high fluorescence of the samples. Therefore, they have been measured using a high-resolution confocal Raman spectrometer. Figure 47 shows the Raman spectra for gypsum and cement group.

Firstly, in the **gypsum group**, characteristic peaks of sodium sulfate minerals are present. A narrow peak, corresponding to $\nu_1$ symmetric stretch vibration mode of sulfate tetrahedra is present at 1010 cm$^{-1}$ and 1033 cm$^{-1}$ for plasterboard and plaster, respectively. These results are in concordance with those obtained by XRD analysis, where different types of sodium sulfate were found (gypsum in plasterboard and bassanite and anhydrite in plaster). Therefore, this up-shifted phenomenon is due to the difference of the H$_2$O in the calcium sulfate structure. Besides this stretch vibration, plaster and plasterboard exhibit doublet for $\nu_2$ symmetric bending of sulfate tetrahedra as (425, 494 cm$^{-1}$) and (420, 498 cm$^{-1}$) respectively. The peaks at 1037 cm$^{-1}$ for the plaster and 1010 cm$^{-1}$ for the plasterboard are $\nu_3$ antisymmetric stretch vibration modes, and peaks at 620 and 670 cm$^{-1}$ in gypsum (plasterboard) and 635 and 680 cm$^{-1}$ in plaster are $\nu_4$ antisymmetric bending vibration modes [14]. For **cement spectrum**, band at 468 cm$^{-1}$ is present associated with the quartz, associated with the presence of sand in all these materials. For concrete and mortar, also carbonate is present, showing a characteristic band at 1090 cm$^{-1}$. For sand, bands at 200 and 127 cm$^{-1}$ are probably associated with the presence of feldspars.
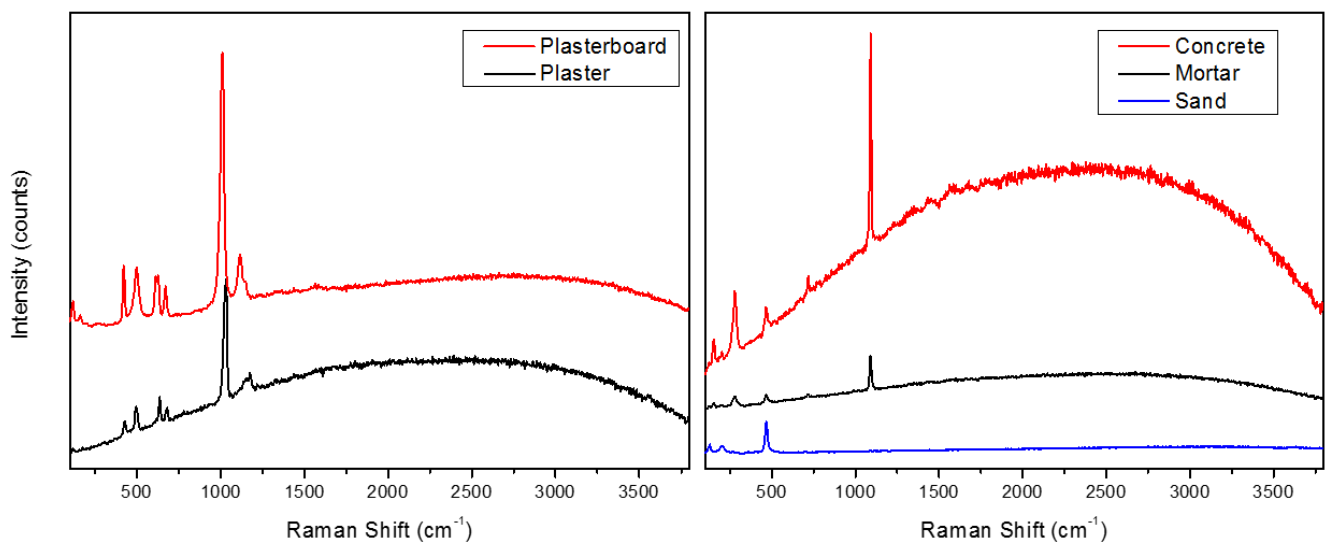


Figure 47. Average Raman spectra of the pattern materials: a) gypsum group materials (plaster and plasterboard) and b) cement group materials (concrete, mortar and sand).

## Differential Thermal Analysis/Thermogravimetry (DTA-TG) and hot stage microscopy

In order to analyze the thermochemical behavior of each pattern material, DTA-TG and hot stage microscopy were made. Each group of materials showed

similar behavior; therefore, results will be presented by groups in order to simplify the comments. Figure 48 shows the DTA-TG of the **Ceramic group**. TG curves show a weight loss of adsorbed water up to ~110 ⁰C followed by the loss of organic-based burn out up to 400 ⁰C in a two-steps weight decrease, corresponding to a mass loss between 0.25 - 1.5%, except in the case of red body tiles, which present a mass loss remarkably higher (c.a. 30%) at 1200 ⁰C. Secondly, when it comes to DTA curves, in all the materials of this group, one endothermic and one exothermic broad peak can be seen at ~ 573 and ~ 980 - 1060 ⁰C respectively. Both peaks are related with the presence of quartz, as confirmed by XRD. The first peak shows the α-quartz to β-quartz polymorphic transformation while the second peak is associated with the formation of new crystalline phases, possibly mullite or anorthite.
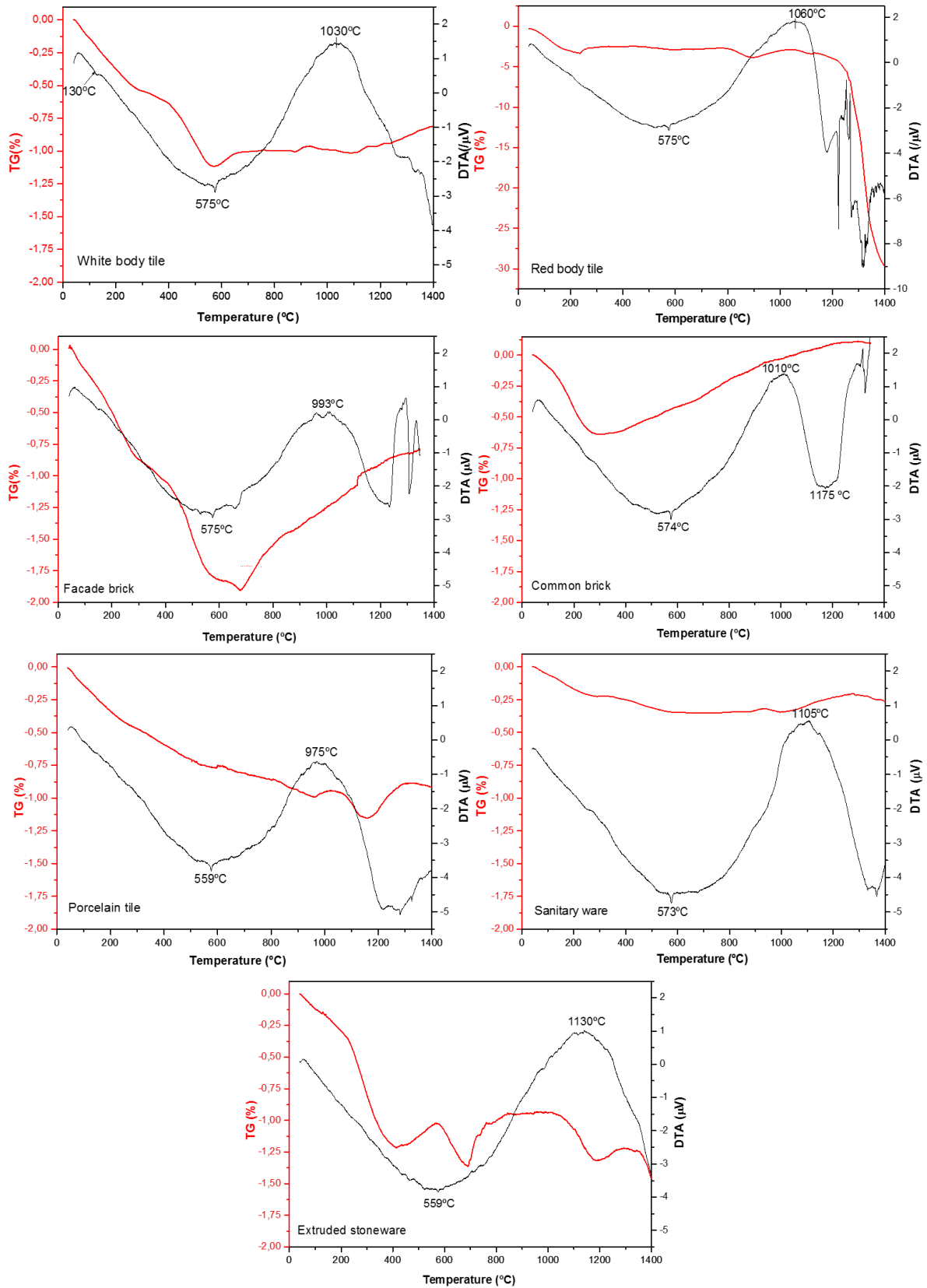
Figure 48. Differential thermal analysis (red) and thermal gravimetric analysis (black) of ceramic's group up to 1400 ºC: common and facade bricks, white and red body tiles and sanitary ware, porcelain tile and extruded stoneware (in order of appearance).

For the **gypsums's group**, results of DTA-TG are shown in Figure 49. Firstly, the TG curve shows a 2-stage weight decrease: the first step is associated to the first dehydration process ($CaSO_4 \cdot 2 H_2O \rightarrow CaSO_4 \cdot \frac{1}{2} H_2O$). This weight loss of ~ 7 % for plaster and ~ 14 % for plasterboard presents a sharp decrease in the heat flow at 159 and 138 ºC respectively. Further dehydration forms the anhydrite ($CaSO_4 \frac{1}{2}H_2O \rightarrow CaSO_4$). With an exothermic effect at approx. 340 ° C converts the anhydrite to calcium sulfate β., Finally, the last endothermic narrow peak at c.a. 1200 ºC is associated with the the conversion of β calcium sulfate to α calcium sulfate. Sulfate decomposition can be seen in additional mass loss at temperatures above 1250 ° C. The remaining process showed in DTA curve can be related to impurities and additives in the gypsum [15].
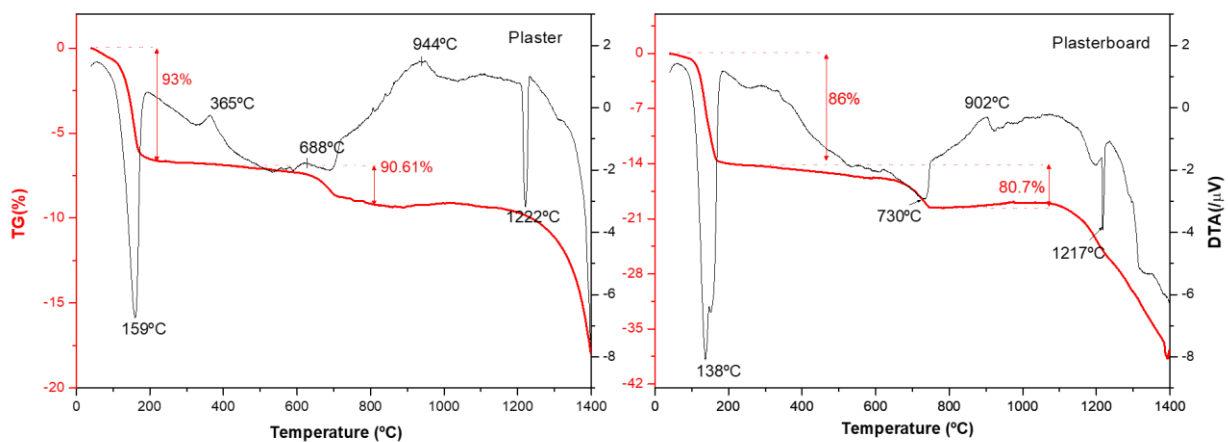


Figure 49. DTA (red) and TG (black) of gypsum's group up to 1400 ºC: plaster (left) and plasterboard (right).

DTA-TG obtained curves of group 3 materials are shown in Figure 50. In this case, sand shows completely different curves than concrete and mortar, which are very similar between them. Sand ATD-TG curves correspond mainly to $SiO_2$ in quartz phase, where two broad bands can be seen, corresponding to the α-quartz to β-quartz polymorphic transformation (endothermic, 573 ºC) and to the formation of new crystalline phases, possibly mullite or anorthite (exothermic, 1100 ºC). The TG curve shows a small increase of weight, which can be due to the phase transformations, or to the oxidation change of iron. On the other hand, concrete and mortar, shows similar DTA-TG curves. Firstly, the temperature range from room temperature to 400 ºC correspond to the dehydration region. In this region, losses corresponding to calcium silicate hydrate (commonly known as CHS gel) are shown. This range also includes the uncombined water losses, present in the pores of the material. The range that goes from 400 ºC to 500 ºC corresponds to the dehydroxylation zone, for which portlandite is responsible. An endothermic band that appears in the ATD line, without loss in TG, corresponds to the α-quartz to β-quartz polymorphic transformation. Finally, between 600 ºC and 800 ºC a decarbonation region, in which the losses corresponding to calcite, can be seen. [16][17]
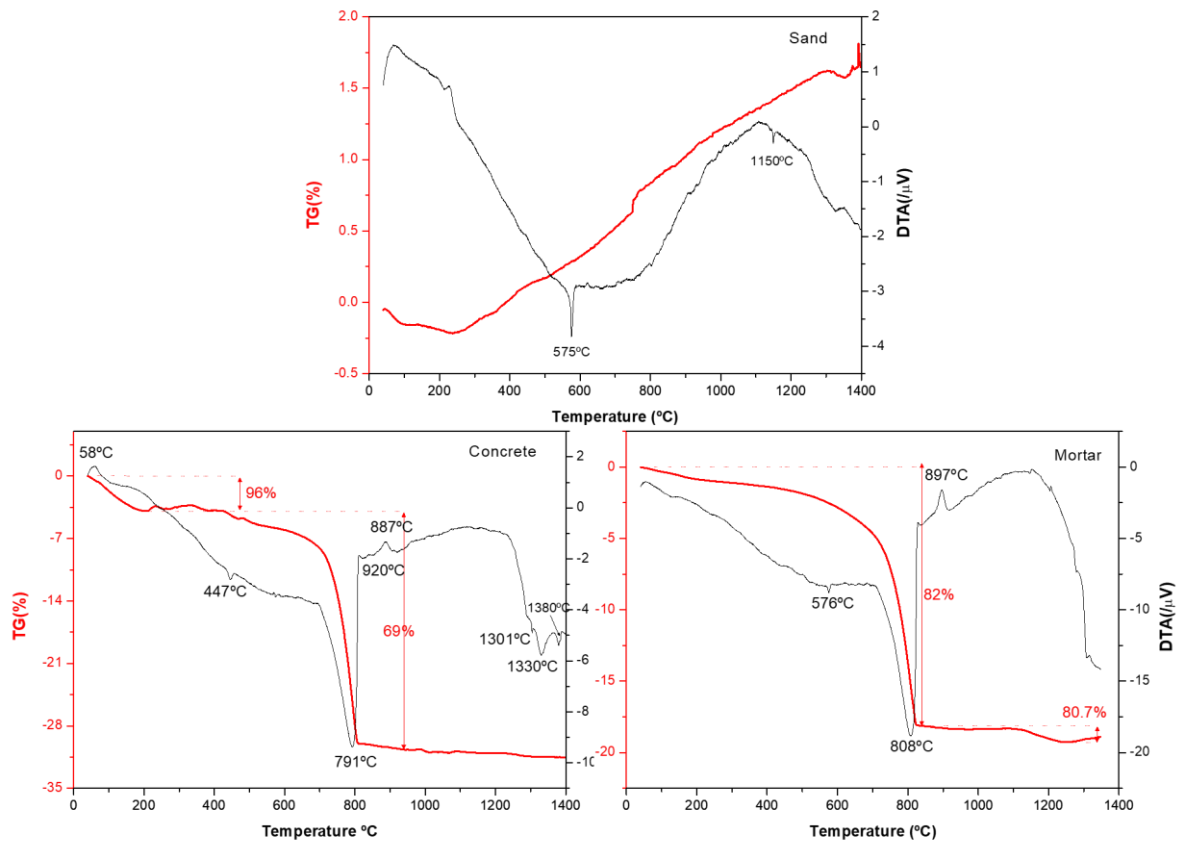
Figure 50. DTA (red) and TG (black) of cement's group up to 1400 ºC: sand (upper), concrete (down left) and mortar (down right).

Table 13. Summary of the weight losses and temperature range in which they occurs.

| | Material | Weight loss (%) | Temperature range (ºC) |
|---|---|---|---|
| Group 1: | White body tile | 1.1 | 500-600 |
| | Red body tile | 4 | 800-900 |
| | Façade brick | 2 | 500-700 |
| | Common brick | 0.6 | 100-300 |
| | Porcelain tile | 1.25 | 1100-1200 |
| | Sanitary ware | - | |
| | Ext. stoneware | 1.25 | 200-400 |
| | | 1.4 | 600-700 |
| | | 1.4 | 1100-1200 |
| Group 2: | Plaster | 7 | 100-180 |
| | | 9.5 | 650-800 |
| | | 18 | 1220-1400 |
| | Plasterboard | 14 | 100-180 |
| | | 20 | 680-780 |
| | | 39 | 1100-1400 |
| Group 3: | Sand | - | |
| | Concrete | 30 | 500-800 |
| | Mortar | 18 | 400-800 |

According to this information, hot stage microscopy was carried out (Tab 7). As commented above during the discussion of the DTA-TG results, these materials can be subgrouped depending on the densification range that they show. Firstly, in the ceramic material group, sanitary ware and porcelain tile shows a higher densification temperature, up to 1320 in the case of the sanitary ware. On the other hand, both types of bricks and body tiles need lower temperatures for their sintering, up to 1150 ºC.

Table 14. Densification range and maximum temperature in ºC obtained by hot stage microscopy.

| | Material | Densification range (ºC) | T max (ºC) | Densification percentage (%) |
|---|---|---|---|---|
| Group 1: | Ext. stoneware | 970 -1490 | 1365 | 35 |
| | Sanitary ware | 950 - 1320 | 1380 | 35 |
| | Porcelain tile | 875 - 1200 | 1132 | 37 |
| | Facade brick | 985 - 1170 | - | 38 |
| | Common brick | 1020 - 1140 | 1090 | 35 |
| | Red body tile | 920 - 1220 | 1150 | 38 |
| | White body tile | 950 - 1250 | - | 38 |
| G. 2: | Plaster | 920 - 1202 | 1395 | 43 |
| | Plasterboard | 790 - 1100 | 895 | 25 |
| Group 3: | Sand | 950 - 1350 | 1240 | 8 |
| | Mortar | 805 - 1160 | 1303 | 8 |
| | Concrete | 735 - 1065 | 830 | 5 |

**Summary**

A general summary with the discussed characterization results is provided in Table 15.

Table 15. General classification and characterization summary of the construction materials. Legend: (t): triplet, (d): doublet.

| Material type | | Material | XRD | | Spectroscopies | | Densification range (ºC) |
|---|---|---|---|---|---|---|---|
| | | | Main crystalline phase | Vitreous phase (%) | UV-Vis-NIR main response (nm) | FT-IR main response (cm⁻¹) | |
| Ceramic | Brick | Common brick | Quartz | n.d. | 400, 500 and 670 | 1100, 570 and 440 | 1020-1140 (35%) |
| | | Façade brick | | n.d. | | | 985-1170 (38%) |
| | Tile | Red body tile | | n.d. | 2200 (highest absorption for the ext. stoneware) | | 920-1220 (38%) |
| | | White body tile | | n.d. | | 1100, 935 570 and 440 | 950-1250 (38%) |
| | | Porcelain tile | | 32 | | 1100 and 440 | 875-1200 (35%) |
| | | Ext. stoneware | | 35 | | 1080 and 440 | 970-1490 (35%) |
| | Wares | Sanitary ware | | 47 | | 1100 and 570 | 950-1320 (35%) |
| Aggregates | | Sand | | n.d. | | 1100, 777 and 440 | 950-1350 (8%) |
| | | Mortar | | n.d. | 1900 and 2200 | 1450 and 877 | 805-1160 (8%) |
| | | Concrete | Calcite | n.d. | 1400, 1900 and 2200 | | 735-1065 (5%) |
| Gypsums | | Plaster | Bassanite | n.d. | 1400-1550 (t), 1930-1950 (d) and 2200-2300 (t) | 3500-3400 1685-1624 1116, 1005 and 670-600 | 920-1200 (43%) |
| | | Plasterboard | Gypsum | n.d. | | | 790-1100 (25%) |

## 7.6. Planning for the rest of the activities

Once the laboratory scale grinding process and the characterization of the materials is accomplished, the next activities of the WP2 for this study are the following ones:

i) Study of water-based medium for the chemical composition modification of the materials before milling.

ii) Optimize resulting colloidal suspension to enhance the compaction of the ceramic pieces and the subsequent processes of mass transfer during ceramic sintering.

iii) Verify quality of the resulting materials in terms of morphological, physical and chemical characteristics (CSIC).

Due to the the lack of real sorted materials at this point of the project, real recycled materials cannot be tested until they are provided. Considering this, studies with new construction materials will be developed. Therefore, morphological, physical and chemical characteristics will be only for these materials and not for the real CDW sorted fractions. However, this approach is expected to be close to those results with recycled materials and data with the real sorted materials will be compared as soon as possible once they are available.

iv) Upscale pre-industrial batches and perform tests to confirm compliance with requirements from WP3.

An approximate Gant diagram with planification of the next months is provided in Table 16.

Table 16. Gant diagram with the planning for the rest of activities.

| Task | m12 | m13 | m14 | m15 | m16 | m17 | m18 | m19 | m20 | m21 | m22 |
|------|-----|-----|-----|-----|-----|-----|-----|-----|-----|-----|-----|
| i    |     |     |     |     |     |     |     |     |     |     |     |
| ii   |     |     |     |     |     |     |     |     |     |     |     |
| iii  |     |     |     |     |     |     |     |     |     |     |     |
| iv   |     |     |     |     |     |     |     |     |     |     |     |

## 7.7. Preliminary conclusions

A laboratory scale grinding process for ceramic fractions has been designed and tested. Three consecutive steps were performed: centimeter size reduction, conventional mills and attrition mills. Particle size analysis were carried out by SEM and laser diffraction method, obtaining $d_{50}$ ranges of 3 - 10 μm and 2.8 - 5 μm for rapid and attrition mill stages respectively. The use of dry milling or alternative solvent is needed for the attrition milling of calcium sulfate-bearing materials, such as plaster and plasterboard because these materials tend to aggregate in aqueous medium. By means of XRF, XRD, Raman, FTIR and UV-

Vis-NIR spectroscopies, the composition has been fully described. Furthermore, classification elements of these materials based on these results have been proposed.

## 7.8. Bibliography

[10] M.C. Casagra, RECYCLING OF SOLID WASTER IN THE PRODUCTION OF CERAMIC FLOOR TILES, n.d.

[11] D. Kioupis, A. Skaropoulou, S. Tsivilis, G. Kakali, Valorization of Brick and Glass CDWs for the Development of Geopolymers Containing More Than 80% of Wastes, Minerals. 10 (2020) 672. doi:10.3390/min10080672.

[12] E. Knittle, W. Phillips, Q. Williams, An infrared and Raman spectroscopic study of gypsum at high pressures, n.d.

[13] M.E. Fleet, Infrared spectra of carbonate apatites: v2-Region bands, Biomaterials. 30 (2009) 1473–1481. doi:10.1016/j.biomaterials.2008.12.007.

[14] A.Y. Liu, A. Wang, J.J. Freeman, RAMAN, MIR, AND NIR SPECTROSCOPIC STUDY OF CALCIUM SULFATES: GYPSUM, n.d.

[15] D. Lázaro, E. Puente, M. Lázaro, P.G. Lázaro, J. Peña, Thermal Modelling of Gypsum Plasterboard Assemblies Exposed to Standard Fire Tests, n.d.

[16] M. Torres-Carrasco, A. del Campo, M.A. de la Rubia, E. Reyes, A. Moragues, J.F. Fernández, New insights in weathering analysis of anhydrous cements by using high spectral and spatial resolution Confocal Raman Microscopy, Cem. Concr. Res. 100 (2017) 119–128. doi:10.1016/j.cemconres.2017.06.003.

[17] O. Mikhailova, A. del Campo, P. Rovnanik, J.F. Fernández, M. Torres-Carrasco, In situ characterization of main reaction products in alkali-activated slag materials by Confocal Raman Microscopy, Cem. Concr. Compos. 99 (2019) 32–39. doi:10.1016/j.cemconcomp.2019.02.004.

# 8. Advanced technologies for sorting, comminuting and processing wooden EBM

## 8.1. Description of the problem

Available data from Eurostat states that about 8,2 Million tonnes of non-hazardous wood waste from construction were generated in Europe in 2012. In addition, there might be wood waste included in the reported amount of mixed waste from construction. Especially in Finland (but also in Sweden and Norway) a significant part of the CDW is wood waste due to the large share of wood in housing construction.

The utilization of C&D wood waste in energy production has so far been the primary option in Europe. This is mainly due to the fact that energy use, where fossil fuels, biomass and wood chips are replaced and transportation distanced are minimized, is often the best economically and environmentally option also with the climatic conditions taken into account. The second reason for the current situation is that during the use phase, the quality of wood may under certain condition deteriorate and the wood waste is not always suitable for recycling or reuse. Also, the pre-treatment of wood materials containing impurities is quite labour intensive. The third constraint is coming from existing legislation, which restrict the recycling of C&D wood waste in many times.

## 8.2. State of the art/technology

C&D wood waste is typically collected in containers on the demolition site and later sorted by the waste management company for further use. Sorting of C&D wood waste can also be done on the demolition site. The C&D wood waste fraction for further use will be crushed to smaller pieces by different kinds of shredders, crushers and choppers like hammer mills, rotary cutters, screw crushers and disc crushers. The processing line of C&D wood waste can also include different kinds of separators like screens, magnetic separators and air separators to remove impurities like stones and sand as well as metal and plastic particles. Manual separation of impurities is also used in many cases.

The utilization of C&D wood waste in energy production has so far been the primary option in Europe. For energy use C&D wood waste is chipped to woodchips or crushed. In Figure 51 a simplified current value chain related to energy use of C&D wood waste is presented. The second largest usage of C&D wood waste is the use of C&D wood waste as a raw material in the production of particle boards. Other usages of C&D wood waste are for examples landfill, composting, animal beddings, composites and ground covers. Impregnated wood fractions are always removed before C&D wood waste is processed to other products than energy feedstock.
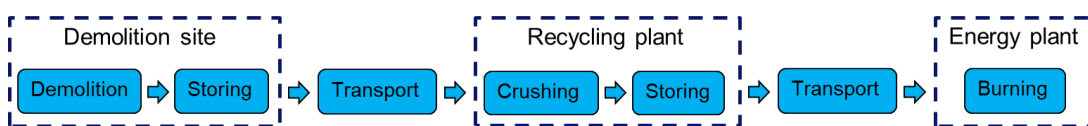


Figure 51. Simplified current value chain related to energy use of C&D wood waste.

In recent years, a lot of research and development activities have been carried out related to the recycling of C&D wood waste to different kinds of products. The utilization of C&D wood waste in the production of pulp, wood panels and biofuels was studied in the DEMOWOOD project, and the use in wood-plastic composite production was studied in the IRCOW and HISER projects. One outcome of the HISER project was an optimized processing concept for C&D wood waste in wood-plastic composite production (Figure 52). In the HISER project it was also shown that the mechanical performance of wood-plastic composites based on C&D wood waste was at a good level and comparable to commonly used wood-plastic composites in decking applications, and therefore offers very attractive raw material alternatives for wood-plastic composite production.
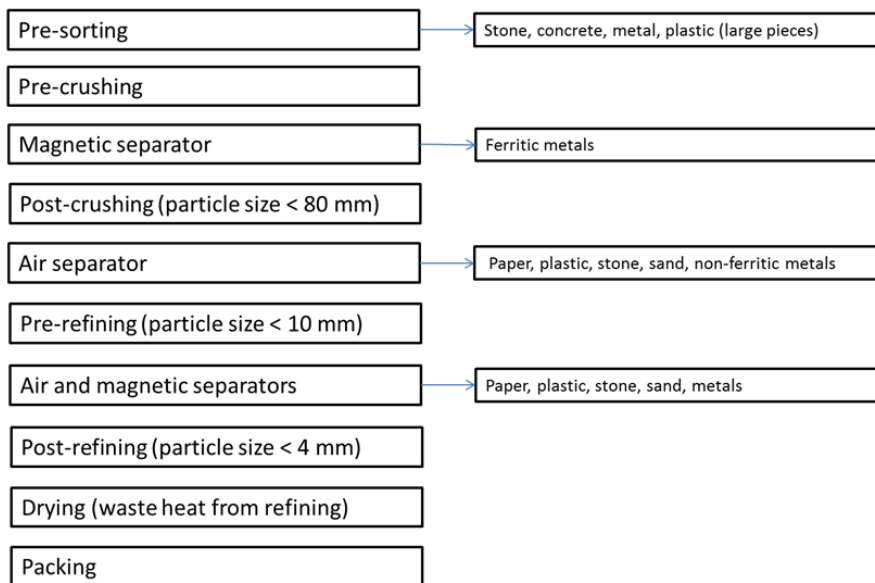


Figure 52. The flow chart of the C&D wood waste processing concept.

Fast pyrolysis of biomass is a technology entering into commercial phase and currently there are three commercial plants under construction with the aim to produce pyrolysis liquids from lignocellulosic feedstocks. Two of these new plants are designed by BTG-BTL and are located in Lieksa, Finland, owned by Green Fuel Nordic and in Gävle, Sweden, owned by Pyrocell. In addition, one plant by Ensyn is under construction in Port-Cartier, Quebec, Canada. Typical feedstock for these plants include sawdust and forest residues. C&D wood waste is not utilized at the moment. The pyrolysis liquid from these plants is used for heat production, or planned to be refined into transportation fuels or renewable chemicals.

## 8.3.  Extended methodology

**High-efficiency sorting and comminuting solutions for C&D wood**

The objective is to upgrade an integrated crushing and sorting system for the production of high-quality wood fibers (>96 wt%).

The basic idea is to optimize sorting, crushing, cleaning and refining processes of C&D wood waste to the requirements of the end products and manufacturing processes of products and based on this optimization work develop new resource and cost-efficient recovery concepts. Special attention is paid on the design and integration of novel gravitation and air-flow assisted material classification systems. Developed concepts separate impurities effectively and classify the cleaned raw materials into desired fractions. Concepts can be integrated into one system if it's appropriate.

C&D wood waste is received in the handling terminal. Visual inspection and separation by hand of bigger impurities (stones, concrete, metal and plastic particles) is done before crushing. The C&D wood waste can be sorted by hand also into different categories according to origin and purity like a clean wood fraction, painted wood fraction, plywood fraction and particle/fibre board fraction before crushing. At the crushing phase, the particle size of C&D wood is decreased below 100 mm. After crushing different kinds of cleaning and separation equipment like a magnetic separator, sieves and air separators are used to remove impurities like metals, gravel, sand, plastic and paper from the crushed C&D wood. The particle size of crushed and cleaned C&D wood is further downsized by chippers and/or hammer mills depending on the end use. This phase also includes additional cleaning operations to ensure that C&D wood doesn't include impurities, which can be harmful at post-processing phases and can deteriorate the end product quality.

Different kinds of processed C&D wood fractions will be produced for laboratory scale tests as well as case studies related to the development and production of thermal insulation materials and pyrolysis lignin.

**Fast pyrolysis and purification process**

The objective is to develop a new fast pyrolysis and lignin separation process to obtain a pyrolytic lignin fraction from demolition wood based pyrolysis liquid. The separated lignin fraction will be used in subsequent production of biophenolic resin.

First, the raw material will be characterized in fuel properties as well as in elemental and metal composition. Safety of the process will be evaluated based on the impurities present in the feedstock. As the feedstock used is demolition wood, it may contain components that cause health risks during pyrolysis. These include components such as arsenic from impregnated wood, halogens from fire retardants and large amounts of nitrogen from resin. Arsenic and halogens are toxic as such and nitrogen can form hydrogen cyanide during pyrolysis. After the feedstock characterization and process safety evaluation, the optimization of the pyrolysis conditions will be carried out with a bench scale bubbling fluidized bed pyrolysis unit with a feed capacity of 1 kg/h. During these experiments, three different process temperatures will be tested and mass balances will be determined. The organic liquid and lignin fraction yield will be followed up and based on the organic liquid yield and quality, optimal conditions are chosen for the pilot scale fast pyrolysis test run. The pyrolysis pilot unit at VTT is a circulating fluidised bed reactor with a feed capacity of 20 kg/h. One 100 h long test run will be carried out to produce enough liquid for the lignin fraction separation, which will be carried out separately after the pyrolysis pilot experiment. Optimization of

the lignin fraction separation will be started at the laboratory scale with the liquids produced at the bench scale pyrolysis experiments. Parameters to be optimized include the temperature, residence time and utilization of solvents during separation. Lignin separation efficiency and lignin quality (molecular weight distibution and hydroxyl froup content) will be followed. After the optimization, 250 g of lignin separated from bench pyrolysis products can be delivered to MEGA for initial resin synthesis tests. After the pyrolysis pilot experiment, a 6 kg batch of separated lignin will be delivered for MEGA for the optimization of resin synthesis protocol with the aim to reach 50 % replacement of phenol with pyrolysis lignin. Finally, 250 kg of separated lignin will be delivered for the actual resin production.

## 8.4. Materials (source, sampling, preconditioning)

A first material batch for ICEBERG tests was delivered by Purkupiha to Tiihonen at November 2020. The material contained clean and painted/glued demolition wood and plywood/chipwood, both clean and coated.



Figure 53. Demolition wood from Purkupiha before processing.

For crushing/refining and material tests the demolition wood was sorted manually with a crapple crane into three different classes: clean wood, coated/clued/painted wood and building boards.

## 8.5. Activities in progress

**Material production**

First refining tests with three different refiners and a pure C&D wood fraction were carried out. Raw material was pre-crushed with a hammer crusher, cleaned with a magnetic separator and milled with a hammer mill with an 8 mm sieve (Figure 54).



Figure 54. C&D clean wood fraction after processing with hammermill equipped with 8 mm sieve.

A clean C&D wood fraction was processed further with three different types of refiners; a hammer mill with 2.7 mm sieve, a Pallmann PSKM double stream mill with 8 mm sieve and a disc refiner (Figure 55).



Figure 55. Pure C&D wood fractions after processing with hammer mill (left), Pallmann PSKM (middle) and disc refiner (right).

The first C&D wood materials for pyrolysis were produced from all three different raw material categories; clean wood, coated/clued/painted wood and building boards. Processing was carried out with a pre-crusher, magnetic cleaner and hammer mill with 8 mm sieve. After processing all materials were dried below

10% moisture content in a warm air bed dryer. Dried C&D wood materials were further milled with a hammer mill equipped with a 2.7 mm sieve and classified with a vibrating sieve between 0.5 to 1.0 mm for pyrolysis tests (Figure 56).



Figure 56. Processed clean C&D wood fraction for pyrolysis tests.

**Insulation material**

Sample bags from materials got from the first refining tests were send for visual evaluation to Soprema (insulation material producer). The main conclusions were

- All refined materials consist of wood particles and there wasn't enough fiberization
- Produced pin chips were too small for production-scale refining processes at the Soprema plant

Based on these conclusions, the following approach was selected: Tiihonen will process C&D wood to wood chips and Soprema will carry out refining steps.

**Pyrolysis**

Feedstock characterization is completed and there were no significant quantities of impurities present in feedstock. Bench scale pyrolysis experiments at three different temperatures (480˚C, 500˚C and 520˚C) have been conducted successfully and mass balances for all experiments have been determined. The highest organic liquid yield of 54 wt% on dry basis was obtained at the process temperature of 480 ˚C. For the produced pyrolysis liquids, detailed physiochemical characterization, metal content analyses and determination of chemical composition have been carried out. In addition to pyrolysis experiments, optimization of pyrolysis lignin separation from pyrolysis liquid has been started at the laboratory scale. Initial lignin separation tests were done with the old pyrolysis liquid produced from waste wood in a previous project, but the experiments were continued with the liquids produced at the bench scale trials from the ICEBERG feedstock. Two different approaches to the lignin separation have been tested. The first approach is the utilization of water to force the phase separation of pyrolysis liquid into a heavy lignin rich phase and a lighter aqueous

phase where water soluble impurities are concentrated. The other approach is to use water with the addition of solvent to enhance the lignin separation into the solvent phase and to reduce the amount of water needed for the process. The benefits and drawbacks and the efficiencies of these two approaches in lignin separation will be clarified in further laboratory experiments.

## 8.6. Planning for the rest of the activities

**Outline and construct material classification system**

The material classification for pilot scale tests is planned to be done with pre-sorting using a crapple loader when feeding the pre-crusher. Cleaning impurities like metals, mineral particles and insulation material residues will be done with a magnetic and air assisted gravitational separator, which separates both heavy and light particles from C&D wood. Cleaning and classification systems will be outlined and construct during the Spring 2021.

**Insulation material**

At the first phase Tiihonen will produce 50 kg of wood chips from a clean C&D wood fraction for refining tests carried out by Soprema. Soprema will evaluate the success of refining and produce thermal insulation panels based on the refined clean C&D wood fraction for testing. Based on the results of the first phase also other C&D wood fractions can be tested. Finally, Tiihonen will produce approximately 10 tons of wood chips from C&D wood for a case study (demonstration).

**Pyrolysis**

Testing of water and solvent based lignin separation will continue at laboratory scale. Also the lignin properties, such as the molecular weight distribution and the hydroxyl groups will be determined. 250 grams of lignin is planned to be separated for MEGA for the initial resin production tests.

A pyrolysis pilot test run has been scheduled for the April (week 15) and the test run preparation has been started. The aim of the test run is to produce 1000 kg of pyrolysis liquid for the lignin separation experiments.

Once the large batch of oil is produced, first 6 kg of pyrolysis lignin will be separated for MEGA for resin recipe tests. Finally, the separation process is scaled up with the aim to produce 250 kg of lignin for resin production trials.

## 8.7. Preliminary conclusions

**Insulation material**

There wasn't enough fiberization in the fibre materials produced by Tiihonen for use in the production of thermal insulation panels. Also produced pin chips were too small for production-scale refining processes at the Soprema plant. Based on

these conclusions, the following approach was selected: Tiihonen will process C&D wood to wood chips and Soprema will carry out refining steps.

## Pyrolysis

Bench scale pyrolysis experiments were conducted successfully. The highest organic liquid yield of 54 wt% on dry basis was obtained at the process temperature of 480 ˚C. Based on the successful experiments, a pyrolysis pilot test run has been scheduled for April 2021 (week 15). Regarding the lignin separation experiments, two different approaches have been tested: utilization of pure water or water with added solvent. Benefits, drawbacks and the efficiencies of these two approaches of lignin separation will be clarified in further laboratory experiments.

## 9. Advanced technologies for purification and processing of both CDW and synthetic gypsum

### 9.1. Description of the problem

Gypsum plasterboards used in construction are constituted of an inner layer of gypsum that may contain additives sandwiched between two outer layers of lining paper. Plasterboards must abide by different requirements and regulations, such as fire protection, water resistance, durability, impact resistance and sound protection. These specifications are controlled by the types of gypsum and additives used in the manufacturing process, with additives usually used to provide fire protection and water resistance.

Gypsum used in plasterboard manufacturing is usually a blend of mineral gypsum and synthetic gypsum, which contain different types and concentrations of inorganic impurities. The synthetic gypsum is obtained during the removal of sulphur dioxide produced in coal-fired power plants and is known as desulphurisation gypsum (DSG). During plasterboard manufacturing, gypsum or calcium sulphate dihydrate ($CaSO_4.2H_2O$) is first calcined at a temperature between 100-180 °C for several hours to produce calcium sulphate hemihydrate ($CaSO_4.\frac{1}{2}H_2O$). Then, calcium sulphate hemihydrate, also known as plaster of Paris, is rehydrated with water to produce gypsum crystals that form a moderately hard material as they set.

Plasterboard waste streams are generated during construction, refurbishment and demolition projects. The collected plasterboard waste usually carries small amounts of other construction materials such as concrete, foam, paint, plastic, wood, ceramics, glass and ferrous metals. It may also contain non-construction materials due to cross-contamination or poor on-site segregation practices. Nowadays, gypsum in plasterboard waste can be recycled through several physical separation methods that comprise of manual segregation, grinding, sieving and magnetic separation. However, recycling and use of CDW gypsum is still very low in the European Union, despite it being a material that can be recycled indefinitely through calcination and rehydration. As a result, most of the CDW gypsum ends in landfills, where it can decompose and release toxic hydrogen sulphide gas (Figure 57**¡Error! No se encuentra el origen de la referencia.**).

Directive 2008/98/EC sets down a 70% target for the preparing for re-use, recycling and other material recovery of non-hazardous construction and demolition waste by 2020. Furthermore, Directive (EU) 2018/851 indicates that the European Commission will consider new targets for re-use and recycling for construction and demolition waste by 31 December 2024. The European Union, through the Life+ Gypsum to Gypsum (GtoG) project, developed quality criteria for recycled gypsum in terms of purity, free moisture content, maximum particle size, total organic carbon, salts content, heavy metals content and pH. The recycled gypsum quality criteria established a minimum purity of 80 wt%, which compares with the purity value recommendation of at least 85 wt% from the Eurogypsum Recycling Working Group and more than 85 wt% from the British standard document BSI PAS 109.
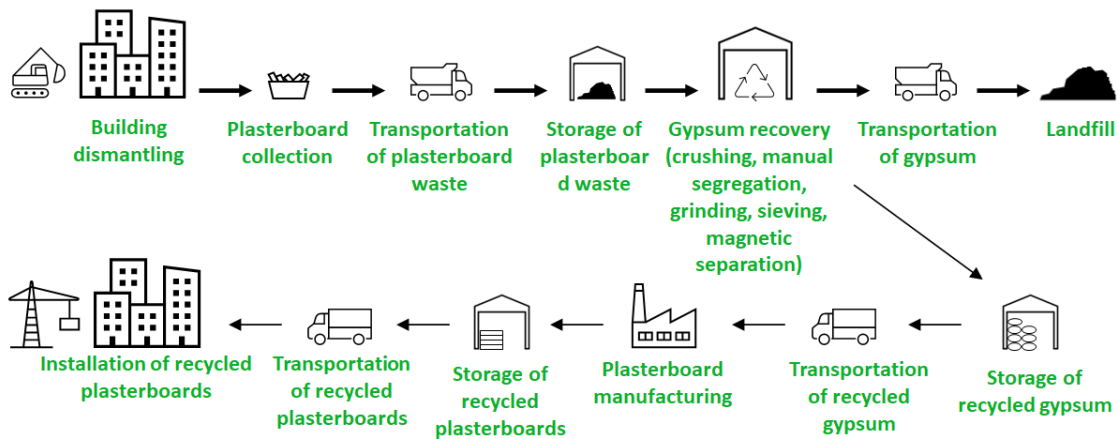
Figure 57. Flowchart of current practice for CDW gypsum processing.

Higher purity gypsum is desirable to reduce the detrimental effects of impurities on gypsum properties. However, one of the main challenges in recycling CDW gypsum comes from the difficulty to achieve consistent purity levels higher than 92 wt% via current treatment technologies. Although gypsum purity levels ranging from 75% to 90% can be achieved, this depends mainly on the quality of the plasterboard waste received, as current treatments have limited efficiency and customisation possibilities. As a result, the highest practical rate of recycled gypsum in new plasterboards is currently around 20 wt%.

In addition, the decline in production of DSG in Europe is a future threat for plasterboard manufacturers and alternative sources of synthetic gypsum are needed to reach contents of 35 wt% of recycled gypsum in new plasterboards. Recycling of synthetic gypsum requires the removal or neutralisation of impurities encapsulated in the gypsum crystals, as these impurities lower the calcination temperature, producing undesirable calcium sulphate phase distributions that lower the water demand of the plaster produced.

Therefore, the main aim of this work is to achieve recycled gypsum with purity levels above 96 wt% through the development of a novel gypsum purification process.

## 9.2.  State of the art/technology

There are two recycling processes that have been used in recent years to purify synthetic gypsum, namely hydrocyclone separation of gypsum to remove water-soluble impurities, and acid leaching of gypsum to extract heavy metals.

Hydrocyclones are simple equipment, without moving parts and of easy operation and maintenance that are used to separate solids from a liquid stream. They consist of a cylindrical section coupled to a conic section that has at its end an aperture called spigot (Figure 58). The suspension to be separated is introduced under pressure and tangentially to the cylindrical section, which houses a coaxial tube called the vortex finder. Most solid particles are carried in the underflow stream, which is discharged through the spigot, whereas fine particles, together

with most of the water, are carried in the overflow stream, which is discharged through the vortex finder.
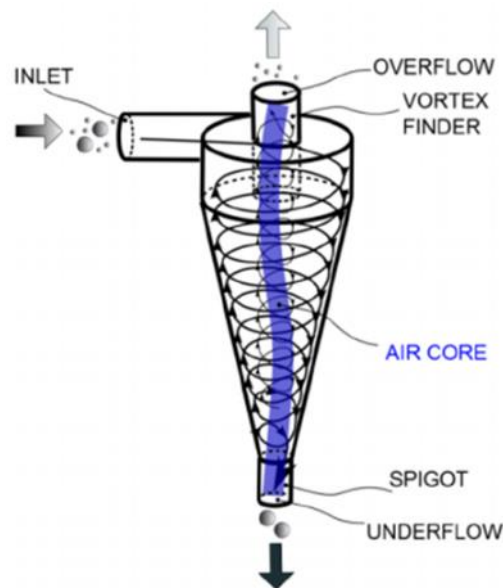


Figure 58. Schematic representation of hydrocyclone operation.

Hydrocyclones can achieve high separation efficiencies when applied to particulate materials with sizes in the range of 5-400 microns. The diameter of the hydrocyclone determines the particle cut-size achieved, with small diameter hydrocyclones (10-100 mm) able to separate particle sizes in the micron range. Furthermore, recirculation of the overflow to the feed mixing tank and higher operating temperatures can increase the separation efficiency. At a fixed spigot diameter (underflow), increasing the vortex finder diameter (overflow) increases the solid concentration ratio but reduces solid recovery. The same effect occurs when decreasing the spigot diameter whilst maintaining the vortex finder diameter fixed. Hydrocyclones are commonly used in flue gas desulphurisation units to separate DSG from other by-products. This equipment has also been proved efficient in the removal of soluble impurities in phosphogypsum when using particles sizes below 300 microns. Therefore, a hydrocyclone plant setup will be evaluated for the purification of gypsum particles less than 300 microns. This process will be tested for both synthetic and CDW gypsum.

Acid leaching is usually carried out with sulphuric acid ($H_2SO_4$), nitric acid ($HNO_3$), hydrochloric acid (HCl) or mixed acids such aqua regia (1:3 mol/mol $HNO_3$/HCl). Among these acids, sulphuric acid is the cheapest, and therefore, the most used. Acid leaching can be performed in some processes at atmospheric pressure in an open tank or at high pressure in an autoclave. The main advantages of leaching at atmospheric pressure compared to high pressure leaching are lower capital expenditure, lower construction and maintenance costs, easier start-up and shutdown, lower corrosion problems, lower energy consumption, easier process control and easier recycling of process water. The main disadvantages are higher acid consumption and slower extraction kinetics, which lead to longer residence times.

Acid leaching conditions such as temperature, residence time, solid/liquid ratio, sulphuric acid concentration, stirring speed during acid leaching have been evaluated with synthetic gypsum in the past. Higher temperature, longer residence time, and reduction of gypsum particle size increase the acid leaching efficiency, whereas recirculation of the leaching solution may also increase the process efficiency. However, acid leaching has not been tested with CDW gypsum and an optimum acid leaching methodology to maximise the removal of impurities has not been developed. Furthermore, acid leaching not only can remove inorganic impurities present in CDW and synthetic gypsum but also may have a positive impact on the gypsum crystal shape, which controls the bonding properties of gypsum, and may dissolve part of the cellulose of the paper fibres present in CDW gypsum, reducing the organic matter content.

Physical purification based on hyperspectral imaging (HSI) developed in Section 2 of this report followed by hydrocyclone and acid leaching purification will increase the purity of recycled gypsum above 96 wt%. The main innovation comes from the combination and adjustment of these technologies to recovered products from different sources (CDW and synthetic gypsum) in a single purification treatment to achieve consistently high purity. This treatment will be able to cope with the variability in the quality of the plasterboard waste received, guaranteeing a constant purity level that will enable high incorporation of recycled gypsum (35 wt%) in the production of new plasterboards.

## 9.3. Extended methodology

The preferred plant design for gypsum purification is shown in Figure 59. This plant design was selected by LU after reviewing the literature on gypsum purification and posterior consultation with ENVA and GYPS partners.
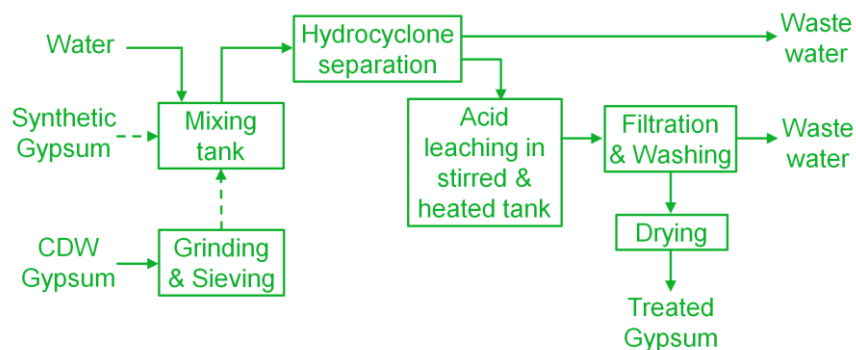


Figure 59. Gypsum purification plant design.

Grinding and sieving are necessary to produce very fine particles of CDW gypsum (less than 250 microns in our tests) to increase the amount of impurities on the gypsum particle surface, and thus, maximise the removal of impurities in the hydrocyclone and acid tank. The mixing tank is necessary to create the slurry for hydrocyclone operation whereas filtration, washing and drying are processes to recover the recycled gypsum after the acid treatment. The equipment that will determine the efficiency of the gypsum purification process are the hydrocyclone

and the acid tank. Therefore, this section will mainly focus on the separation of impurities in the hydrocyclone and in the acid tank through leaching.

Hydrocyclone separation

A wide range of commercial hydrocyclones for mineral separation are available in the market. Possible hydrocyclones for gypsum purification, their cost (if quoted) and specifications are presented in Table 17. Among the different alternatives, the preferred equipment is the Salter hydrocyclone due to its relatively low cost, easy operation and high versatility.

Table 17. Characteristics of commercial hydrocyclones considered for the gypsum purification plant.

| *Description and specifications of commercial hydrocyclones* | | |
|---|---|---|
| *Manufacturer* | *Equipment (Cost)* | *Specifications* |
| Weir | CVX40 2" Cavex hydrocyclone (free of charge but 2 month delivery time) | Corrosion resistant, low cost, maximum operating temperature of 50 ºC, provided with 2 additional spigots and 2 vortex finders, maximum solid loading of 20 wt%. |
| Salter | SC224-P 2" hydrocyclone (£912) | 3 spigot sizes, 3 vortex finders, maximum operating temperature of 50 ºC, maximum solid loading of 15% (optimum 10-12 wt%). |
| GTEK | FX75 polyurethane hydrocyclone ($350) | Maximum particle size of 1 mm, maximum solid loading of 25 wt%. |
| Gromatex | C15 steel hydrocyclone lined with rubber (£6200) | Maximum solid loading of 25 wt%. |
| Metso | MHC50 carbon steel hydrocyclone lined with polyurethane | 25 cm diameter, 1.5 m height, weight of 125 kg, minimum operating pressure of 35 kPa, minimum slurry feed flow of 7.8 L/s. |

Figure 60 displays the lab-scale hydrocyclone plant setup and the hydrocyclone components. Correct hydrocyclone operation is characterised by a slurry flow pattern in the underflow that lies between roping (straight flow) and spraying.
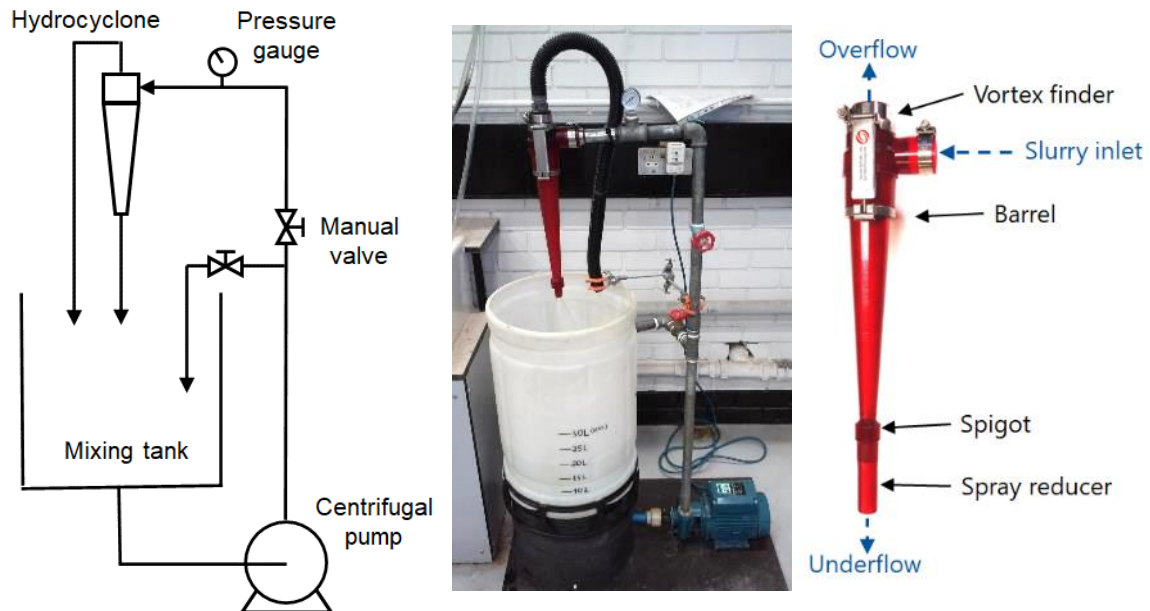


Figure 60. Schematic representation and actual lab-scale hydrocyclone setup including hydrocyclone components.

Acid leaching

Acid leaching tests were performed with a borosilicate beaker, a hot plate and an overhead stirrer inside a fume cupboard. Distilled or purified water was used to prepare the acidic solutions. The temperature of the gypsum suspension was measured with an independent thermocouple placed inside the beaker.

Filtration and drying

After hydrocyclone tests and acid leaching tests, the slurry was filtrated using a Buchner filtration kit connected to a vacuum pump. In the case of acid leaching tests, distilled or purified water was used to wash the gypsum cake until the pH of the filtrate was around 6. Then, the samples were dried in an oven at 45 °C for either 12 or 24 hours, depending on the water content of the samples. The temperature was kept at 45 °C to prevent conversion of calcium sulphate dihydrate to calcium sulphate hemihydrate, which can change the gypsum phase distribution in the sample and its calcination behaviour. Then, the dried samples were crushed with a mortar and pestle to produce a powder for further characterisation.

## 9.4.   Materials (source, sampling, preconditioning)

Around 30 kg of plasterboard waste streams from construction, refurbishment and demolition were collected at different recycling sites.

- The plasterboard offcuts from construction were collected and crushed to a powder by ENVA at their recycling site in Nottingham and supplied to LU on 30/09/2020. This plasterboard waste is fairly clean although it may contain small amounts of impurities such as foam, plastic film, packaging strapping, shards of heavy plastics, wood, electric cable, aluminium edge stripping, stainless steel brick ties, hooks, brackets, fragments of glass, paper and food.

- The refurbishment plasterboard waste was collected at Lenton Household Waste and Recycling Centre in Nottingham on 15/10/2020. This waste contains around 5 % by weight of impurities such as screws, nails, edging strips, tape, packaging, wood, plastic rail plugs, all types of fasteners, brick ties, cardboard, newspaper, foams, bricks, glass and food.

- The demolition plasterboard waste was collected at ENVA recycling site in Leicester on 28/10/2020. This waste contains similar impurities to those found in refurbishment plasterboard waste but they amount to around 10-15 % by weight.

In addition, phosphogypsum, mineral or natural gypsum , and plaster of Paris were obtained.

- Fertiberia, a phosphoric acid manufacturer located in Huelva (Spain), provided 30 kg of phosphogypsum on 03/12/2020.

- Mineral gypsum and plaster of Paris were supplied by GYPS on 09/12/2020 and 05/11/2020, respectively. These materials will be used as reference during characterisation tests.

Several citric acid manufacturers were contacted to obtain citrogypsum but it was not possible to source this material due to the economic downturn caused by COVID-19.

Figure 61 presents the different plasterboard wastes collected at the recycling sites. The plasterboard waste from construction was collected as a powder whereas the plasterboard wastes from refurbishment and demolition were collected directly from the skip or stockpile. Contaminants were also collected to have a representative sample of each waste.

| | |
|---|---|
| Incoming bagged plasterboard offcuts from construction at ENVA recycling plant (Nottingham, UK) | Processed plasterboard material from construction at ENVA recycling plant (Nottingham, UK) |
| Skip with refurbishment plasterboard waste at Lenton Household Waste and Recycling Centre (Nottingham, UK) | Plasterboard in demolition waste stockpile at ENVA recycling plant (Leicester, UK) |

Figure 61. Construction, refurbishment and demolition plasterboard wastes.

Either 0.75 kg or 1.5 kg of plasterboard waste from construction, refurbishment and demolition were processed by manual segregation, crushing and sieving (Figure 62). The level of contaminants in refurbishment and demolition plasterboard waste were respectively 10 wt% and 24 wt%, which are much higher than those typically found by ENVA at their recycling site (5 wt% and 10-15 wt%).

The demolition plasterboard waste contained foam, mortar and paint (Figure 63). Small amounts of glass were found in the construction plasterboard waste and small amounts of foil were found in the demolition plasterboard waste.

The plasterboard wastes were ground carefully with a mortar and pestle to less than 2 mm in order to separate and quantify impurities. All crushed plasterboard wastes contained paper fibres as impurities. The gypsum wastes containing paper fibres and having particle sizes below 2 mm were ground to less than 250 microns to produce the feedstock for hydrocyclone separation and acid leaching tests.

| Plasterboard wastes | Paper | Gypsum wastes + Paper fibres |
|---|---|---|
| Construction (0.75 kg) | 1 wt% | 99 wt% |
| | | |
| Refurbishment (1.5 kg) | 10 wt% | 90 wt% |
| | | |
| Demolition (1.5 kg) | 12 wt% | 76 wt% |
| | | |

Figure 62. Plasterboard wastes as received (left) and after segregation of paper (middle) and gypsum waste with paper fibres (right) through crushing and sieving using the sieve with aperture of 2 mm.

| Foam | Mortar (left) and paint (right) | |
|---|---|---|
| < 1 wt% | 10 wt% | < 1 wt% |
| | | |

Figure 63. Foam, mortar and paint in demolition plasterboard waste.

## 9.5.  Activities in progress

Hydrocyclone tests

Initial hydrocyclone tests were performed with 10 L and 30 L of water in the mixing tank to identify those size configurations for vortex finders and spigots that produced the correct water flow pattern in the hydrocyclone. The recycle valve to the mixing tank and the hydrocyclone inlet valve were kept fully open during the

tests. Three vortex finder sizes of 9, 11 and 14 mm and three spigot sizes of 3.2, 4.5 and 9.4 mm were tested and the nine possible combinations were evaluated.

Only combining the 11 mm and 14 mm vortex finders with the 4.5 mm and 9.4 mm spigots provided correct water flow patterns. The volumetric water flow rate in the underflow and the underflow/overflow volumetric flow ratio when using these four configurations was determined (Table 18). The highest flow rates and underflow/overflow ratios were obtained with the 9.4 mm spigot. The hydrocyclone with the 14 mm vortex finder and 9.4 mm spigot was chosen for the tests with CDW and synthetic gypsum slurries because the underflow/overflow ratio is closer to 1.

Table 18. Volumetric water flow rate in the hydrocyclone's underflow and underflow/overflow ratio for the combinations of vortex finders and spigots with optimum water flow pattern.

| Experimental values | | | | |
|---|---|---|---|---|
| Vortex finder size (mm) | Spigot size (mm) | Water in mixing tank (L) | Volumetric flow rate in Underflow (L/min) | Underflow/Overflow ratio |
| 11 | 4.5 | 10 | 1.51 ± 0.03 | 0.15 |
| 11 | 4.5 | 30 | 1.61 ± 0.04 | 0.15 |
| 11 | 9.4 | 10 | 7.52 ± 0.19 | 1.59 |
| 11 | 9.4 | 30 | 7.60 ± 0.11 | 1.47 |
| 14 | 4.5 | 10 | 1.19 ± 0.03 | 0.10 |
| 14 | 4.5 | 30 | Not determined | Not determined |
| 14 | 9.4 | 10 | 6.05 ± 0.17 | 0.72 |
| 14 | 9.4 | 30 | 6.23 ± 0.23 | 0.73 |

Then, tests were performed with paper fines less than 250 microns to elucidate if this impurity, which is present in CDW gypsum, can be separated with the hydrocyclone due to its lower density compared to gypsum. It was found that the concentration of paper fines in the underflow was 2.43 g/L and the concentration of paper fines in the overflow was 2.39 g/L. Therefore, the hydrocyclone cannot separate this impurity from CDW gypsum.

Hydrocyclone tests with CDW gypsum (refurbishment and demolition) and phosphogypsum were carried out with 20 L of slurry (15 % gypsum on a weight basis), which was obtained after adding 3.27 kg of gypsum to 18.6 L of municipal water. The residence time of each test was 3 hours and the temperature of the slurry throughout the test varied between 21 °C and 24 °C.

Figure 64 shows the hydrocyclone operation with CDW gypsum and phosphogypsum. Samples were collected at the underflow every hour using borosilicate beakers. A sample was also collected at the overflow after 3 hours. Samples were collected in the beaker for 5 seconds to determine the gypsum

concentration and volumetric flow rate. The CDW gypsums produced foam in the mixing tank. The collected refurbishment gypsum waste did not settle whereas the collected demolition gypsum waste settled slowly. On the contrary, phosphogypsum did not produce foam and settled rapidly in the beaker.
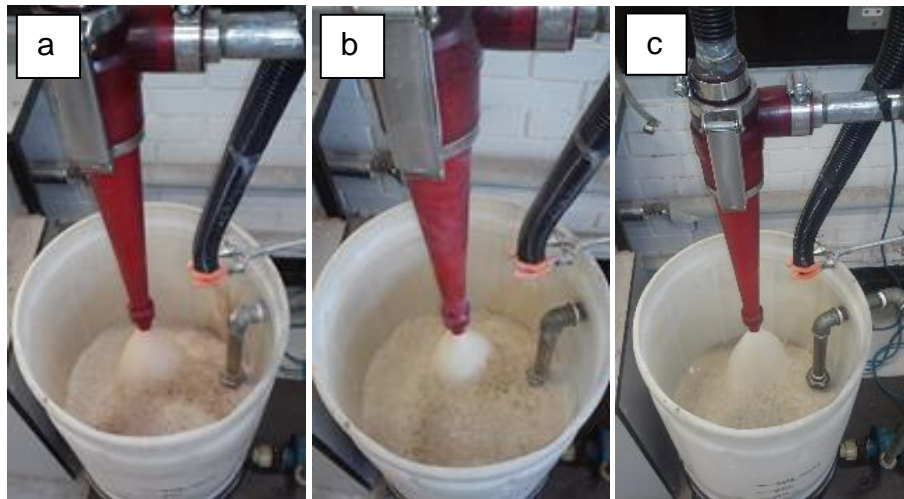


Figure 64. Hydrocyclone operation with refurbishment gypsum waste (a), demolition gypsum waste (b) and phosphogypsum (c).

All collected samples and the foam from refurbishment gypsum waste were characterised through X-ray fluorescence (XRF). Pellets for XRF analyses were prepared with 0.8 g of sample and 0.2 g of boric acid, both in powder form. The blend was placed inside a die with a 5 mm piston and a manual hydraulic press was used to apply 10 tonnes of force to produce the pellet. A Orbis micro-XRF analyser was used at a voltage of 30 kV, current of 0.4 mA and amplifier time of 1.6 µs to acquire the data. The weight percentages of $SO_3$, $CaO$, $SiO_2$, $Al_2O_3$, $Fe_2O_3$, $Mn_2O_3$, $MgO$, $P_2O_5$, $K_2O$, $Na_2O$, $NiO$, $SrO$ and $Cl$ were recorded.

Mineral gypsum can have a purity ranging from 75 wt% to 96 wt%. Therefore, the purity level of CDW gypsum is difficult to quantify because there is no information about the origin and composition of the mineral gypsum that was used during the production of the plasterboard waste. Since the amounts of $SiO_2$ and $Al_2O_3$ in CDW and synthetic gypsum are lower than those in mineral gypsum, the purity level of the samples was calculated as the sum of $CaO$, $SO_3$, $SiO_2$ and $Al_2O_3$ weight contents. The results, presented in Figure 65, indicate that differences in the purity levels of refurbishment gypsum waste, demolition gypsum waste and phosphogypsum collected at the hydrocyclone's underflow are insignificant within experimental error. Therefore, the hydrocyclone separation process is not effective for the removal of impurities present in the CDW and synthetic gypsum studied.

Figure 65. Purity of refurbishment gypsum waste (WGR), demolition gypsum waste (WGD) and phosphogypsum (PG) before and after collection from the hydrocyclone's underflow and overflow at different times.

Acid leaching tests

All acid leaching tests were carried out with a gypsum/solution ratio of 1:3 on a weight basis, with a slurry volume of 350 mL and with a stirring speed of

150 revolutions per minute. The parameter values that have been evaluated for the different samples are presented in Table 19. It is important to note that not all possible combinations have been studied because some parameter values, such as low temperature (24 °C) or low acid concentrations (less than 3 wt%), did not change gypsum purity.

Table 19. Parameter values that have been evaluated during acid leaching tests.

| Experimental values | | | |
|---|---|---|---|
| Sample | Temperature (°C) | Residence time (h) | Sulphuric acid concentration (wt%) |
| WGR | 24, 60, 90 | 0.5, 1, 1.5, 2, 3 | 0, 3, 5, 10 |
| WGD | 60, 90 | 0.5, 1 | 5, 10 |
| PG | 24, 60, 90 | 0.5, 1, 3 | 0, 3, 5, 10 |

Three approaches were evaluated to optimise the acid leaching methodology of gypsum.

i)      Single acid leaching tests

Acid leaching tests were performed to determine the best reaction conditions in terms of temperature, acid concentration and residence time. Acid leaching, filtration and washing were carried out using a borosilicate beaker, hot plate, overhead stirrer and Buchner filtration kit (Figure 66).



Figure 66. Acid leaching equipment (left) and Buchner filtration kit (right).

As previously indicated in Table 19, acid treatments were carried out with sulphuric acid concentrations between 0 and 10 wt%, temperatures between 24 °C and 90 °C and residence times between 30 minutes and 3 hours. The acid treated samples were filtrated, washed and dried prior characterisation.

Figure 67 shows that the purity of acid-treated refurbishment gypsum waste is above the 96 wt% target when leaching is carried out at 90 °C with 5 wt% sulphuric acid for 30-60 minutes or with 10 wt% sulphuric acid for 30 minutes. However, the sample treated with 10 wt% sulphuric acid was difficult to filtrate and dry because of the gypsum cake retained water forming a paste.

Acid treatments with demolition gypsum waste and phosphogypsum were also performed (
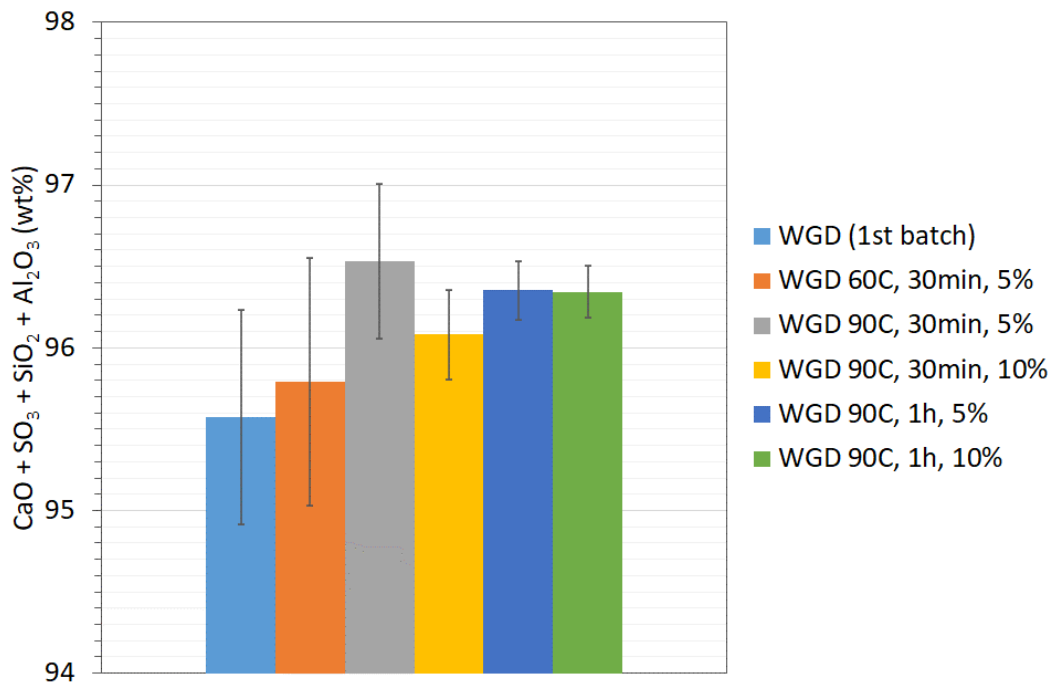


Figure 68 andFigure 69, respectively). The highest purity was achieved when the samples were treated at 90 °C with a 5 wt% sulphuric acid solution for 30 minutes. However, the standard deviation values for some treated samples were higher than ±0.5 wt%, making the results less reliable than those for refurbishment gypsum waste.
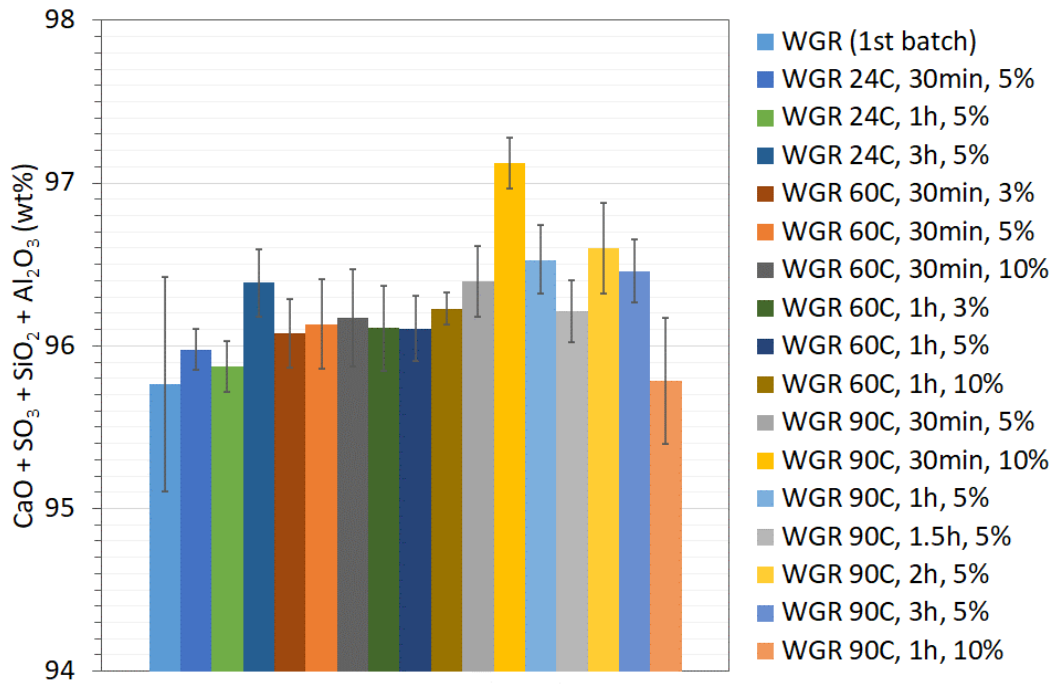
Figure 67. Purity levels of the initial and acid-treated refurbishment gypsum waste (WGR) at different temperatures, residence times and sulphuric acid concentrations.
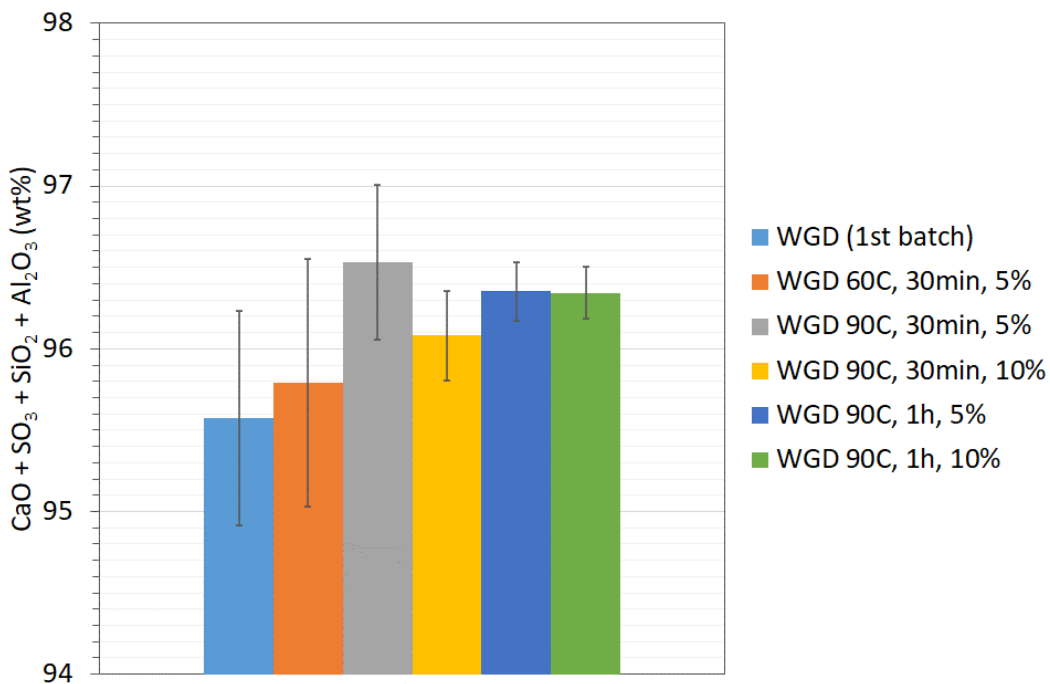


Figure 68. Purity levels of the initial and acid-treated demolition gypsum waste (WGD) at different temperatures, residence times and sulphuric acid concentrations.
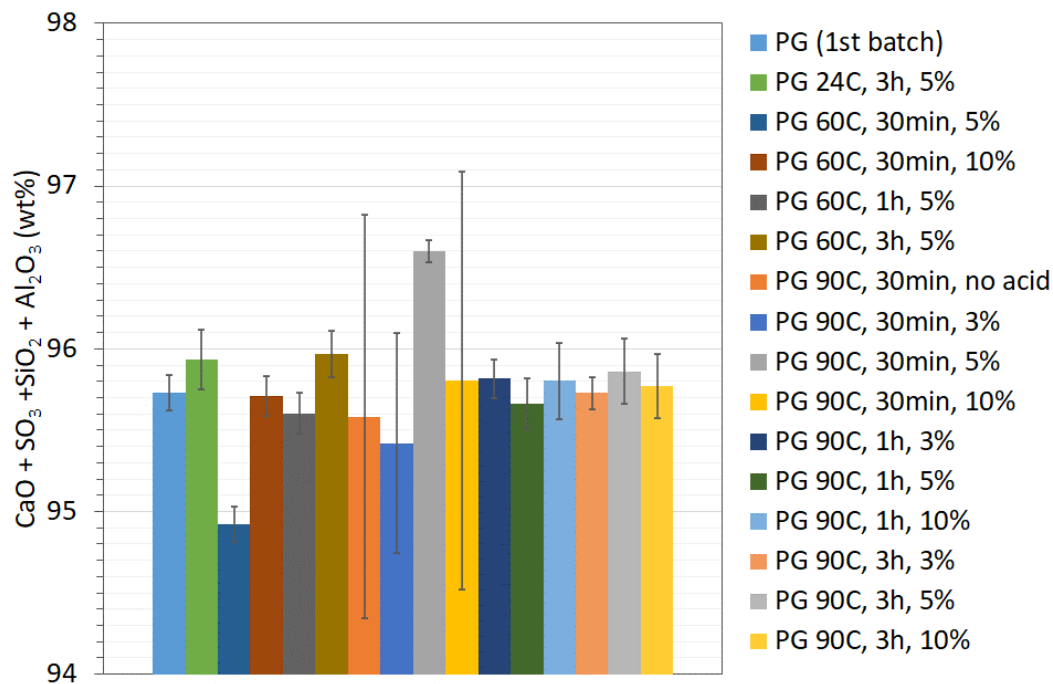
Figure 69. Purity levels of the initial and acid-treated phosphogypsum (PG) at different temperatures, residence times and sulphuric acid concentrations.

Overall, the most effective acid leaching temperature and sulphuric acid concentration are 90 °C and 5 wt%, respectively. The best residence times are 1 hour for the CDW gypsum and 30 minutes for phosphogypsum.

Some acid-treated samples, together with mineral gypsum (reference material) and the initial wastes, were characterised through thermal gravimetric analysis (TGA). This technique can provide information about the presence of impurities and calcium sulphate hemihydrate because:

- Calcium sulphate dihydrate (pure gypsum) loses 21 wt% from room temperature to 250 °C.
- Inorganic impurities do not decompose in this temperature range.
- Calcium sulphate hemihydrate loses around 6 wt%.

Therefore, the weight loss at 250 °C should be 21 wt% if there are no significant amounts of impurities and calcium sulphate hemihydrate.

TGA was performed in a TA Instruments Q5000IR apparatus to determine the calcination behaviour of selected samples. The samples (20 mg) were placed in a sealed aluminium pan with a pierced lid. The initial temperature was 40 °C and the final temperature 250 °C, using a heating rate was 5 °C/min. A nitrogen flow rate of 20 mL/min on the balance was used throughout the test.

Figure 70 displays the weight loss and derivative weight loss as a function of temperature for mineral gypsum, refurbishment gypsum waste, phosphogypsum, and the gypsum wastes after acid leaching at 90 °C with 5 wt% sulphuric acid for 30 minutes. The results indicate that the initial phosphogypsum, acid-treated

phosphogypsum and acid treated refurbishment gypsum waste have a high purity because they undergo a weight loss of around 20 wt%.

The derivative weight profiles of all samples show two maxima in decomposition rate. Acid treatment of refurbishment gypsum waste and phosphogypsum lowers the temperature of maximum decomposition rate. Phosphogypsum shows a bigger reduction in temperature, from 155 °C to 135 °C, whereas refurbishment gypsum waste only shows a 5 °C reduction. This finding indicates that acid leaching increases gypsum purity at the expense of a deterioration in calcination behaviour.
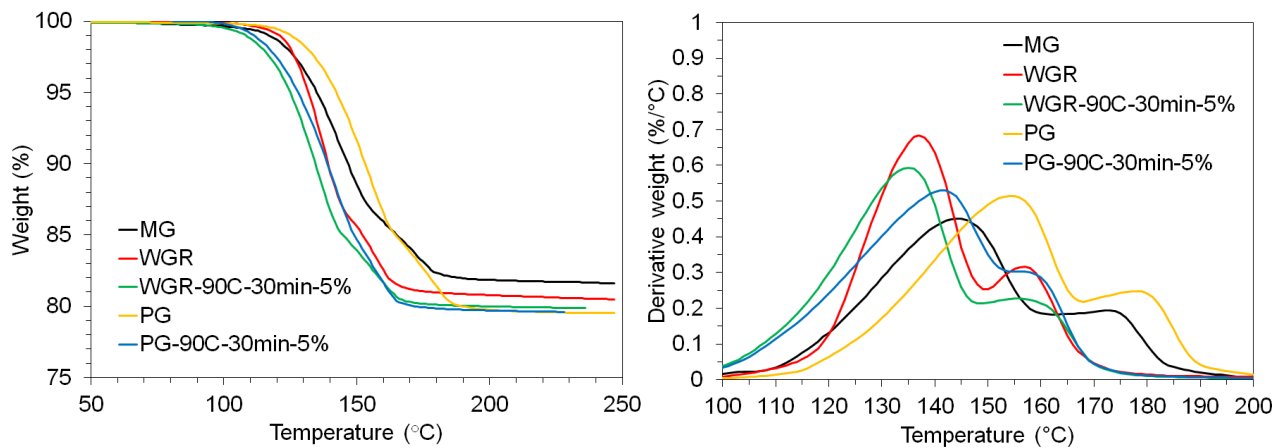


Figure 70. TGA profiles for mineral gypsum (MG), refurbishment gypsum waste (WGR), phosphogypsum (PG), and WGR and PG samples after acid treatment at 90 °C with 5 wt% sulphuric acid for 30 minutes.

Acid leaching tests were also carried out with the gypsum collected at the hydrocyclone's underflow after 3 hours of residence time (Figure 71). These acid treatments (AT) were carried out to determine whether the hydrocyclone separation process could have a positive impact on the acid leaching efficiency.
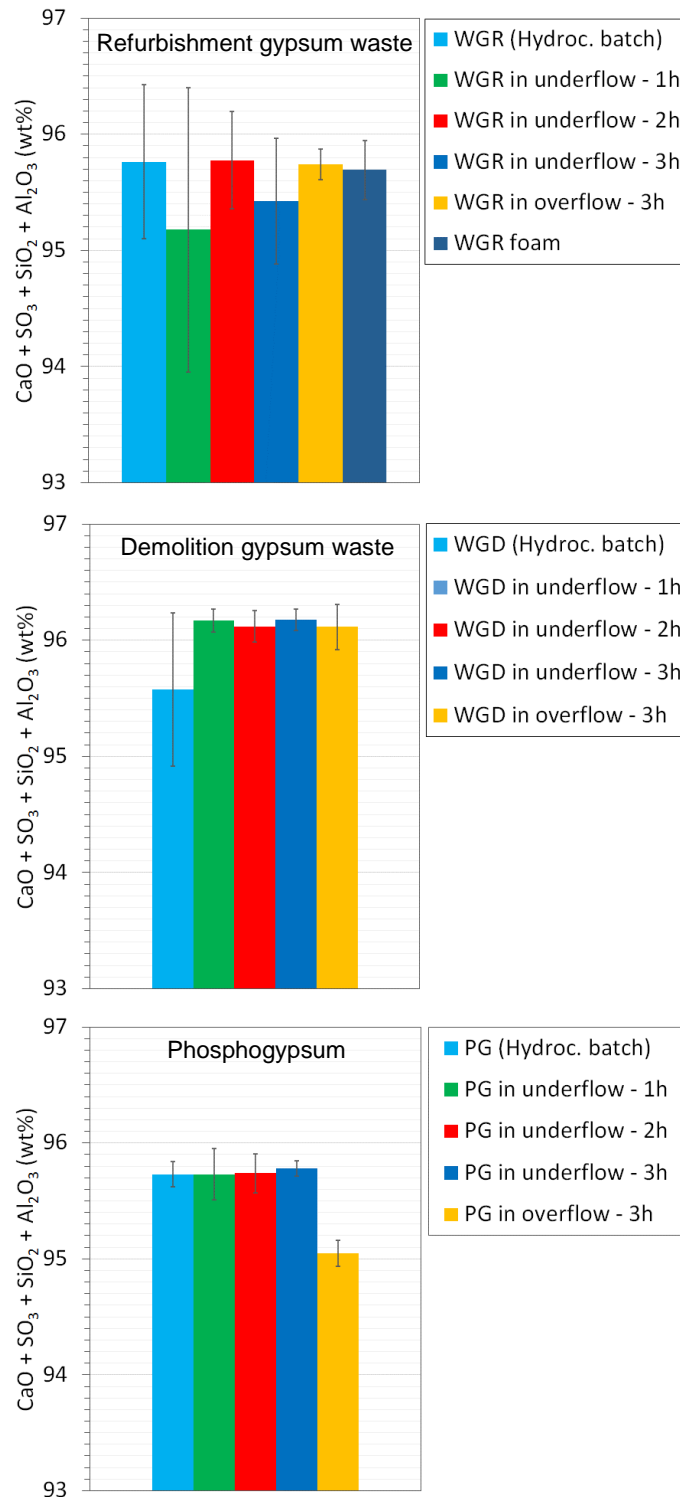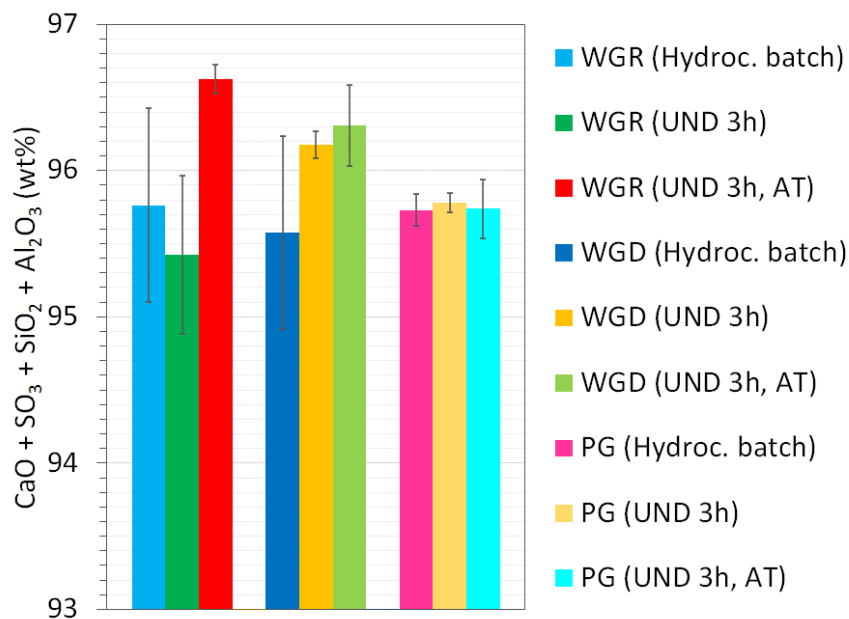
Figure 71. Purity of initial refurbishment gypsum waste (WGR), demolition gypsum waste (WGD) and phosphogypsum (PG), samples collected at the hydrocyclone's underflow after 3 hours (UND 3h) and underflow samples after acid treatment (AT) at 90 °C with 5 wt% $H_2SO_4$ for 30 minutes with phosphogypsum or 1 hour with CDW gypsum.

Acid leaching of the refurbishment and demolition gypsum samples collected at the hydrocyclone's underflow increases the purity of the materials to levels above 96 wt%. However, the purity levels obtained are comparable to those obtained just simply with acid leaching (Figure 67 and Figure 68).

Unexpectedly, acid leaching of phosphogypsum collected at the hydrocyclone's underflow did not have a significant impact on its purity level and remained below the target value of 96 wt%. This finding suggests that the hydrocyclone separation process prevents the removal of phosphogypsum's impurities through acid leaching.

Therefore, hydrocyclone separation does not offer any technical or economic advantage for the acid purification of gypsum wastes.

ii) Acid leaching tests combined with additional methodological steps

The acid treatment methodology was modified to increase the removal of impurities. The following steps were introduced during acid treatment and filtration:

- Addition of gypsum when the acidic solution was at 90 °C.

- Removal of foam produced during acid treatment of CDW gypsum.

- Decanting of the solution with dissolved impurities after the acid treatment.

- Re-dissolution of the gypsum cake in purified water during the filtration/washing step to release entrapped impurities.

- Discarding of red particles depositing at the bottom of the beaker during acid treatment of CDW gypsum.

Second batches of refurbishment gypsum waste and phosphogypsum, which had lower purity than the first batches, were used. The purity values of the acid-treated samples using this methodology are presented in Figure 72.

There is not much improvement in gypsum's purity with these additional steps. This could be explained by the deleterious effect of adding the gypsum samples to the hot acidic solution, which favours gypsum crystal growth and prevents the dissolution of the impurities in the acidic solution.

The red particles that deposited at the bottom of the beaker were separated and characterised through XRF. These particles were separated from acid treatments of demolition gypsum waste. Their composition was almost identical to that of the bulk sample, suggesting that the removal of these particles will have no impact on the purity level of the treated gypsum.
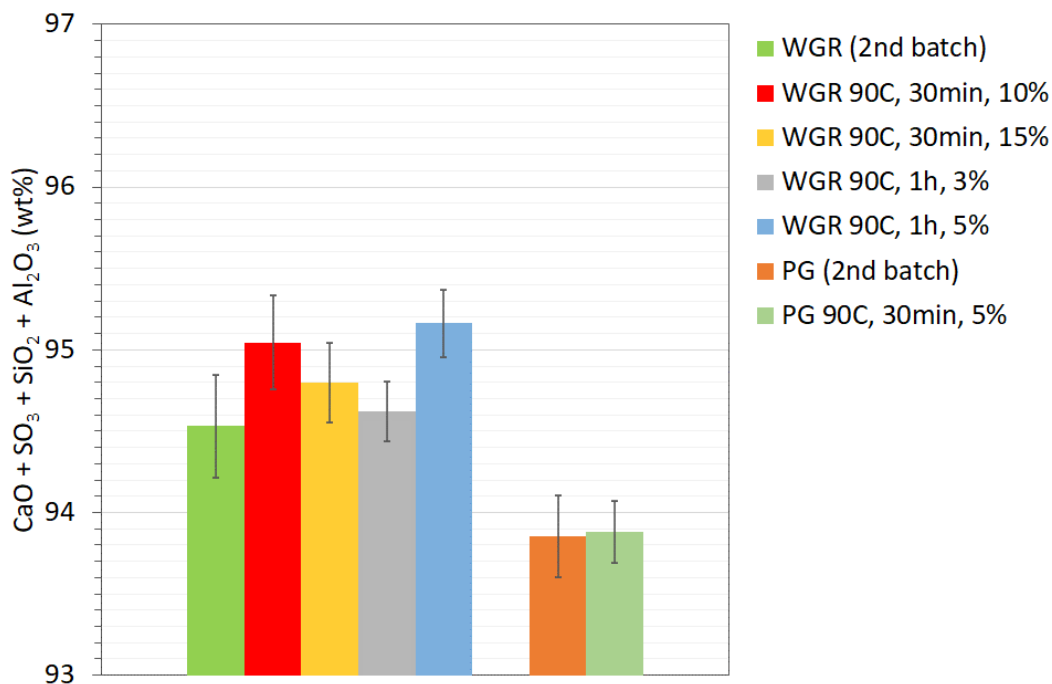


Figure 72. Purity levels of the second batches of refurbishment gypsum waste (WGR) and phosphogypsum (PG) and the acid-treated samples at different temperatures, residence times and sulphuric acid concentrations.

iii) Three acid leaching cycles with pristine sulphuric acid solutions.

Three sequential acid leaching tests were carried out to determine whether several leaching cycles can increase the purity level of gypsum. These tests were carried out with the second batch of CDW and synthetic gypsum.

The acid leaching methodology included all the steps mentioned in the previous section with the difference that gypsum was added to the acidic solution at room temperature and the mixture was heated to 90 °C at a heating rate of around 3-4 °C/min, as in single acid leaching tests. In each cycle, acid leaching was

performed using the best conditions identified in single acid treatments, namely temperature of 90 °C, solution with 5 wt% sulphuric acid and residence time of 30 minutes (phosphogypsum) or 60 minutes (CDW gypsum).

Figure 73 shows that the purity of CDW gypsum and phosphogypsum consistently increased by 2 wt% after the three acid treatments. However, phosphogypsum is the only material that does not reach the target purity of 96 wt% because of the relatively low purity of the batch (less than 94 wt%). Therefore, triplicate acid leaching of CDW and synthetic gypsum at 90 °C with 5 wt% sulphuric acid for 30-60 minutes can produce a recycled material with more than 96 wt% purity as long as the purity of the initial waste is more than 94 wt%. The results also confirm that the acid leaching process is effective when the mixture is heated from room temperature to 90 °C at a heating rate of 3-4 °C/min.
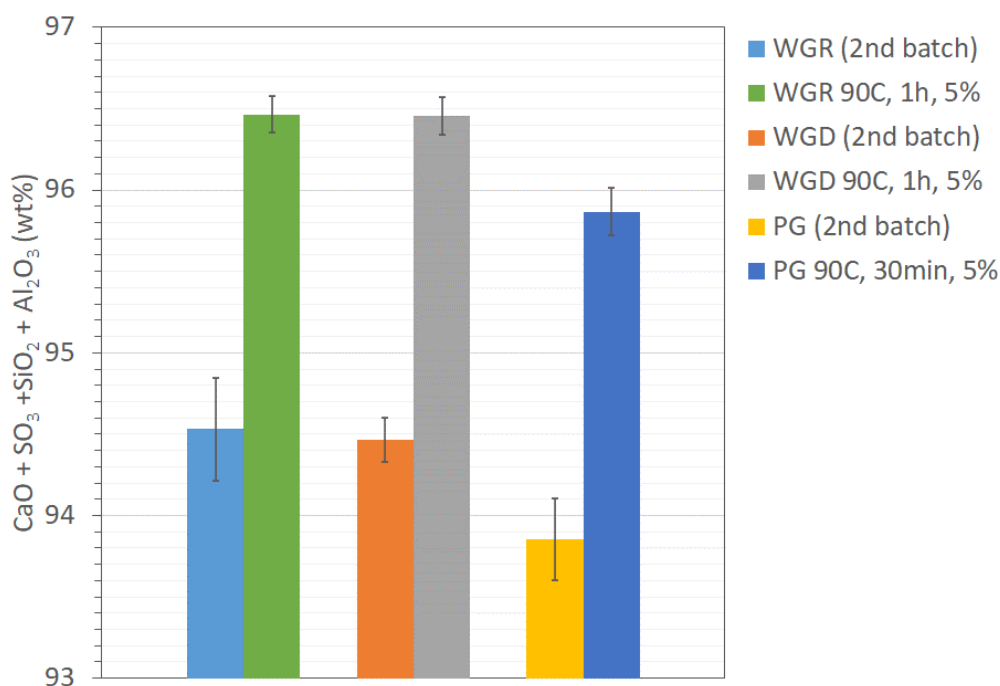


Figure 73. Purity levels of the second batches of refurbishment gypsum waste (WGR), demolition gypsum waste (WGD) and phosphogypsum (PG) and the samples treated in triplicate at 90 °C with 5 wt% $H_2SO_4$ for 1 hour when using the CDW gypsum and for 30 minutes when using phosphogypsum.

To put the results of this approach into context, the diagram in Figure 74 illustrates the level of impurity removal in the CDW gypsum samples through the different stages of the recycling process.
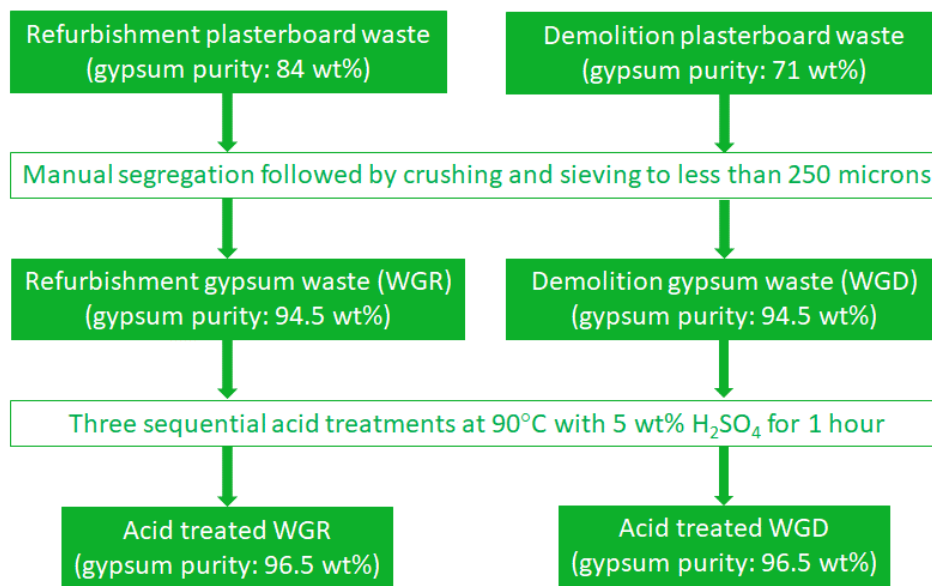
Figure 74. Purity level of refurbishment and demolition gypsum wastes collected at recycling sites through the different stages of the purification process.

The percentage of removed impurities in the samples after the three acid treatments were calculated with the mathematical expression $(C_i-C_t)*100/C_i$, where $C_i$ is the impurity concentration in the initial gypsum sample for the leaching test and $C_t$ is the impurity concentration in the treated gypsum (Table 20). The data for MgO and $Fe_2O_3$ in phosphogypsum are not included because the amounts of these impurities are less than 0.1 wt%. The data indicate that the percentage values of impurity removal are quite similar in the three samples and acid leaching effectiveness decreases in the order: $MgO > Fe_2O_3 > Cl > MnO > P_2O_5$. However, the biggest impact on the gypsum purity level is caused by the removal of $P_2O_5$ because it is the main impurity in CDW and synthetic gypsum (2.5-4 wt%).

Table 20. Impurity removal efficiency after three sequential acid treatments of the gypsum samples.

| *Experimental values* | | | | | |
|---|---|---|---|---|---|
| *Sample* | *$P_2O_5$* | *MgO* | *Cl* | *MnO* | *$Fe_2O_3$* |
| WGR | 21% | 92% | 44% | 43% | 64% |
| WGD | 23% | 83% | 54% | 42% | 70% |
| PG | 25% | - | 56% | 49% | - |

## 9.6. Planning for the rest of the activities

The rest of the activities will focus on refining the acid treatment methodology to achieve the target purity above 96 wt% in the recycled gypsum in a consistent manner and with the lowest number of steps.

However, two modifications have been included to the original work implementation plan. First, it was not possible to source citrogypsum from three European citric acid manufacturers. Therefore, DSG will be sourced from GYPS to replace citrogypsum in the development of the purification process. Secondly, LENZ and GAIKER will develop the hyperspectral imaging system to provide LU with sorted gypsum in June 2021 for acid purification and verification of the results.

In consequence, the corrected work implementation plan to complete the remaining activities to develop technologies for purification and processing of both CDW and synthetic gypsum is as follows:

- DSG characterisation before and after hydrocyclone separation and acid leaching tests using identical process conditions used with CDW gypsum and phosphogypsum. This activity will be completed by the end of May 2021.



- Acid treatments will be completed by the end of May 2021, including the recirculation of spent acidic solution, increasing the slurry volume and gypsum/solution ratio, and increasing the stirring speed. Additional acid leaching tests will be performed with the material provided by the HSI-based sorting system in June 2021 to verify the results obtained with the best acid leaching methodology. The best samples will also be characterised at LU through X-ray diffraction (XRD), to determine the amounts of calcium sulphate hemihydrate and anhydrite, and scanning electron microscopy (SEM) will be used by GYPS to determine the aspect ratio of the gypsum crystals.



- Curves will be constructed with acid leaching parameters that control the efficiency of the purification process. The curves will focus primarily on temperature, acid concentration and residence time, but other parameters evaluated in the next 3 months may be considered if they affect the purity level of the recycled gypsum significantly.

| TASK AND ACTIONS (A) | PROGRESS | START | END | | | | | | | | | | | | | | | | | | | | |
|---|---|---|---|---|---|---|---|---|---|---|---|---|---|---|---|---|---|---|---|---|---|---|---|
| Task 2.5.1: Action 7. Production of curves to predict the properties of treated gypsum based on operation parameters | | | | | | | | | | | | | | | | | | | | | | M7 | |
| A7.1: Curves to predict the composition of treated gypsum as a function of operation parameters | 0% | 27/5/21 | 2/6/21 | | | | | | | | | | | | | | | | | | | | |
| A7.2: Curves to predict the calcination behaviour of treated gypsum as a function of operation parameters | 0% | 31/5/21 | 6/6/21 | | | | | | | | | | | | | | | | | | | | |
| A7.3: Curves to predict the rheology of treated gypsum as a function of operation parameters | 0% | 5/6/21 | 11/6/21 | | | | | | | | | | | | | | | | | | | | |
| A7.4: Curves to predict the setting time of treated gypsum as a function of operation parameters | 0% | 10/6/21 | 16/6/21 | | | | | | | | | | | | | | | | | | | | |

## 9.7.   Preliminary conclusions

The main conclusions to date in the development of advanced technologies for the purification and processing of CDW and synthetic gypsum are:

- Hydrocyclone separation is not effective for the purification of CDW gypsum or phosphogypsum and can even impair the efficiency of a posterior acid leaching of phosphogypsum.

- A single acid treatment of CDW gypsum and phosphogypsum with a 5 wt% solution of sulphuric acid (1:3 gypsum to solution ratio on a weight basis) that is heated at around 3-4 °C/min from room temperature to 90 °C and held at this final temperature for 30-60 minutes increases the purity of the recycled gypsum to more than 96 wt% within experimental error. The increase in purity level is around 1-1.5 wt%, with more than 80% reduction in MgO, more than 60% reduction in $Fe_2O_3$, and more than 40% reduction in Cl. There is a smaller reduction in $P_2O_5$ of around 23%, but this reduction is mainly responsible for the increase in gypsum purity because $P_2O_5$ concentration in CDW and synthetic gypsum is around 2.5-4 wt%.

- Addition of gypsum to a hot acidic solution must be avoided to prevent the growth of gypsum crystals and encapsulation of impurities. On the other hand, decanting of dissolved impurities and redissolution of the acid-treated gypsum cake in purified water can improve the efficiency of the purification process.

- Although acid leaching increases the purity level of gypsum, it also causes a deleterious impact on the treated gypsum's calcination behaviour by reducing its decomposition temperature. This finding will require further investigation through XRD and SEM characterisation.

Acid leaching of waste and synthetic gypsum in three cycles is more effective than a single treatment, as it increases the purity level in the treated materials by 2 wt%. Therefore, this methodology will achieve the target purity of more than 96 wt% if the purity level of the initial CDW and synthetic gypsum is higher than 94 wt%, which can be achieved with preliminary separation of impurities before acid leaching. However, the higher material and energy costs associated with these cycles make this methodology less compelling.

# 10. Advanced technology for purification and recycling of PU/PIR post-consumer foams

## 10.1. Description of the problem

Tons of C&D PU waste are being incinerated (quaternary recycling), disposed in landfills or being grinded down (secondary recycling) with a highly limited scope of reusability. Instead of these deposing processes, the materials could be better used in recycling processes or other production circles with the help of tertiary recycling, where the product is chemical reduced to monomers. For example, as PUR & PIR based insulation boards are often used in the form of sandwich panels between metal sheets, there is quite a lot of PU based waste waiting to be deposed of, which could be recycled to again being used as a resource in producing new boards. This could be achieved with the use of the glycolysis process. As there are a variety of components used in creating a specific product with specific parameters, which are bound to change over the passing years of production and further development of the product in terms of various upgradeable aspects, like pore size and so on, there can´t be a general assembly of one way. Therefore, it is also not possible to degrade these items in the same way without the possibility to take backlashes from resulting deviations that will arise through this diversity. It is of importance to specify the given material based on the overall component and designing a process, which is flexible and easily altered, if some parameters are changed, but in a reasonable fashion. The recycled product also must be cheap in the production costs to generate a gain from it that is higher than the gain it would generate, if it would be incinerated. This could be the case if several cycles of the materials could be achieved till the recycled material is utterly full with different contents from prior degrading agents and therefore incompatible with production lines that need specific responses from the given material. There could be intervened, that more sufficient processes, in terms of separating those not wanted reagents, could be developed in the future, but as it is now, they are not available. But the first problem arrives in terms of long used waste materials from old building places. These could be contaminated with water, microorganisms, and other contaminations that can be soaked in the described material. As some of these will bother further processes, the first tackle would be to have a good separation system. Getting non-mixed demolition waste and this waste material in a dried state, is a highly needed precondition for working with the involved process of degrading the polymer-chain-structure of PIR & PUR insulation boards. As the source of a lot of incoming waste material is questionable or insecure in terms of consistency of the quality, new arrived materials for producing recycled polyols will need to be viewed as a "black-box". Therefore, safety measures need to be taking into account. After successfully establishing the lab-scale experiments, the upscaling process takes place, which must be monitored due to the change of shape and other parameters, which will have an impact on the recycling process. During the first view of the material, there is a need to inspect the state of the material in terms of a variate of parameters, which the following chapters will be more precise about and even give a preliminary conclusions for the projects results so far.

## 10.2. State of the art/technology

There are already some different solvolysis processes known regarding chemically degrading PU waste, where some have shown greater possibilities in terms of industrial production scale in comparison to others. The following text will describe, in a short summary, the different known methods with pointing out the usage in terms of usability, while then concentrating on the chosen method in more detail.

**Hydrolysis**

The method of hydrolysis is the chemical reaction of the urethane with water steam under pressure and high temperature. It splits the ester of the urethane under generation of $CO_2$ as shown in Figure 75. The reaction also produces amines. These amines could be harming substances and therefore an additional step of deamination would be needed, or maybe a phase separation could be used.

| *Schematic of the hydrolysis* |
|---|
| Hydrolysis |

$$R_1 - \overset{\overset{\displaystyle H}{\displaystyle |}}{N} - \overset{\overset{\displaystyle O}{\displaystyle ||}}{C} - O - R_2 \; + H_2O \longrightarrow R_1 - NH_2 + CO_2 + HO - R_2$$
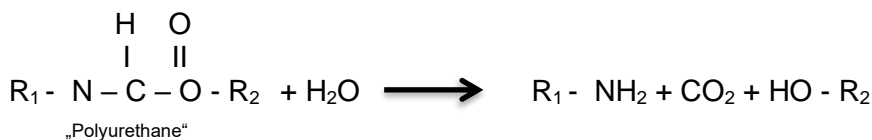
„Polyurethane"

Figure 75. Overview about hydrolysis reaction.

In terms of using the hydrolysis as a method for reducing the polyurethane waste in a chemical way, it can be said, that the needed pressure and temperature are not allowing the process to be used in an industrial size so far as it would be a costly matter. As of now, there would be more research needed to develop a commercial industrial scale usability.

**Aminolysis**

The carbonyl carbon of the urethane is interchanged with an amine group under atmospheric pressure and low temperature as shown in Figure 76:

| *Schematic of the aminolysis* |
|---|
| Aminolysis |

$$R_1 - N - CO - O - R_2 \; + NH_2 - R_3 \longrightarrow R_1 - NH - CO - NH - R_2 + HO - R_3$$

Figure 76. Overview about aminolysis reaction.

As it develops two phases, it would need further steps regarding separation & purification and to find a use for both phases. As of now, the actual available research stopped years ago, so there are no indications that an upscaling process would be technical and economical possible.

**Glycolysis**

The commonly used method for PU recycling at RAMPF Eco Solutions involves the so-called Glycolysis. It is a transesterification reaction. In the transesterification reaction, the glycols (often bivalent alcohols) split the urethane group under the reaction conditions of specific temperature and with higher reactivity during the additive of a catalyst for the split reaction. The OH-Value indicates the hydroxyl groups in a substance. Due to the addition of the glycols, the recycling polyol's OH-Value increases during the dissolving process. These processes are shown as a schema in Figure 77.

| *Schematic of the glycolysis of Polyurethane* |
|---|

Reaction of generating Urethanes

$$R_1 - \underbrace{N = C = O}_{\text{Isocyanate-Group}} + \underbrace{HO - R_2}_{\text{Hydroxyl-Group}} \longrightarrow R_1 - \underbrace{\overset{\displaystyle H}{\overset{\displaystyle |}{N}} - \overset{\displaystyle O}{\overset{\displaystyle ||}{C}} - O}_{\text{Urethane-Group}} - R_2$$

Glycolysis

$$R_1 - \overset{H}{\underset{|}{N}} - \overset{O}{\underset{||}{C}} - O - R_2 + HO - R_3 - OH \xrightarrow[+ \text{ Cat.}]{+ \Delta T} R_1 - \overset{H}{\underset{|}{N}} - \overset{O}{\underset{||}{C}} - O - R_3 - \textcolor{red}{OH} + \textcolor{red}{HO} - R_2$$

„Polyurethane"  Glycol

(R1, R2 → R3)

**Recycling polyol**
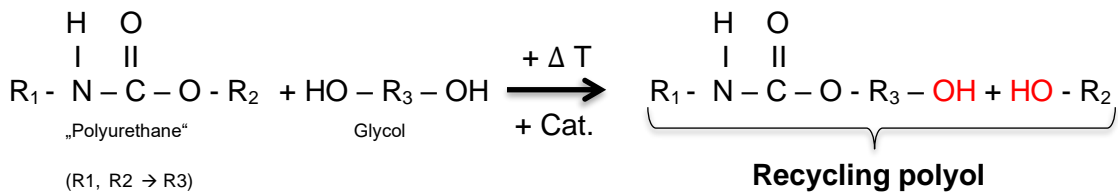
Figure 77. Overview about glycolysis and recycled polyol creation.

The mixture of monomers, hydroxyl-terminated urethanes, polyol and glycol can be reused with addition of isocyanate, as shown in the Figure 77 above.

Additionally, the reactions of the hydrolysis and aminolysis can take place during the glycolysis as side reactions. As the used glycol is used in abundance, the percentage of these additional side reactions is low. But free amines could also be created, depending on the composition of the waste PU. Therefore, it is also needed to analyse the composition of the recycled polyol regarding these components to decide if an additional deamination step is needed for the given material.

## 10.3. Extended methodology

There are some influencing parameters that need to be taken into account for the production of the recycled polyols and also the possibility of contaminated resources needs to be addressed. Therefore, the following parameters, which are used to describe the given procedure in addition to the use of a recipe that is tailored to the given "black-box" material, are as followed described:

- Temperature in °C
- Stirrer speed in RPM
- Dissolving time in min.
- Pressure in bar
- Distillate in mL
- Impurities in g

**Analysation methods**

After the creation of the recycled polyol, it is analysed. The parameters vary in regards of specific parameters that are required for certain production lines. The following Table 21 below shows the regular measured parameters:

Table 21. Regular analysed parameters of polyol content.

| Regular analysed parameters | | | |
|---|---|---|---|
| *Parameters* | *Unit* | *Method* | *Test temperature* |
| Acid-Value | KOH / g | Metrohm Bulletin Nr. 200/2 d | 20 °C |
| OH-Value | KOH / g | Metrohm Bulletin Nr. 322 d | 20 °C |
| Viscosity | mPa*s | DIN 53019 | 25 °C |
| Water-Content | wt% | DIN 51777 | 20 °C |

In cases of new possible products, there are further analysation methods used to determine the following parameters, which are shown in Table 22:

Table 22. Further possible analysations of polyol content.

| Additional analysed parameter | | | |
|---|---|---|---|
| *Parameters* | *Unit* | *Method* | *Test temperature* |
| Gel-Time | Min. | DIN EN ISO 9396 | 50 or 70 °C |
| Heating-Value | kJ/g | DIN 51900 | Gradient |
| MDA Content | wt% | HPLC-Analytic | 50 °C |

## 10.4. Materials (source, sampling, preconditioning)

So far, the used materials in the project are new and uncontaminated PIR & PUR insulation boards. These where produced through SOPREMA from France and an example is shown in Figure 78.



Figure 78. Example of delivered PUR/PIR insulation boards from SOPREMA.

For usability, the given insulation boards where first grinded with a mechanical grinder to a reasonable particle size as shown in Figure 79.



Figure 79. Example for the PUR/PIR insulation boards after grinding for usage, like lab-scale experiments.

Other materials used are lab-scale instruments such as stirrer, flasks, analytic chemicals etc., and also the use of a solvent (glycol) and a catalyst for degrading the polymer-chains to a new usable polyol.

## 10.5. Activities in progress

After grinding the boards into usable particle size for the experiments, lab-scale glycolysis experiments were performed. A polyol sample was produced and delivered to the project partners for further investigations of the usability of the produced recycling polyol.

At the beginning of the experiments, dissolution tests in the used reagents of the grinded boards in the used reagents were performed. The PIR & PUR could be dissolved, but in a very slow rate. Further tests with various catalysts where performed to find suitable degrading reagents that do not disturb the dissolving process. It has to be noted here, that the use of different substances can cause the release of different molecular structures that were mixed in during the insulation board production. Therefore, it could have been possible to release foaming substances or getting mixed reactions that could result from the unknown content of the boards, like the release of exothermic reactions, which could badly influence the used reagents and kinetics of the running batch. Because of that, the different substances where used on a small scale to collect the corresponding data without having lost a lot of research material or risking a unpredictable outcome with higher damage in a worst-case situation. Another focus was placed on finding unsolvable impurities of the recycled boards in the polyol, which was therefore filtered. No such impurities could be found in the recycled polyol from the pure PIR & PUR insulation boards that were received from SOPREMA.

With the collected data from the small lab scale experimentations, the process was upscaled (Figure 80).



Figure 80. Example of a running lab-scale experiment, where a glycolysis is ongoing.

As it can be viewed in Figure 81, vapour is being produced during the dissolving process. Because of this, we used a Liebig condenser to collect the distillate. The collected distillate amount varies as the recipe is being altered. Therefore no further statement could be made at the moment regarding the distillate. After the reaction, the recycled polyol is collected and cooled down. The dissolved and cooled polyol is shown in Figure 81.

Figure 81.Example of a finished polyol from degraded PUR insulation boards.

After confirmation of the possibility to use the glycolysis reaction with the given material during the lab-scale experimentation, the actual development of a recipe to acquire specific parameters for recyclability has started. This includes the further adjustment of the content, like the mass percentage that could be dissolved, the possible adjustments in the reaction time due to increasing or decreasing contents of the recipe with the aim to get the desired specifications but also creating a recycled polyol that wouldn´t be overly expensive due to the additional reagents used. Another factor is the change in parameters like temperature and stirrer speed, which shows significant impact on the dissolving process. The adjustment of these different regarding the specifications that are aimed for takes therefore a lot of time and is still in development.

**Example of analyzed Samples**

In Table 23 are some analyzed samples of the PIR-batches listed and compared to the given aim of the specific parameter range for further use in a production line as a recycled polyol. While PIR-1 is an average of the same batch in a replica of three, PIR-2 shows the first optimization on the recipe while the same recipe with additional deamination is followed in PIR-3, as the content of MDA was high. It also must be pointed out, that a new specification aim was be announced, after the analyzation of the first samples at the testing area of SOPREMA. At the current state, the research needs more research & development regarding the new specifications for the recycled PIR based polyol.

Table 23. Optimizations so far – PIR-Polyol

| Experimental values from recycled PIR-insulation boards | | | | | |
|---|---|---|---|---|---|
| Data | PIR-1 | PIR-2 | PIR-3 | First specification | Final specification |
| OH-value mg KOH / g | 667.3 ± 11.7 | 503.6 ± 1.7 | 490.3 ± 6.9 | 550 ± 50 | 200 ± 50 |
| Viscosity mPa*s @ 25 °C | 1690 ± 95 | 5300 ± 283 | 4320 ± 99 | 3000 ± 2000 | 3000 ± 2000 |

| | | | | | |
|---|---|---|---|---|---|
| Water content w% | n.m.* | 0.33 ± 0.02 | 0.27 ± 0.1 | - | - |
| Production time h | 6.5-7.5 | ~4 | ~5 | max. ~8 | max. ~8 |
| MDA content w% | 2.14 ± 0.15 | 2.35 ± 0.36 | 1.3 ± 0.28 | < 01 | < 0.1 |

As for the results in terms of the PUR-Polyol, Table 24 shows the analysed data. While PUR-1 where the first samples produced in the small lab-scale up, the PUR-2 are the first optimized samples.

Table 24. Optimizations so far – PUR-Polyol

| *Experimental values from recycled PUR-insulation boards* | | | |
|---|---|---|---|
| *Data* | *PUR-1* | *PUR-2* | *Final specification* |
| OH-value mg KOH / g | 468.7 ± 7.8 | 498.2 ± 23.4 | 550 ± 50 |
| Viscosity mPa*s @ 25 °C | 8428 ± 210 | 9059 ± 1243 | 3000 ± 2000 |
| Water content w% | 0.51 ± 0.1 | 0.4 ± 0.05 | - |
| Production time h | ~10-12 | ~6 | max. ~8 |
| MDA Content w% | 0.53 ± 0.1 | 0.33 ± 0.04 | < 0,1 |

One of the main challenges with the PUR based recycled polyol is the time needed for the dissolving process, which is why the first optimization experirments of the PUR-2 batches were aimed to decrease the amount of time needed for the production of the polyol. This worked but we still haven´t reached the specifications that we are aiming for therefore further research is needed.

**Problems:**

During the processes with the pure insulation boards, there are already some discovered problems, which are listed and described in the following summarisation:

- The recycled PIR & PUR polyols are having an olfactory unpleasant scent
  - Probably from free amine content through depolymerisations

- Analysed samples regarding amine content showed more than the nontoxic level of 0.1 wt%
  - Testing needs further investigation, high content could be influenced through other substances, like previously used catalysts during the production of the insulation boards

- Used catalysts could possibly have a negative effect on the recyclability of the polyol
  - Further investigation on the possibility to swap or using different concentration levels needs to be analysed

- The specific specifications for the recycled PUR & PIR polyols, regarding the recyclability by SOPREMA, couldn´t be achieved till now

## 10.6. Planning for the rest of the activities

As the problems that are discovered so far are listed in the previous section, the focus for the next activities is on developing the recycled polyol that meets the specifications and altering the production process to be as clean as possible.

For the next step, it would then be to upscale the process step by step, from 10 kg to 100 kg batches and analyse the generated process parameters and polyols. Because of this, there will be more experiments done in a systematic upscaling process, because every change in diameter can influence the reaction in the whole. So can the RPM that the given stirrer has in the medium. Another problem on the higher scale- could arise from the material weight at particle size, as low-weight particles tend to develop an arching effect in the conveyer, which could be needed to be addressed.

The next step would be to use the recipe on an industrial scale (tons) and again analyse these produced data. In this process, the know-how from RAMPF will be used and compared to the newly produced data while evaluating the costs and other parameters that maybe will be subject to change with the project partners.

While this is the case for the upscale event regarding to pure materials from PIR & PUR insulation boards from SOPREMA, access to waste material from buildings will also be required. Because of the precondition of the material that needs to be taken into account, further communication with the project partners will be happening, as the separation from possible impurities is a major factor as first step in the recycling process.

The acquired waste material needs to be analysed and reviewed to see if the developed recipe can be used to degrade the material via the glycolysis process and if major new problems, like impurities could be found.

Another aspect will be the research in terms of mixed waste material, where a separation of PIR & PUR isn´t present or a separation process couldn´t split these components either. Therefore, mixed PU needs again being experimented and analysed, as the difference in PIR & PUR, which comes mainly from different contents of isocyanate usage during the production, has an impact on the used degrading reagents and therefore are not degraded in the same way.

Also, the communication with SOPREMA and Keey Aerogel are major points in terms of the usability factor of the produced recycling polyols. Closer cooperation will be done when more and more samples are delivered and tested, while the specifications could change, depending on the resulting characteristics of the new products.

## 10.7. Preliminary conclusions

The progress in terms of the PU & PIR insulation boards so far shows, that it is indeed possible to degrade the boards via the use of a solvolysis-process (more specifically glycolysis).

The process involved however is still in the middle of development to achieve, not only the possibility of processing the insulation boards from EBM/RBM/ into a polyol, but also using these polyols as a production component for new valuable products, like new insulation boards.

Therefore, further investigations regarding the combination of various aspects, like the use and concentration of degrading catalysts, time influence on the homogeneity of the polyol, cost of the heating process, etc. are still needed.

## 11. Advanced technology turning silica based waste into Silica Closed Loop granular Aerogels

### 11.1. Description of the problem

Buildings account for 78% of the total construction in the EU-28. They occupy a floor area of 25 billion m², account for 40% of the EU´s energy consumption, 36% of its $CO_2$ emissions, around 25% of the total waste generated and 54% of demolition materials are landfilled with a high burden of associated environmental impacts (loss in embodied energy, $CO_2$ emissions, soil pollution and water consumption) (1). Recent reports reveal that the EU28 generates around 350 million tons of construction, renovation and demolition waste (CDW) (2). It seems crucial to find the best possible strategy in order to reuse, recycle and increase the valorisation of the different goods and components of buildings. In addition, the European Green Deal is enforcing rules on energy performance of buildings (3). New methods/materials for insulation are being developed to reduce $CO_2$ emissions. Silica aerogel is one of the most promising material for thermal insulation applications due to their nanopores with a fine, open-pore structure. Currently, silica aerogel is commercially available in different forms such as, powders, granules, monoliths, and blankets (aerogel composites). However, the price of silica aerogel related to the high cost of raw material (silica precursor) is clearly the biggest barrier of this material in the building sector.

Both energy consumption/$CO_2$ emission reductions and demolition waste valorisation can be achieved by a novel closed-loop circular economy model of a high-performance building insulation material from End of Life building materials (EBM).

The objective of this task is to develop an optimized continuous production line (1000 l/day) of highly homogeneous silica closed-loop granular aerogels (λ<0.016 W/mK) from high silica content EBM (e.g. glass and siliceous concrete), using silicic acid hydrothermal synthesis and multi-solvent Low Temperature Super-Critical Drying (LTSCD), decreasing raw material consumption by 6% (mass) and cost by 50% compared with the most optimized current practice (final production cost ranging between 400-500 €/m$^3$).

The 0.5 ton of obtained silica precursor and 5m$^3$ of silica aerogel granules from this task will be used for the production of ceramic wall tiles, plasterboard, ultra-lightweight concrete elements, and PU-based aerogel panels in WP3.

### 11.2. State of the art/technology

In the past 20 years, silica aerogel has attracted increasingly more attention due to their extraordinary properties in various applications. Silica aerogel is a solid nanostructured material with high porosity (~95%), high specific surface area (up to 1,000 m²/g), high optical transmission (90%), low density, and excellent heat insulation properties. The silica aerogel manufacturing process generally consists of 3 main steps:

1)      Gel formation - As a result of hydrolysis and condensation processing of the silica precursor, a nanostructured solid network is formed in different forms (powder, granular, moulding and impregnated blankets).

2)      Solvent exchange - The solvent exchange is needed for the production of silica aerogel based on an aqueous solution such as sodium silicate, since water is poorly miscible with $CO_2$ during the supercritical drying process.

3)      Drying process – The drying is to preserve the microstructure as well as shape from compaction and further changes. The drying process can be conducted in three different techniques such as ambient drying, freeze drying, and supercritical drying. Each drying process has its own advantages and disadvantages. LTSCD is recognized as the most environmental suitable and adequate process to obtain high-quality aerogels.

Conventional silica aerogels are available in different forms such as, powders, granules, monoliths, and blankets (aerogel composites) depending on the applications. Silica aerogel granules are commonly used to enhance the thermal performance in  building applications such as interior/exterior insulating plasters, insulation boards, and daylighting glass panels. However, their applications have been limited due to their high production cost including raw material and manufacturing process.

Concerning the high cost of raw materials, scientific researchers attempt to use the alternative silica sources such as bio-based materials, waste materials, and organic chemicals to produce a silica precursor instead of using high-cost commercial silica solution. Foletto et al (2006) reported that sodium silicate was produced by reacting rice husk ash (RHA) with aqueous sodium hydroxide. About 90% of the silica contained in the RHA into sodium silicate was converted in a closed system at 200 °C. Keawthun et al. (2014) prepared a sodium silicate solution from different waste glasses using hydrothermal and fusion methods. The study indicated that an alkaline fusion treatment of waste glass at 650 °C with sodium hydroxide for 60 min. gives a 90 wt% silica extraction. In 2017, Piskin et al. synthesized hydrophobic silica aerogel using gold mine waste as silica source. The synthesized silica aerogels were used in the production of insulating plaster. The results showed that the addition of 20 wt% silica aerogel in plaster decreased 63% thermal conductivity compared to the natural plaster without aerogel. In the VEEP project, it has been reported that a low thermal conductivity aerogel composite can be prepared using sodium silicate solutions obtained from concrete and demolition waste (CDW) recycled materials.

Toward a cost-effective manufacturing process of silica aerogel, only a batch process is currently employed. This process is not suitable in efficient industrial production due to cost and time consumption. Therefore, the development of a continuous process is essential and a process optimization in each step is necessary.

Keey Aerogel and Tecnalia proposed the combination of a low-cost silica precursor using EBM and a highly efficient continuous aerogel production in supercritical drying technology. The hydrothermal synthesis will be optimized to obtain the silica precursor from EBM. Then, the silica aerogel synthesis will be optimized. The granulated silica aerogel will be produced continuously in

supercritical conditions. The semi-industrial installation will be validated to obtain competitive commercial silica aerogel properties.

## 11.3. Extended methodology

The methodology of research approach is described as the following;

1. Silica precursor synthesis - The different types of EBM will be tested using a hydrothermal process. The reaction conditions will be optimized and the best EBM will be selected for aerogel production.
2. Aerogel synthesis optimization - The aerogel production process will be optimized in each step to achieve the low-cost silica aerogel product. The new method of aerogel synthesis will be conducted and the properties of silica aerogel will be characterized, for example density, thermal conductivity, particle size distribution, and hydrophobicity.
3. Silica aerogel production
    a. Validation of continuous aerogel production at lab scale – The process of granulated silica aerogel manufacturing will be validated. The process conditions such as solvent, temperatures, and cutting parameters will optimized.
    b. Design and installation of the continuous LTSCD system.
    c. Optimization and validation of continuous LTSCD in semi-industrial scale.
    d. Production of homogeneous silica aerogel granules for the production of ceramic wall tiles, plasterboard, ultra-lightweight concrete elements, and PU-based aerogel panels in WP3.

## 11.4. Materials (source, sampling, preconditioning)

Three types of EBM will be tested for hydrothermal synthesis. The characteristics of each EBM are presented in Table 25. and Figure 82.

Table 25. Raw materials employed in the hydrothermal process

| *Source material* | *Acronym* | *Origin* |
|---|---|---|
| Glass wastes | GW | Spain |
| CDW | SC1 | Spain |
| CDW | SC2 | Netherlands |

Figure 82. Pictures of the glass waste and CDW samples SC1 and SC2

The chemical composition of the raw materials employed in the hydrothermal process is evaluated by X-Ray Fluorescence. Table 26 shows the chemical composition of all materials that have been employed and tested within Task 2.7.

The materials submitted to the hydrothermal process need to present a high content of silica. As it can be observed in Table 26., the content of silica for raw materials varies from 71 to 78 wt% depending on the sample. The glass waste sample presents high content of silica, $Na_2O$, CaO and MgO. On the other hand, CDW recycled samples present apart of silica, a high content of CaO.

Table 26. Weight percent of the oxides found in the raw materials tested in Task 2.7.

| Sample | % | | | | | | | | | | | | | |
|--------|------|-------|------|------|-----------|------|------|-----------|-----------|------|------|--------|------|----------|
| | $SiO_2$ | $Na_2O$ | CaO | MgO | $Al_2O_3$ | $K_2O$ | $SO_3$ | $Fe_2O_3$ | $As_2O_3$ | $TiO_2$ | Cl | $ZrO_2$ | NiO | $P_2O_5$ |
| GW | 71,5 | 13,5 | 8,85 | 4,44 | 0,65 | 0,20 | 0,17 | 0,084 | 0,07 | 0,049 | 0,031 | 0,014 | 0,014 | 0,013 |
| SC1 | 59,9 | 0,12 | 20,4 | 0,43 | 1,73 | 0,46 | 0,30 | 0,73 | - | 0,094 | 0,036 | 0,019 | 0,013 | 0,038 |
| SC2 | 77,8 | 0,17 | 10,4 | 0,83 | 2,50 | 0,48 | 0,40 | 0,64 | - | 0,12 | 0,033 | 0,012 | 0,015 | 0,030 |

## 11.5. Activities in progress
### 11.5.1. Silica precursor synthesis

**Hydrothermal process and waterglass characterization**

The aim of this task is to adapt and optimize a silica extraction process in order to find the optimum extraction conditions in the Silicic Acid Hydrothermal Synthesis stage.

In this route, the glass waste and CDW as described before has been hydrothermally treated with a NaOH solution under high temperature and pressure during a specific time.

From the hydrothermal reaction, a sodium silicate solution (known as waterglass solution) is obtained. In this reaction, besides the waterglass, the formation of a solid subproduct is also observed (which is not desired). These hydrothermal tests have been performed in a 0.5 L reactor available in TECNALIA. The scheme of the hydrothermal process is shown in Figure 83.

**Glass and silica based waste material**
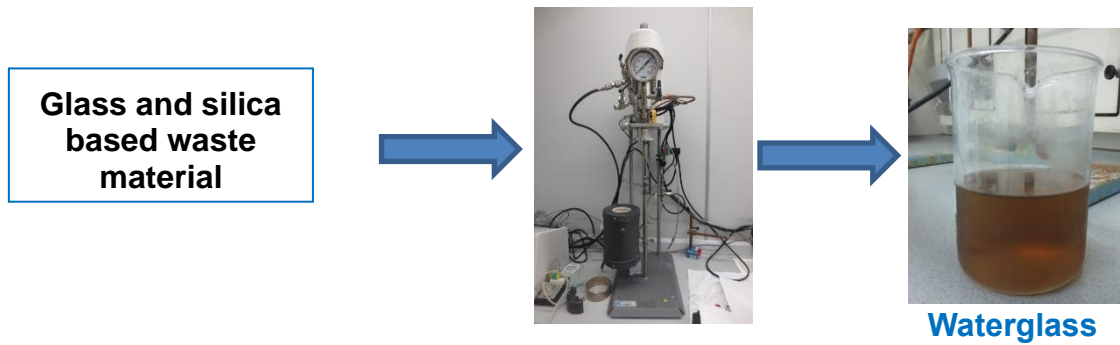
**Waterglass**

Figure 83. Scheme of the hydrothermal process.

The general approach has been to mill the samples (<4 mm) before their hydrothermal treatment in order to get a better yield in the silica extraction hydrothermal process. The obtained waterglass solutions have been characterized in order to analyse the content of the extracted silica. A gravimetric method has been used for measuring the concentration of $SiO_2$ contained in the water-glass solution and the concentration of $Na_2O$ has been determined by a titration method according to ISO standards (ISO 1690:1976 and ISO 1692:1976). This allows the calculation of:

i) the silica extraction yield by means of equation 1.

$$\% \text{ Silica extraction} = [SiO_2]_{ex}/[SiO_2]_o *100 \qquad (1)$$

where $[SiO_2]_{ex}$ is the concentration of silica in waterglass and $[SiO_2]_o$ is the silica concentration present in the raw/recycled fraction material. ii) the $SiO_2$:$Na_2O$ molar ratio (Mr).

Commercial waterglass samples have values around 3.0. However, this does not mean that waterglass solutions with lower values of Mr than 3 are not suitable for aerogel synthesis.

Table 27 shows the best results of the characterization of waterglass samples obtained from glass waste and CDW recycled fractions submitted to the extraction process. Values of silica extraction yield and $SiO_2$:$Na_2O$ molar ratio are listed in these tables.

Table 27. Waterglass solutions obtained from raw materials.

| Sample treated | Silica extraction yield (%) in the waterglass | Molar ratio SiO2/Na2O in the waterglass |
|:---:|:---:|:---:|
| GW | 60 | 1.35 |
| SC1 | 32 | 1.68 |
| SC2 | 63 | 2.07 |

The highest silica extraction yield is achieved with SC2 sample with a value of 63%. The value of Mr is equal to 2.07. This could be explained because this material presents the highest concentration of silica in its composition and a CaO content much lower than the SC1 sample. On the other hand, comparing with glass waste, SC2 has a slightly higher CaO content but much lower MgO content in this composition, resulting in the best performance in the hydrothermal process. As it was stated, in all reactions a solid subproduct is formed. Some of the solids have been characterized by XRF showing that some zeolites are formed. This means that during the silica extraction as waterglass there are other competitor reactions taking place between the silica and the $Al_2O_3$, CaO, MgO present in the recycled material. Based on these results, it was decided to select the SC2 material as a promising material for the silica extraction via the hydrothermal process.

### 11.5.2. Silica aerogel production

**Validation of continuous aerogel production in lab scale**

The continuous silica aerogel production at lab scale using granulation technology was validated. The process conditions such as solvent, temperatures, and different parameters were optimized.

The cutting parameters were adjusted to obtain a particle size between 1-2 mm which is generally required for construction applications. The particle size distribution of the obtained silica aerogel granules was analyzed using Malvern mastersizer 3000 device. The results were compared with the commercial silica aerogel granules as shown in Figure 84. It has been observed that the obtained silica aerogel granules from the jet cutting method were uniform in size, with a relatively narrow particle size distribution with mean particle size 1700 micron.
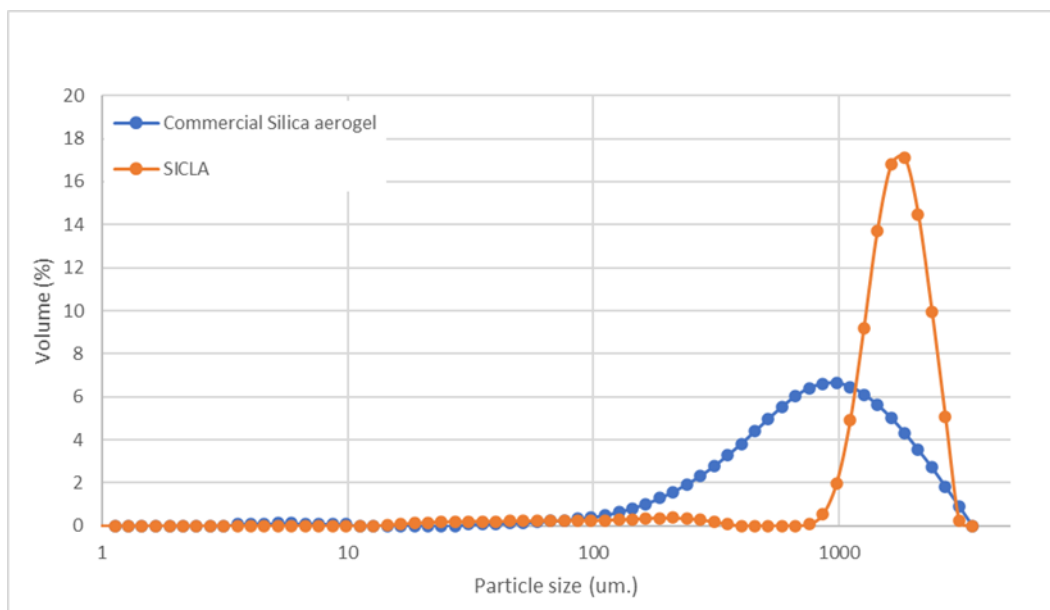


Figure 84. Particle size distribution of silica aerogel granules using jet cutter

To validate the production of silica aerogel granules using a jet cutter, the nanostructure of obtained silica aerogel granules was observed using a FEI-SEM Quanta 400 scanning electron microscope (**SEM**) operated at 100 kV at Institute de science des matériaux de Mulhouse (IS2M). The SEM micrograph of silica aerogel granules are presented in Figure 85. It was confirmed that the obtained silica aerogels had a nanostructure with particle size <10 nm.
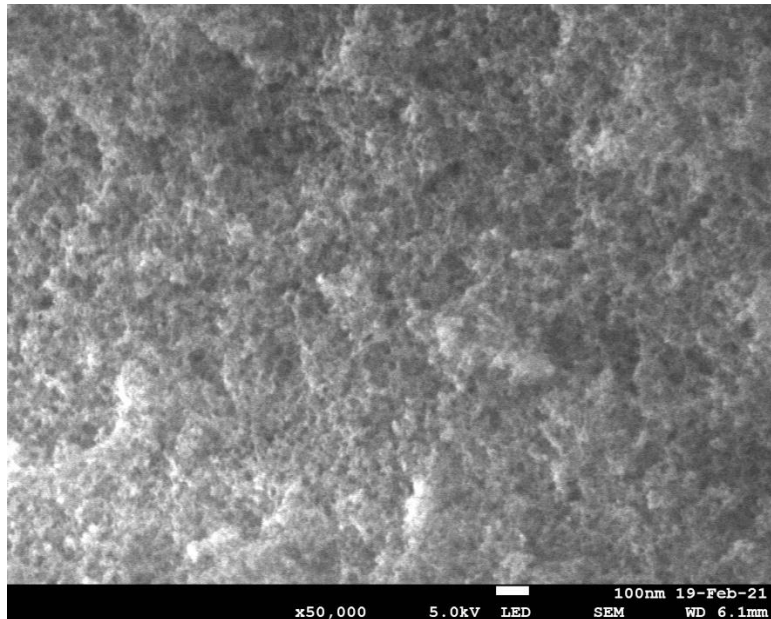


Figure 85. SEM micrograph of silica aerogel granules using jet cutter

### 11.5.3.   Design and installation the continuous LTSCD system

The designed production capacity is 2,000 m³/year. The equipment and piping systems were ordered to be installed in April 2021.

## 11.6. Planning for the rest of the activities

The plan for the rest of the activities is shown in Table 28.

Table 28. Planning for next Task 2.7 activities.

| Tentative date | Plan Activity |
|---|---|
| April 2021 | Installation of continuous silica aerogel production system |
| April/May 2021 | Production of silica precursor from EBM for WP3 |
| May 2021 | Optimization of the aerogel synthesis condition using silica precursor from EBM |
| April-May 2021 | Alternative silica aerogel synthesis to reduce/avoid ion-exchange resin process |
| June 2021 | Optimization continuous silica aerogel production in lab /semi-industrial scale |
| April-August 2021 | Characterization of silica aerogel granules |

## 11.7. Preliminary conclusions

As it has been described in this deliverable, the objective has been successfully achieved. The hydrothermal process permits the extraction of silica as waterglass from different raw materials and recycled CDW samples which have a high content of silica in their initial composition.

All materials are composed of silica but also of other metals that can interfere negatively in the silica extraction process. The presence of CaO, $Al_2O_3$ and other oxide metals can compete in the formation of sodium silicate by the precipitation of silica in the form of other siliceous species (zeolites) which are found in the subproduct solid. For the selection of the glass and silica-based waste material for the fabrication of the aerogel, two factors should be considered: i) the performance of the material, thus, the silica extraction yield and value of Mr and ii) the availability of the material itself.

Considering these two aspects, it can be concluded that the CDW material SC2, up to 63% of silica extraction yield, is the most promising material for the preparation of aerogel products within ICEBERG project. This CDW material SC2 will be used for optimization and scale up to produce silica precursor and silica aerogel granules for the production of ceramic wall tiles, plasterboard, ultra-lightweight concrete elements, and PU-based aerogel panels in WP3. A lab-scale continuous silica aerogel manufacturing process was validated and silica aerogel granules with homogenous particles were obtained with mean particle size 1700 micron. The SEM micrograph confirmed that the obtained silica aerogels had a nanostructure with particle size <10 nm. The design of continuous silica aerogel production was finalized and it will be installed within April 2021.

## 11.8. References

1.European Commission-DG ENV (2011) "Management of CDW in EU". Final Report elaborated by BIO Intelligence Service.

2. Vegas et al (2015), Upgrading the quality of mixed recycled aggregates from CDW by using near-infrared sorting technology, Const. and Build. Materials 75, 121-128.

3. Energy performance of buildings directive [Internet]. Energy - European

Commission. 2019 [cited 2020 May 21]. Available from:

https://ec.europa.eu/energy/topics/energy-efficiency/energy-efficient-buildings/energy-perfor

mance-buildings-directive_en

4. E.L. Foletto, E. Gratieri, L. Hadlich de Oliveira, and S.L. Jahn, Conversion of rice hull ash into soluble sodium silicate, Materials Research. (2006) vol.9

5. M. Keawthun, S. Krachodnok, and A. Chaisena, Conversion of waste glasses into sodium silicate solutions, Int.J.Chem.Sci. (2014) vol.12(1)

6. N.K. Mermer, M.S. Yilmaz, O.D. Ozdemir, and M.B. Piskin, The synthesis of silica-based aerogel from gold mine waste for thermal insulation, J.Therm.Anal.Calorim. (2017)

## 12. Conclusions

The present document overviews the main results obtained in the frame of the ICEBERG project dealing with the development of novel technologies and strategies to produce high purity RBM materials. Key conclusions of the activities performed in the first year of the Project are summarized next:

- A complete characterization study has been performed on mixed ceramic fractions obtained from EBM. Results show the ability of spectroscopic techniques to identify different materials, and set the fundamental basis to identify the composition of the particles in mixed ceramic fractions by means of Hyperspectral Imaging (HIS), and the application of advanced image processing algorithms. Based on this technology and the particle recognition models that are being developed, a pilot scale (1 t/h) sorting line will be prototyped.

- The main operational parameters of a novel concrete recycling process have been stablished. Consortium partners are working on the implementation of a modular 20t/h thermal attrition unit that will separate the incoming material into clean recycled sand and hydrated cement rich powder, but also glued particles spall to increase the recovery of clean sand.

- A LIBS based quality assessment methodology has been developed to assess the presence of pollutants in EoL concrete. The sensitivity of the technology for the determination of different contaminants, and the optimum measurement conditions have been identified. Further work is on-going to implement a functional demonstrator based on this technology, and to combine it with a RFID based traceability system.

- A carbonation process for the upcycling of concrete demolition waste has been developed and optimized. The process probed itself able to reduce water absorption and generate high quality RCA.

- A laboratory scale grinding process for ceramic fractions has been designed and tested. The process, which involves three consecutive steps – centimeter size reduction, conventional milling and attrition milling, shall contribute to improve the homogeneity and quality of recycle ceramic fractions.

- An integrated process for the production of high quality wood fibres from wood containing demolition waste is under optimization. The advantages and drawbacks of different candidate processes have been comparatively investigated.

- An advanced purification process for CDW and synthetic gypsum is under development. While hydrocyclone separation has proved limited effectiveness in the separation of CDW gypsum, the purity of the outcoming material could be significantly improved through the combined or individual use of acid and leaching treatments. Additional experimental studies are scheduled to stablish an optimised gypsum purification process.

- A glycolysis process has been successfully applied to the recycling of PU and PIR foams. Work is in progress to define the optimum conditions to obtain polyol from wasted foams, and to reuse the recovered compounds in the production of valuable products, such as new insulation boards

- A hydrothermal process has been successfully developed to extract silica and waterglass from silica rich construction and demolition waste. Considering the interferences caused by the presence of contaminants, SC2 material was identified as the most promising input material. Using this material, a lab-scale continuous silica aerogel manufacturing process was validated, and silica aerogel granules with homogenous particles were obtained with adequate mean particle size. The design of continuous silica aerogel production was completed, and a demonstrator will be implemented in the forthcoming months.